

CHAPTER 15

Two- and Three-Dimensional Numerical Simulation of Mobile-Bed Hydrodynamics and Sedimentation

Miodrag Spasojevic and Forrest M. Holly, Jr.

15.1 INTRODUCTION

15.1.1 When Is Multidimensional Mobile-Bed Modeling Necessary?

Although present understanding and conceptualization of mobile-bed processes are still far from complete, one-dimensional mobile-bed numerical models have been used with some success in engineering practice since the early 1980s. As described in Chapter 14 of this manual, such models are most often applied to situations involving extended river reaches and extended time periods, typically to determine the long-term response of a river to natural or man-made changes imposed upon its hydrologic and sediment regime. The mobile-bed and hydrodynamic processes in one-dimensional models must necessarily be expressed in terms of cross-sectional properties such as average velocity, average depth, hydraulic radius, and overall shear stress. Quantities such as bed scour and fill, bed-load transport, sediment-load concentration, and bed-material composition must also be expressed as total cross-sectional values. Although some modelers have developed means of extracting limited two-dimensional information from one-dimensional models, for example, through assumed transverse distributions of shear stress and depth-averaged velocity, the fundamental computation is one-dimensional. Demands on computational resources are generally not a significant factor or expense, and traditional field-data collection efforts are similar to those needed for steady- or unsteady-flow flood modeling.

Whatever their utility for studies of extended time periods and river reaches, one-dimensional models cannot resolve local details of flow and mobile-bed dynamics. Such local details might involve the plan-view distribution of deposition patterns in a reservoir; the scour and deposition patterns associated with flow around the ends of spur dikes or other

river training works; or the scour and deposition provoked by bridge piers. For such problems, two- or three-dimensional models provide the possibility of resolving these kinds of local details, albeit at the cost of significantly increased program complexity and computational resources. In time, if computing power continues to increase at its current breathtaking pace, one may envisage use of two- or three-dimensional models even for large-scale problems such as those amenable only to one-dimensional models at the present time. At present, two- and three-dimensional use is limited to problems requiring resolution of local details over relatively short time periods, often as a complement to one-dimensional models of larger spatial and temporal scope.

15.1.2 Is the Additional Complexity of Multidimensional Mobile-Bed Modeling Justified?

It is often argued, and indeed has been argued since the advent of industrialized computational hydraulics in the 1970s, that the increased complexity and data needs of “the next level of modeling complexity” are not justified given our imperfect understanding of certain physical processes, the inadequacy of field data, and the uncertainty inherent in model results. The authors believe that this is a spurious argument. First, experience has shown that input data needs that may not seem justified at today’s level of modeling capability will soon be justified by tomorrow’s capabilities. Second, why should one compound the uncertainty in model results by adding inadequate field data to a simplified version of complex natural processes? Third, and perhaps most important, more complex models (in this case, two- and three-dimensional ones) obviate the need to describe all the complex and nonhomogeneous processes in a river cross section in terms of global cross-sectional average properties such as mean velocity, discharge, hydraulic radius, and average bed shear. In a two-dimensional

depth-averaged model, one still must relate near-bed processes to the depth-averaged properties in the water column, such as depth-averaged velocity and bed shear stress, but at least the heterogeneity of processes across the channel can be represented. In a three-dimensional model, near-bed processes can be related to the hydrodynamic properties at a computational grid point immediately adjacent to the bed and localized in a plan-view sense.

Therefore the authors believe that whether or not the particular features and requirements of a study mandate the use of multidimensional modeling, the model representation of physical processes can only be improved—or at least made more rational—by adopting a two- or three-dimensional approach. This may not be feasible for all studies because of computer-resource constraints, as described in the following section. But the authors believe it is time to begin planning for a study by asking, in the interest of better representation of physical processes, “Can this be done with a two- or three-dimensional model, or do we have to resort to a one-dimensional approach?” rather than “Can this be done with a one-dimensional model, or do we have to resort to a two- or three-dimensional approach?”

15.1.3 Limitations of Computer Resources

One obvious reason to answer the above question “we’ll have to go one-dimensional” is the limitations of computer resources. Memory and disk space are not generally limiting, even for three-dimensional modeling. But the sheer central processing unit (CPU) time requirements of three-dimensional models, even in a parallel-processing environment, obviate any possibility of using them for extended spatial extents and simulation durations within the time frame of a study, at least as of this writing. For example, depending on the computing hardware in use, one-dimensional mobile-bed models covering the order of hundreds of kilometers can be used to perform simulations of the order of decades with a turnaround time on the order of several hours. By contrast, a fully three-dimensional mobile-bed model might require days of CPU time just to obtain a single steady-state solution over a river reach on the order of 20 kilometers. This three-dimensional demand is considerably less if the hydrostatic pressure assumption replaces the vertical momentum equation; and the CPU time per time step in a true unsteady calculation is generally less than that required to obtain a single accurate steady-state solution. Such CPU time requirements depend directly on the number of sediment size classes being transported, the number of subsurface bed strata considered, the type of computational grid (structured or unstructured), and other factors. Nonetheless, computer CPU time requirements can be a significant factor militating against the use of three-dimensional modeling given the calendar time constraints of a typical engineering study.

The CPU time demands of two-dimensional modeling fall somewhere in between those of one-dimensional and three-dimensional, but turnaround time can still be a decisive issue depending on the temporal and spatial extent of the modeling effort.

15.1.4 Structure of This Chapter

The remainder of this chapter is structured to provide not only the model user and developer, but also the model “consumer” (i.e., the one paying the bill), with a framework for understanding the conceptual bases of multidimensional models, alternatives for mathematical representation of relevant physical processes, alternative computational grid representations and their associated approximate numerical solution methods, and a sense of what can go wrong. Within this chapter, the authors use the terms “mobile-bed modeling,” “sediment modeling,” and “sediment-process modeling” interchangeably.

Section 15.2 provides a brief overview of typical problem types and available techniques and modeling systems for each. Section 15.3 summarizes the mathematical and numerical bases of the two- and three-dimensional hydrodynamic models that underpin any mobile-bed modeling. Section 15.4 provides an overall conceptual framework for modeling sediment transport and bed evolution. The next three sections, 15.5, 15.6, and 15.7, go into detail in the treatment of sediment processes on or near the bed, those in suspension, and the exchange between the two domains. Section 15.8 deals with the need for empirical closure relations and their role in modeling systems, whereas Section 15.9 focuses on numerical-solution issues related to sediment processes. Section 15.10 provides some background on field data needs and the role of such data in model construction, calibration, and verification. Section 15.11 provides limited examples of two- and three-dimensional mobile-bed model studies. Finally, Section 15.12 provides the authors’ view of the state of the art and future perspectives in multidimensional mobile-bed modeling.

The authors assume that the reader has a general familiarity with the vocabulary of numerical hydraulics, and also with some of its general techniques and support tools. Some of the relevant sections refer to the reader to background texts on computational hydraulics, computational fluid dynamics, and grid generation.

The authors do not pretend to have prepared this chapter from a purely objective framework. Most of the developments and examples build on the authors’ own experiences with their particular conceptualization of the mobile-bed problem and simulation systems they have developed and used. It is hoped that this enables the reader to acquire solid depth and detail on at least one approach to the problem. The authors have tried to use their own frame of reference as a basis for less detailed description of conceptual, mathematical, and numerical approaches used by others.

15.2 PROBLEM TYPES AND AVAILABLE TECHNIQUES AND MODELING SYSTEMS—A SURVEY

15.2.1 Introduction

In preparation for the more detailed developments in subsequent sections, the authors present here a survey of typical

problems for which two- or three-dimensional mobile-bed modeling may be required. The purpose is to draw attention to the features of each type of problem that may require corresponding features and techniques in a modeling system and to give an admittedly incomplete set of references to two- and three-dimensional modeling systems and applications currently available for each problem type. Table 15-1

Table 15-1 Summary of Model Capability Requirements

Section	Type of problem	Two-dimensional (depth-averaged)	Three-dimensional required?	Hydrostatic assumption in three dimensions?	Unsteady flow capability required?	Sediment mixture capability required?	Distinct treatment of bed-load/suspended-load processes?
15.2.2	Reservoir sedimentation	Often sufficient	If reentrainment into outlet structures is studied	OK if entrainment into outlet structures not studied	Sequence of steady flows usually OK	Required	Required unless inflow is fully bed load
15.2.3	Settling basins/tanks/clarifiers	Generally not relevant	Necessary for representation of interaction between geometry and sedimentation patterns	OK if flow is quiescent	Generally not necessary	Required unless sediment load is homogeneous	Not generally required
15.2.4	Riverbend dynamics and training works	Not applicable without special incorporation of secondary flow effects	Needed to capture secondary-flow effects	OK if detailed flow around structures is not an issue	Desirable for study of effects of hydrograph	Required unless sediments are entirely uniform	Required in most alluvial rivers
15.2.5	Mobile-bed dynamics around structures	Not applicable	Required	Generally not acceptable, because vertical accelerations are important	Generally not necessary	Required unless sediments are entirely uniform	Required in most alluvial rivers
15.2.6	Long-term bed evolution in response to imposed changes	Generally irrelevant	For focused local study within larger one-dimensional model	May be necessary for long-term simulation	Must accommodate series of annual hydrographs	If required for the overall one-dimensional model	If required for the overall one-dimensional model
15.2.7	Sorbed contaminant fate and transport	May be appropriate	May be required	OK if flow-structure-sediment interaction is not of primary interest	Likely necessary for studies of resuspension during floods	May not be required if focus is entirely on contaminated fine sediments	Suspension advection-diffusion required

summarizes this inventory. The authors limit their attention to subcritical flow, because supercritical flow capability is rarely needed for problems in which mobile-bed activity is of primary interest.

15.2.2 Reservoir Sedimentation

Chapter 12 of this manual is devoted to the issue of reservoir sedimentation, for which prediction and management simulation are best accomplished using two-dimensional (plan-view) models. The present chapter also includes an example application of a two-dimensional model to reservoir sedimentation (Section 15.11).

Although one-dimensional models have been, and indeed still are, used for reservoir sedimentation, by definition they can only resolve the longitudinal distribution of sedimentation, from the headwaters to the dam. Many reservoirs flood not only the incised river channel, but also adjacent floodplain areas; in addition, many have significant lateral embayments and islands. One-dimensional models can resolve such features only in terms of equivalent transverse cross sections, at best including distinct one-dimensional flow paths around islands (in models permitting looped channel structures) and one-dimensional segments extending into lateral embayments.

Of course three-dimensional modeling can also be used for reservoir sedimentation, and might be used if computational resources were available and especially if the local entrainment of sediment into outlet works was to be studied. The general absence of significant recirculation in reservoir flow, as well as the generally low velocities and lack of training structures, argues for a depth-averaged approach being sufficient. However, only a three-dimensional model can resolve and simulate the effects of reservoir density currents if these play a significant role in the sedimentation processes of a particular site. Vertically two-dimensional models have been used for the study of reservoir sedimentation in this case, but these are width-averaged and therefore can only approximately resolve the effects of lateral embayments.

Reservoir sedimentation simulation does not generally require full representation of unsteady-flow hydrodynamics. It is usually necessary only to simulate long-term hydrographs, and this can be done using a series of steady-state inflows and water-surface elevations if necessary. Similarly, sedimentation rates (by size fraction) can be determined for such a series of steady-flow situations and used to generate equivalent sedimentation quantities over time.

When three-dimensional models are employed for reservoir sedimentation, it is generally acceptable to use the vertically hydrostatic pressure assumption in lieu of the vertical momentum equation (see Section 15.3.3). Vertical accelerations are generally not strong in a typical reservoir, at least outside the vicinity of structures. The hydrostatic pressure assumption results in significant reduction in computational time compared to fully three-dimensional formulations.

However, if the local entrainment of deposited sediment into outlet works is being studied, a fully three-dimensional treatment (i.e., with the vertical momentum equation included) may be required.

Reservoir sedimentation studies should be based on simulation models that accommodate sediment mixtures, through individual size classes or some other mechanism. The longitudinal (streamwise) differential sorting is intimately related to the differential transport modes of different sediment sizes (e.g., bed load for inflowing gravels or sands and suspended load for inflowing silts and washload) and to the variation of these transport modes from the upstream depositional delta to the downstream deep pool.

It is very important that both bed-load and suspended-load processes be represented in reservoir sedimentation models, unless there is no suspended load or washload in the inflowing streams. It is characteristic of a reservoir that suspended load or washload in the relatively steep, rapid, shallow inflow may transition through a bed-load mode of movement in the middle or downstream portions of the reservoir, where velocities are low, before being ultimately deposited on the bed. Similarly, fine material deposited during a previous event may become reentrained into bed load or suspended load during dynamic reservoir operations and/or extreme hydrologic inflow events, subsequently to be redeposited further downstream. A model must recognize these distinctly different mechanisms of transport and the associated differences in the time scale of sediment movement to capture the longitudinal sorting of deposited sediment.

A nonorthogonal curvilinear structured grid is usually needed for two- or three-dimensional reservoir modeling, especially to represent a sinuous flooded river channel within the overall embayment. Unstructured grid capability is not generally needed unless it is necessary to reproduce the detailed flow around structures as part of the study.

Reservoir sedimentation modeling is not highly demanding of sophisticated turbulence models, because most of the mobile-bed activity is deposition, and strong jet effects do not generally occur in reservoirs. However, if diffusion of a washload plume in the reservoir is an important factor in downstream deposition, or if sedimentation effects around structures within the reservoir (including intakes) are important in a three-dimensional model, then a simple turbulence model may not be adequate.

When deposited-material compaction and consolidation are included in a study, bed-layering capability is required in the two- or three-dimensional mobile-bed model. Consolidation calculations require knowledge of the age of deposits, and this in turn requires distinct accounting of deposited material, for example, in distinct layers.

Examples of two- and three-dimensional models that have been used for the study of reservoir sedimentation include those of Spasojevic and Holly (1990a; 1990b); Savic and Holly (1993); Olsen et al. (1999); and Fang and Rodi (2000).

15.2.3 Settling Basins

Simulation of deposition in engineered settling basins (including sedimentation tanks and clarifiers) is similar to that of reservoir sedimentation, but is somewhat less demanding, at least as long as the sediment is noncohesive, as assumed throughout this chapter. For purely volumetric analyses, one-dimensional modeling may be sufficient. It is difficult to imagine situations in which depth-averaged two-dimensional modeling is needed, though width-averaged two-dimensional approaches may be appropriate. These permit examination of the vertical structure of deposition. Generally, though, three-dimensional modeling is most likely needed. Indeed, the main purpose for performing a model study of a sedimentation basin is to analyze the interaction between the confined, engineered geometry of the basin and the deposition patterns, as input to the design process. Boundary effects are ubiquitous, and are naturally accommodated by three-dimensional modeling. Unless there are strong vertical accelerations near the inlet or the outlet, the hydrostatic pressure assumption may be adequate. Unsteady-flow dynamics is generally not relevant to continuous-flow sedimentation basins, so steady-flow models to determine sedimentation rates may be quite appropriate.

Unless the inflowing sediment is truly of uniform size, it is generally necessary that the modeling accommodate differential particle sizes, especially because this can have a direct bearing on the longitudinal deposition patterns in the sedimentation basin.

To the extent that reentrainment of deposited sediments in the basin is not an issue, it may not be necessary for the model to accommodate bed-load processes and their exchanges with the water column. However, if possible reentrainment near the outlet is under study, it may be necessary to include a full representation of bed-load dynamics and exchange with the water column.

Because settling basins tend to have regular geometric shapes, a simple Cartesian structured grid may be sufficient. Because the diffusive transport of suspended sediments entering the basin can be an important factor in its design, it is important for the model to include at least a one-equation model for turbulence in the horizontal plane. Bed layering is of importance only if sediment reentrainment in flushing operations is anticipated, and then only if significant stratification of sediment sizes is expected.

An example of a model study of sedimentation basins is that of Olsen and Skoglund (1994).

15.2.4 River-Bend Dynamics and Training Works

Three-dimensional modeling must be used for the study of mobile-bed processes in river bends and around their associated training works (bendway weirs, spur dikes, etc.). One-dimensional models simply cannot resolve the detailed interaction between flow and sediment within the

cross section. Two-dimensional depth-averaged models cannot normally resolve the secondary currents that are an essential part of this process.

However, some investigators have implemented various special techniques that enable depth-averaged models to approximate secondary flow in bends. Flokstra (1977) substituted semi-empirical velocity distributions for helicoidal flow (obtained from a power law) into the dispersion terms of the depth-averaged equations. Jin and Steffler (1993) introduced the depth averaged moment-of-momentum equations to provide a measure of the intensity of the secondary flow. Duan et al. (2001) computed flow and bed-shear stress by using the depth-averaged model CCHE2D. Empirical functions of three-dimensional flow characteristics, formulated using the results of the three-dimensional model CCHE3D, were used to transform the flow and bed-shear stress into approximate three-dimensional distributions.

In three-dimensional bendway modeling, it is possible to adopt the hydrostatic pressure assumption if the details of water and sediment movement around training structures, or water intakes, are not of primary interest. Otherwise a full three-dimensional treatment is required.

Full unsteady-flow capability, as reflected in an unsteady-inflow hydrograph, is not of primary interest for this type of study, although the ability to simulate the effects of an annual hydrograph may be important, if only through a succession of steady flows. If, on the other hand, the dynamic flood effects of a rapidly varying hydrograph are important to mobile-bed response, full unsteady-flow capability is needed. As mentioned earlier, the combination of fully three-dimensional (nonhydrostatic) flow and full unsteadiness may require computational resources that preclude simulations of any meaningful length in prototype time. If the problem under study involves fairly rapid and/or substantial bed changes in response to some intervention, these changes may provoke corresponding changes in the free-surface elevations and slopes. This may then require either a series of steady-flow computations or truly unsteady simulation to capture the feedback from bed changes to the flow field.

In most alluvial rivers, bed topography and geomorphology are intimately related to the nonhomogeneity of transported sediments, whereby coarser material responds to near-bed currents and shear stresses quite differently from suspended material. Therefore bendway modeling invariably requires the capability to accommodate multiple sediment size classes, as well as the distinct differences between bed-load and suspended-load transport mechanisms.

Riverbend modeling requires a curvilinear grid. It may be orthogonal in regular channels such as the Missouri River, but generally must be nonorthogonal to permit correct representation of natural riverbank and island geometries. When local structure details must be represented (spur dikes, etc.), an unstructured-grid approach may be necessary.

A relatively high level of turbulence modeling (e.g., $k-\epsilon$) is required, because strong jet diffusive effects around structures may be encountered and be decisive in determining the configuration of deposition zones in the wake of such structures.

Bed-layering capability may not be important for these studies, unless erosion into previously deposited layers of varying composition is foreseen. A particular situation might be erosion into strata provoked by river-training works successfully shifting the channel away from one bank.

Examples of river-bend mobile-bed modeling include those of Wang and Adeff (1986); Minh Duc et al. (1998); Gessler et al. (1999); Holly and Spasojevic (1999); Fang (2000); Wu et al. (2000); Spasojevic et al. (2001); and Spasojevic and Muste (2002). Section 15.11 of this chapter includes an example of a three-dimensional application.

15.2.5 Mobile-Bed Dynamics around Structures

This area and the previous one have considerable overlap; indeed, the details of mobile-bed response near training structures in river bends may well be of importance to relatively large-scale modeling of geomorphology in river bends. However, there is also a class of problems for which attention is focused on the structure itself, especially in habitat remediation studies. For example, V-notch weirs, wing dikes, and notched spur dikes may be configured to create low-velocity habitat, requiring a rather delicate balance between sediment through-flow and flow obstruction. Other applications of engineering importance are scour around bridge piers and abutments; scour/stability considerations for pipelines on the riverbed; and stability of structures associated with recreational facilities such as casino boat cofferdams, marinas, and beach-protection works.

Two-dimensional models cannot do justice to this problem. It is tempting to think that a depth-averaged approach may enable at least a plan-view analysis of the effect of the structure on currents and recirculation/deposition. But the flow around such structures and their associated scour holes can be strongly three-dimensional. In addition, such flow can be characterized by significant vertical accelerations, which cannot be captured using the hydrostatic pressure assumption in a three-dimensional model. Therefore this class of problems generally requires fully three-dimensional, i.e., nonhydrostatic modeling.

Full unsteady-flow dynamics is not normally required for this class of study. It may be necessary to run a series of studies of flows to study structure response throughout the expected hydrograph range of conditions, but the dynamic effects per se are generally not of great importance. It should be recognized, however, that insofar as the upstream boundary conditions to such a model, including both bed-load and suspended-load inflows, may reflect the hysteresis effects associated for flood dynamics, the true unsteadiness may have to be taken into account in the formulation of boundary conditions for the series of steady-state conditions.

Except in special circumstances of rivers having uniform sediment, it is generally necessary for the modeling system to accommodate multiple sediment sizes and recognition of the distinctly separate modes of sediment movement on the bed and in suspension. There can be considerable local sorting of sediments in the complex flows around structures, for example, when sediments in suspension are deposited in the recirculation zone behind a structure and then may undergo continued slow transport as bed load, perhaps back toward the structure in some cases.

It is very difficult to provide effective representation of near-field flow around structures with a structured grid. At the very least, this must be a nonorthogonal curvilinear grid, and an unstructured grid is highly desirable. Similarly, this modeling situation puts a premium on an effective high-order turbulence model (e.g., $k-\epsilon$), because the diffusive exchange of momentum and sediment across zones of highly nonuniform velocity is the very essence of the problem.

Bed layering is generally not of great importance for near-field structure modeling, unless scour into antecedent nonuniform strata is an important issue.

Examples of model studies of mobile-bed dynamics around structures include those of Olsen and Melaaen (1993); Brors (1999); and Spasojevic and Muste (2002). Other examples of local-scour model predictions include those of Zaghloul and McCorquodale (1975) and Jia et al. (2001). Section 15.11 of this chapter includes an example of a three-dimensional application to a problem of structure configurations for habitat restoration.

15.2.6 Long-Term Bed Evolution in Response to Imposed Changes

One-dimensional models remain the method of choice for the study of long-term changes in river morphology over extended river reaches. Such changes include upstream regulation, changes in upstream sediment supply, water and sediment diversion/extraction, bank stabilization, and channelization. It can be necessary to focus on these long-term changes within a particular bend or short segment of river, often involving the presence of structures, within the larger context of the extended one-dimensional model. This focused interest is very likely to require three-dimensional modeling, especially if flow-structure-sediment interaction is an issue (e.g., sedimentation in water intakes, maintenance of navigation conditions). This triggers requirements for the same kinds of model capabilities as those described above in Sections 15.2.4 and 15.2.5, and in addition may well require the simulation of multiple annual hydrographs, either in a fully unsteady or a quasi-steady mode.

To the extent that this activity implies the embedding of a local three-dimensional model within a one-dimensional or two-dimensional one, the issue of deriving three-dimensional boundary conditions (e.g., upstream velocity and suspended-sediment concentration fields, bed-load distribution across

the section) from the one- or two-dimensional results, possibly within each time step, is a challenging one. It implies at the very least that the local three-dimensional model boundaries be taken at one-dimensional model cross sections that have relatively parallel and transversely uniform flow, if possible. It may also imply that there must be some feedback from the local three-dimensional model to the cross sections of the overall one- or two-dimensional model, though this may not be necessary.

If the local three-dimensional model is to be run in an unsteady mode, the hydrostatic pressure assumption is very likely to be necessary simply to keep computation time within reasonable limits (see Section 15.3.3). The three-dimensional model's need for treatment of nonuniform sediments, separation of bed load and suspended load, and other such factors is slaved to the comparable requirements for the overall one-dimensional model, depending on the sediment regime in the river.

The grid for an embedded three-dimensional model can generally be a structured curvilinear one, orthogonal in a fairly regular channel but nonorthogonal otherwise. Turbulence model demands are modest, because by definition this type of study is focused on identifying long-term changes rather than local and short-term details of flow and sediment movement; generally a one- or two-equation model should be sufficient—see Section 15.3.4. Bed layering may be quite important, if the long-term evolution of the river includes erosion into antecedent nonuniform strata, including strata that are laid down during the long-term simulation itself.

Although the authors are not aware of a specific application involving direct embedding of a two- or three-dimensional mobile-bed model in an overall one-dimensional extended model, there have been applications of two- and three-dimensional models to long-term bed evolution in specialized reservoir sedimentation contexts (Savic and Holly 1993; Fang and Rodi 2000). In addition, several models have been applied to long-term bed evolution in laboratory contexts.

15.2.7 Sorbed Contaminant Fate and Transport and Cohesive Sediment Problems

Modeling of sorbed contaminant fate and transport, be it one-, two-, or three-dimensional, is one of the most challenging activities in mobile-bed modeling. It combines the uncertainties of mobile-bed modeling with the uncertain description of sorption-desorption processes in the multiple transport modes of an alluvial system. In addition, these processes are most important for fine sediments, including cohesive sediments, for which the entrainment, transport, and deposition mechanics can be episodic rather than continuous and are poorly understood. Chapters 4 and 20 of this manual deal with the problems of transport of fine sediment and associated contaminants.

The particular problems associated with sorbed contaminant modeling are essentially the same whether the underlying mobile-bed modeling is one-, two-, or three-dimensional. The overall scope and focus of the study determines the level of dimensionality, whether unsteady capability is necessary, whether the hydrostatic pressure assumption is permissible, etc.

In sorbed contaminant modeling, contaminated fine material, once entrained or otherwise introduced into the system, is transported primarily as suspended load, i.e., essentially at the speed of the water velocity. Therefore it is mandatory that the modeling approach explicitly include advection-diffusion of suspension as a transport mechanism.

The source-sink term for advection-diffusion of suspension is particularly problematic when fine, especially cohesive, sediments are involved. Entrainment of cohesive sediments is understood to occur as episodic bursts of "mass entrainment" once a critical shear stress is exceeded, rather than as a progressive and continuous entrainment driven by the notion of an excess of shear stress over critical, as is generally accepted for noncohesive sediment. Cohesive sediment also tends to flocculate, or clump together once in suspension, and this behavior strongly influences its deposition tendencies and rates. Because salinity is an important parameter governing flocculation, a model must be capable of simulating transport (i.e., advection-diffusion) from a tidal boundary condition in parallel with fine-sediment and sorbed-contaminant transport in an estuary in many cases.

Given the episodic nature of cohesive-sediment dynamics, and the fact that studies of sorbed-contaminant fate and transport are likely to be focused on the risk of reentrainment of contaminants during flood events, this kind of modeling is likely to require unsteady-flow capability. But to the extent that flow-structure-sediment interaction is not an important feature of the study, it may be permissible to base modeling on the hydrostatic pressure assumption, thus enabling unsteady computations within reasonably computer time requirements.

Bed-layering capability is an important feature of models used for sorbed contaminant fate and transport, notably when alternate deposition-entrainment cycles are to be studied. During flood events, entrainment of contaminated sediments is generally from material laid down, and perhaps covered, during previous extended depositional periods. It is only through explicit representation of this layering process, with distinct differentiation of sediment and contaminant characteristics within layers, that this resuspension process can be faithfully represented.

Sorbed-contaminant modeling does not, in and of itself, invoke any special grid requirements; these follow from the physical situation as described in earlier sections. Turbulence modeling can be quite important, because diffusive transport of fine material in suspension can be an

important component of the contaminant fate and transport. Similarly, bed layering can be quite important, because contaminated sediments may lie in antecedent deposition strata that are disturbed through erosion during exceptional floods.

There do not appear to be recent examples of multidimensional sorbed-contaminant modeling in the literature. Earlier examples include those of Onishi and Trent (1982); Onishi and Thompson (1984); and Onishi and Trent (1985).

15.2.8 Summary

A common thread running through these discussions of typical modeling situations is that in mobile-bed modeling, there is a tradeoff between model complexity and computer (and human) resources. This is particularly true in the fully three-dimensional unsteady-flow domain (without the hydrostatic pressure assumption), in which, as of this writing, model complexity and fidelity are ultimately limited nearly by the calendar time available for the study. At the other extreme of one-dimensional modeling, computer resources are rarely a limiting factor; but the expert interpretation needed to draw meaningful results from a simplified one-dimensional schematization of reality may be as limiting as computer resources in the three-dimensional case. Two-dimensional modeling falls somewhere between these extremes. Ultimately the modeler must weigh the strengths, weaknesses, and costs of alternative modeling approaches against the objectives and resources of the particular study.

15.3 MATHEMATICAL BASIS FOR HYDRODYNAMICS IN TWO AND THREE DIMENSIONS

15.3.1 Introduction and Scope

Hydrodynamic and mobile-bed process modeling are intimately related. Although this chapter, and indeed this entire manual, are focused on sediment and mobile-bed processes, it is important for the reader to understand how the formulations and numerical solution of the hydrodynamic processes interact with those of the mobile-bed processes.

The purpose of this section is to provide a summary overview of the hydrodynamic-process formulations generally used in mobile-bed models. The general three-dimensional and two-dimensional equations are presented first, and then issues of simplification of the vertical momentum equation (hydrostatic assumption), solution techniques, coordinate transformations, and turbulence closure models are discussed in turn.

15.3.2 Summary of Basic Equations

Although the fields of direct Navier-Stokes and large-eddy simulation hydrodynamic modeling are receiving considerable

attention in the field of computational fluid dynamics, the hydrodynamic formulations used in mobile-bed modeling, at least as of this writing, remain based on the Reynolds-averaged Navier-Stokes equations.

15.3.2.1 The Reynolds-Averaged Navier-Stokes Equations The Reynolds-averaged Navier-Stokes equations are derived from the incompressible-fluid Navier-Stokes equations through temporal averaging of instantaneous velocities over an appropriate time scale. This operation results in a shift of the stresses associated with the momentum exchange of correlated fluctuating velocities from the momentum-advection terms to Reynolds stress terms. These Reynolds stresses must then be resolved using an appropriate turbulence model, as discussed in detail in Chapter 16 of this manual.

Water mass conservation is expressed through the Reynolds-averaged mass conservation (continuity) equation

$$\frac{\partial u}{\partial x} + \frac{\partial v}{\partial y} + \frac{\partial w}{\partial z} = 0 \quad (15-1)$$

in which

x , y , and z = Cartesian coordinate directions and $u(x, y, z, t)$,
and $w(x, y, z, t)$ = time-dependent Reynolds-averaged velocities in the x , y , and z directions respectively, t being the time.

The Reynolds-averaged u -, v -, and w -momentum conservation equations are written

$$\begin{aligned} \frac{\partial u}{\partial t} + \frac{\partial(uu)}{\partial x} + \frac{\partial(vu)}{\partial y} + \frac{\partial(wu)}{\partial z} \\ = fv - \frac{1}{\rho_0} \rho g \frac{\partial z'}{\partial x} - \frac{1}{\rho_0} \frac{\partial p}{\partial x} \\ + \frac{1}{\rho_0} \left(\frac{\partial \tau_{xx}}{\partial x} + \frac{\partial \tau_{yx}}{\partial y} + \frac{\partial \tau_{zx}}{\partial z} \right) \end{aligned} \quad (15-2)$$

$$\begin{aligned} \frac{\partial v}{\partial t} + \frac{\partial(uv)}{\partial x} + \frac{\partial(vv)}{\partial y} + \frac{\partial(wv)}{\partial z} \\ = -fu - \frac{1}{\rho_0} \rho g \frac{\partial z'}{\partial y} - \frac{1}{\rho_0} \frac{\partial p}{\partial y} \\ + \frac{1}{\rho_0} \left(\frac{\partial \tau_{xy}}{\partial x} + \frac{\partial \tau_{yy}}{\partial y} + \frac{\partial \tau_{zy}}{\partial z} \right) \end{aligned} \quad (15-3)$$

$$\begin{aligned} \frac{\partial w}{\partial t} + \frac{\partial(uw)}{\partial x} + \frac{\partial(vw)}{\partial y} + \frac{\partial(ww)}{\partial z} \\ = -\frac{1}{\rho_0} \rho g \frac{\partial z'}{\partial z} - \frac{1}{\rho_0} \frac{\partial p}{\partial z} \\ + \frac{1}{\rho_0} \left(\frac{\partial \tau_{xz}}{\partial x} + \frac{\partial \tau_{yz}}{\partial y} + \frac{\partial \tau_{zz}}{\partial z} \right) \end{aligned} \quad (15-4)$$

in which

- $f = 2\Omega \sin\phi$ is the Coriolis parameter, with Ω the angular rotational velocity of the earth and ϕ the latitude;
- $\rho(x, y, z, t)$ = density of a mixture of water and suspended sediment;
- ρ_0 = reference density;
- g = acceleration due to gravity;
- z' = the vertical direction;
- $p(x, y, z, t)$ = pressure; and τ = fluid shear-stress tensor, here presumed to incorporate both molecular stresses and those resulting from the Reynolds averaging process.

Molecular stresses, being much smaller than Reynolds stresses, are often neglected. The Coriolis term, which describes the effect of the earth's rotation on the motion of fluid on the earth's surface, is important only when fairly large water bodies are modeled.

Equations (15-1) to (15-4) are considered the fully three-dimensional Reynolds-averaged set. They must be complemented with an appropriate turbulence closure model, possibly involving a parallel set of partial differential equations, before they can be used in a mobile-bed model, as is discussed below.

Equations (15-1) to (15-4) already evoke the Boussinesq approximation, which is valid for incompressible flows with variable density (the variation of gravity can be neglected in all flows considered in this chapter). According to this approximation, if the variation in density is relatively small, it may be assumed that the variation in density is negligible in all the terms in the equations except the gravitational term.

15.3.2.2 The Hydrostatic-Pressure Simplification In some applications, it is possible to bring considerable simplification to the fully three-dimensional set (Eqs. 15-1 to 15-4) by invoking the hydrostatic pressure assumption. This is tantamount to ignoring any vertical components of fluid acceleration, so that the pressure varies linearly from the surface to any point below it. If the z coordinate direction is taken as vertical ($z \equiv z'$), the assumption is formalized as

$$\frac{\partial}{\partial z} \left(z + \frac{p}{\rho g} \right) = 0 \quad (15-5)$$

in which

$$z + \frac{p}{\rho g} = \zeta(x, y, t)$$

is the free-surface elevation above datum.

Introduction of Eq. (15-5) into Eqs. (15-2 and 15-3), through a suitable rearrangement of the variable-density

gravity term and the pressure term to include the free-surface elevation, yields

$$\begin{aligned} \frac{\partial u}{\partial t} + \frac{\partial(uu)}{\partial x} + \frac{\partial(uv)}{\partial y} + \frac{\partial(uw)}{\partial z} \\ = fv - g \frac{\partial(z_b + h)}{\partial x} - \frac{g}{\rho_0} (\zeta - z) \frac{\partial \rho}{\partial x} \\ + \frac{1}{\rho_0} \left(\frac{\partial \tau_{xx}}{\partial x} + \frac{\partial \tau_{yx}}{\partial y} + \frac{\partial \tau_{zx}}{\partial z} \right) \end{aligned} \quad (15-6)$$

and

$$\begin{aligned} \frac{\partial v}{\partial t} + \frac{\partial(vu)}{\partial x} + \frac{\partial(vv)}{\partial y} + \frac{\partial(vw)}{\partial z} \\ = -fu - g \frac{\partial(z_b + h)}{\partial y} - \frac{g}{\rho_0} (\zeta - z) \frac{\partial \rho}{\partial y} \\ + \frac{1}{\rho_0} \left(\frac{\partial \tau_{xy}}{\partial x} + \frac{\partial \tau_{yy}}{\partial y} + \frac{\partial \tau_{zy}}{\partial z} \right) \end{aligned} \quad (15-7)$$

in which

- $z_b(x, y)$ = bed elevation above datum and
 $h(x, y, t)$ = flow depth;

i.e., the free-surface elevation is expressed as $\zeta = z_b + h$. The free-surface elevation (or the flow depth) thus replaces the pressure as one of the four dependent variables, and this vastly simplifies the numerical solution of the set. In fully three-dimensional nonhydrostatic modeling, the solution for the pressure field is quite difficult and computationally demanding. The hydrostatic pressure assumption makes it possible to first obtain the free-surface elevation ζ or the flow depth h , for example by solving the depth-averaged two-dimensional problem. The free-surface elevation then becomes a known variable in the second-step solution of the remaining three-dimensional equations.

Equations (15-6) and (15-7) retain the density-gradient terms to account for possible density changes due to changes in suspended-sediment concentration. The density-gradient terms, resulting from the rearrangement of gravity and pressure terms in Eqs. (15-2) and (15-3), are simplified by replacing $\frac{p}{\rho}$ with $g(\zeta - z)$, which amounts to combining the hydrostatic-pressure assumption and the Boussinesq approximation. Density, and therefore density-gradient terms, are evaluated from suspended-sediment concentrations through an appropriate empirical relation.

Equations (15-5), (15-6), and (15-7) make up the hydrostatic-pressure simplification of Eqs. (15-2), (15-3), and (15-4). The continuity equation, Eq. (15-1), remains the same in both systems.

15.3.2.3 The Depth-Averaged Equations The hydrodynamic equations for two-dimensional (depth-averaged) mobile-bed modeling are obtained through formal depth-averaging of the full three-dimensional set, Eqs. (15-1),

(15-6), and (15-7). Depth-averaged variables are defined as follows:

$$\tilde{f} = \frac{1}{h} \int f dz. \quad (15-8)$$

The depth-averaged mass conservation (continuity) equation then becomes

$$\frac{\partial h}{\partial t} + \frac{\partial(h\tilde{u})}{\partial y} + \frac{\partial(h\tilde{v})}{\partial z} = 0. \quad (15-9)$$

The depth-averaged \tilde{u} -momentum conservation equation is

$$\begin{aligned} & \frac{\partial(\tilde{u}h)}{\partial t} + \frac{\partial(\tilde{u}\tilde{u}h)}{\partial x} + \frac{\partial(\tilde{v}\tilde{u}h)}{\partial y} \\ &= f\tilde{v}h - gh \frac{\partial(z_b + h)}{\partial x} - \frac{g h^2}{2\rho_0} \frac{\partial p}{\partial x} \\ &+ \frac{1}{\rho_0} \left[\frac{\partial}{\partial x} (\tilde{\tau}_{xx} h) + \frac{\partial}{\partial y} (\tilde{\tau}_{xy} h) \right] \\ &+ \frac{\tau_{sx} - \tau_{bx}}{\rho_0} - \frac{1}{\rho_0} \left[\frac{\partial}{\partial x} \int_h \rho (u - \tilde{u})(u - \tilde{u}) dz \right. \\ &\left. + \frac{\partial}{\partial y} \int_h \rho (u - \tilde{u})(v - \tilde{v}) dz \right] \end{aligned} \quad (15-10)$$

and the depth-averaged \tilde{v} -momentum conservation equation is

$$\begin{aligned} & \frac{\partial(\tilde{v}h)}{\partial t} + \frac{\partial(\tilde{u}\tilde{v}h)}{\partial x} + \frac{\partial(\tilde{v}\tilde{v}h)}{\partial y} \\ &= -f\tilde{u}h - gh \frac{\partial(z_b + h)}{\partial y} - \frac{g h^2}{2\rho_0} \frac{\partial p}{\partial y} \\ &+ \frac{1}{\rho_0} \left[\frac{\partial}{\partial x} (\tilde{\tau}_{xy} h) + \frac{\partial}{\partial y} (\tilde{\tau}_{yy} h) \right] \\ &+ \frac{\tau_{sy} - \tau_{by}}{\rho_0} - \frac{1}{\rho_0} \left[\frac{\partial}{\partial x} \int_h \rho (u - \tilde{u})(v - \tilde{v}) dz \right. \\ &\left. + \frac{\partial}{\partial y} \int_h \rho (v - \tilde{v})(v - \tilde{v}) dz \right] \end{aligned} \quad (15-11)$$

In these equations, τ_{sx} and τ_{bx} are the x -direction shear stress at the water surface and bed, respectively, and similarly for τ_{sy} and τ_{by} . The terms containing the products, such as $(u - \tilde{u})(v - \tilde{v})$, represent effective stresses associated with the correlation in deviations of local velocities from their depth averages, and are commonly referred to as the dispersion terms.

15.3.2.4 Turbulence Closure One commonly used simplified approach to solve the “turbulence closure problem”

is to express the Reynolds stresses through the Boussinesq eddy-viscosity model (for more detail see Chapter 16 of this manual). The Boussinesq eddy-viscosity model assumes that the Reynolds stress is related to the mean rate of strain (through the so-called eddy viscosity), and to the turbulent kinetic energy. The turbulent kinetic-energy term is usually absorbed into the pressure-gradient term, whereas the mean rate of strain is sometimes subject to further simplification. Thus the Reynolds stress τ_{xx} in Eq. (15-2), for example, can be replaced by $v_t(\partial u / \partial x)$, where v_t is the eddy viscosity. This leads to a new set of equations that, when complemented by an appropriate turbulence model to estimate the eddy viscosities, are now ready to be discretized for numerical solution (possibly after additional coordinate transformation; see below), as follows for the hydrostatic case:

The Reynolds-averaged three-dimensional u -momentum conservation equation is

$$\begin{aligned} \frac{\partial u}{\partial t} &= - \frac{\partial(uu)}{\partial x} - \frac{\partial(uv)}{\partial y} - \frac{\partial(uw)}{\partial z} \\ &+ f v - g \frac{\partial(z_b + h)}{\partial x} - \frac{g}{\rho_0} (\varsigma - z) \frac{\partial p}{\partial x} \\ &+ \frac{1}{\rho_0} \left[\frac{\partial}{\partial x} \left(v_t \frac{\partial u}{\partial x} \right) + \frac{\partial}{\partial y} \left(v_t \frac{\partial u}{\partial y} \right) + \frac{\partial}{\partial z} \left(v_t \frac{\partial u}{\partial z} \right) \right] \end{aligned} \quad (15-12)$$

The Reynolds-averaged three-dimensional v -momentum conservation equation is

$$\begin{aligned} \frac{\partial v}{\partial t} &= - \frac{\partial(vu)}{\partial x} - \frac{\partial(vv)}{\partial y} - \frac{\partial(vw)}{\partial z} \\ &- fu - g \frac{\partial(z_b + h)}{\partial y} - \frac{g}{\rho_0} (\varsigma - z) \frac{\partial p}{\partial y} \\ &+ \frac{1}{\rho_0} \left[\frac{\partial}{\partial x} \left(v_t \frac{\partial v}{\partial x} \right) + \frac{\partial}{\partial y} \left(v_t \frac{\partial v}{\partial y} \right) + \frac{\partial}{\partial z} \left(v_t \frac{\partial v}{\partial z} \right) \right] \end{aligned} \quad (15-13)$$

The depth-averaged two-dimensional \tilde{u} -momentum conservation equation is

$$\begin{aligned} \frac{\partial \tilde{u}}{\partial t} &= - \frac{\partial(\tilde{u}\tilde{u})}{\partial x} - \frac{\partial(\tilde{u}\tilde{v})}{\partial y} \\ &- f\tilde{v} - g \frac{\partial(z_b + h)}{\partial x} - \frac{gh}{2\rho_0} \frac{\partial p}{\partial x} \\ &+ \frac{1}{\rho_0 h} \left[\frac{\partial}{\partial x} \left(v_t \frac{\partial \tilde{u}}{\partial x} h \right) + \frac{\partial}{\partial y} \left(v_t \frac{\partial \tilde{u}}{\partial y} h \right) \right] \\ &+ \frac{\tau_{sx} - \tau_{bx}}{\rho_0 h} \end{aligned} \quad (15-14)$$

The depth-averaged two-dimensional \tilde{v} -momentum conservation equation is

$$\begin{aligned} \frac{\partial \tilde{v}}{\partial t} = & -\frac{\partial(\tilde{v}\tilde{u})}{\partial x} - \frac{\partial(\tilde{v}\tilde{v})}{\partial y} - f\tilde{u} \\ & - g\frac{\partial(z_b + h)}{\partial y} - \frac{gh}{2\rho_0}\frac{\partial p}{\partial y} \\ & + \frac{1}{\rho_0 h} \left[\frac{\partial}{\partial x} \left(v_t \frac{\partial \tilde{v}}{\partial x} h \right) + \frac{\partial}{\partial y} \left(v_t \frac{\partial \tilde{v}}{\partial y} h \right) \right] \\ & + \frac{\tau_{sy} - \tau_{by}}{\rho_0 h} \end{aligned} \quad (15-15)$$

As in the case of similar derivations for constituent transport equations, the Boussinesq eddy viscosity coefficient v_t is an artificial construct intended to capture the residual shear-stress effects of correlations in velocity deviations from temporal and/or depth averages. As such, the values of eddy viscosity appearing in the three-dimensional equations must be obtained from an appropriate three-dimensional eddy-viscosity model. Eddy-viscosity models vary from very simple, such as constant eddy-viscosity or zero-equation models, to more advanced, such as two-equation $k-\varepsilon$ or $k-\omega$ models (Chapter 16). The corresponding eddy viscosities appearing in the depth-averaged equations must be obtained from an appropriate depth-averaged eddy-viscosity model. The diffusion terms in depth-averaged hydrodynamic models, i.e., the effective stresses generated by the depth-averaging process, are typically modeled analogously to and combined with corresponding Reynolds stresses. The additional contribution to eddy viscosity arising from the depth averaging can be accounted for indirectly by adjusting one of the constants in the depth-averaged $k-\varepsilon$ model (see Rodi 1993).

Equations (15-12) and (15-13) and the continuity equation, Eq. (15-1), are the basis for the flow model built into the CH3D-SED code, used in Sections 15.11.2 and 15.11.3 of this chapter. The flow model built into the MOBED2 code, which is used in example 15.11.4 of this chapter, is based on Eqs. (15-14) and (15-15) and the continuity equation, Eq. (15-9).

15.3.3 Role of Hydrostatic Pressure Assumption

The previous section presented three-dimensional hydrodynamic equations both without and with the hydrostatic pressure assumption. Hydraulic engineers are quite accustomed to invoking hydrostatic pressure in the solution of most problems, without having to recall that it implicitly assumes that pressure differences associated with vertical fluid accelerations are unimportant for the problem under study.

As discussed in the previous section, invocation of the hydrostatic pressure assumption vastly simplifies the three-dimensional hydrodynamic problem. Indeed, as of this writing

the computational time required to do a multiple-day unsteady simulation with the hydrostatic assumption is of the same order of magnitude as that required to obtain a single steady-state solution with the fully nonhydrostatic equations. Therefore it is important to consider the circumstances under which it is permissible to invoke the hydrostatic pressure assumption in three-dimensional mobile-bed modeling.

As a general rule, it is necessary to use fully three-dimensional, nonhydrostatic modeling whenever local details of mobile-bed dynamics around structures are of interest. Such structures include river training works such as dikes and bendway weirs, as well as habitat-restoration structures such as v-notched dikes, chevron weirs, or notched weirs. Experience has shown that calculated local velocity fields around structures, particularly near the bed, can be quite different for the hydrostatic and nonhydrostatic cases. This is of course due to the effects of vertical acceleration components near the intersection of the structure and the bed. Because the details of local scour and deposition in the immediate vicinity of such structures can depend quite strongly on the local velocity fields, the hydrostatic assumption can have an indirect but very important influence on mobile-bed behavior near the structure.

However, the overall mobile-bed response to using the hydrostatic-pressure assumption in the calculation of secondary currents has seldom been quantified. Therefore, it is difficult to give some general rule as to when the hydrostatic assumption is and is not acceptable. At the extreme limits, it is perhaps obvious that it is acceptable for studies of overall cross section response to changes in hydrologic or sediment regime, where local flow and sedimentation details are not of primary importance. By contrast, it is perhaps obvious that the hydrostatic assumption is not acceptable in studies focused uniquely on local sedimentation details around structures. In between these extremes, the acceptability of the assumption is a matter of judgment. Whenever it is possible to make preliminary comparative model runs with and without the hydrostatic assumption, in order to glean some insight into the apparent importance of vertical accelerations to the overall sedimentation pattern under study, this should by all means be done.

In the end, the ability to use the full nonhydrostatic equations on one hand, and the ability to perform truly unsteady calculations over some extended period of time on the other, appear as of this writing to be mutually exclusive. However, one would expect fully unsteady, nonhydrostatic modeling to become increasingly feasible as the exponential growth in computational power continues.

15.3.4 Solution Techniques and Their Applicability

Approximate numerical solution techniques for the two- and three-dimensional hydrodynamic equations generally fall into one of three categories: finite-difference methods (see, e.g., Shimizu et al 1990; Spasojevic and Holly

1990a; 1990b; 1993; and Lin and Falconer 1996); finite-element methods (see, e.g., Thomas and McAnally 1985; Wang and Adeff 1986; Brors 1999; Jia and Wang 1999; and the RMA-10 model at the Coastal and Hydraulics Lab, U.S. Army Corps of Engineers); or finite-volume methods (see, e.g., Olsen and Melaaen 1993; Minh Duc et al. 1998; Olsen et al. 1999; and Wu et al. 2000). Although there are important differences between finite-element and finite-volume approaches, both can be associated with unstructured grids and thus are grouped together here. It should be mentioned that the method of characteristics has been successfully applied to two-dimensional computation of rapidly varied flow, in particular for dam-break computation (see, e.g., Fennema and Chaudhry 1990), but generalization of codes based on this method to mobile-bed capability does not appear to be in the offing.

Finite-difference methods are based on approximation of partial derivatives by divided differences on a space-time grid. Such grids are called "structured," in that they comprise quadrilaterals (possibly curvilinear), all of which are defined by the same set of coordinate contours parallel (in transformed space) to the physical x , y , and z axes. Considerable computational economy can be achieved by structuring solution algorithms to proceed along single grid lines in each of the three directions, replacing the need to solve three-dimensional or two-dimensional problems with the solution of multiple one-dimensional problems, usually coupled through multiple iterations. However, this computational economy is obtained at the expense of grid inflexibility and/or excessive computer memory requirements. If the computational grid must be refined (i.e., more grid lines introduced) to provide high resolution in the vicinity of a structure or sharp natural feature, this grid refinement must extend throughout the computational domain, even though it may not be necessary far away from the local feature of interest. Nonetheless, the finite-difference method generally offers a simplicity of programming and intuitive conceptualization of the problem that are not so natural with finite-element methods.

Finite-element and finite-volume methods are integral-based approaches in the sense that they are derived not through approximations of partial derivatives, but rather through consideration of conservation laws applied to volumetric elements and careful evaluation of fluxes (mass, momentum) across nonparallel faces of the elements. The finite-element method is based on the notion of minimizing residuals in an average or integral sense over a volumetric (or surficial) element. The finite-volume method is more directly based on primitive conservation laws and can be interpreted as equivalent to a finite-difference method when quadrilateral or elements are selected as a special case (such an interpretation is not possible when tetrahedral, i.e., triangle-based, elements are used).

Application of the integral principles to one volumetric element is dependent only on the fluxes coming from or going to adjacent elements. This leads to the notion of an unstructured grid, where grid refinement around a local feature is

accomplished through packing of small-scale volumetric elements around the feature. This packing or refinement is purely local, in that the local small scale does not propagate through the mesh of the entire solution domain. Thus local grid refinement can be accomplished without triggering the excessive memory requirements of structured grids. In addition, unstructured grids naturally accommodate dynamic (adaptive) grid refinement driven by spatially variable error detection.

The grid-refinement flexibility of finite-element/volume methods is obtained at the price of computational efficiency. Generally the multiple iterative one-dimensional computations that are possible on a structured (finite-difference) grid cannot be implemented on an unstructured one, because the very notion of continuous coordinate contours, along which partial derivatives are approximated, does not exist. Solution algorithms must generally be fully two- or three-dimensional, incurring the large computational time requirements of matrix inversion, often iterative. In practical terms, the flexibility of unstructured grids is obtained at the cost of practical limits to the duration of unsteady-flow simulations. Such practical limits may become less important as parallel processing becomes increasingly available.

The accurate computation of advection (of momentum or mass) is particularly challenging, and some hydrodynamic codes solve for advection in a separate, dedicated step using a numerical method best suited to the hyperbolic nature of the advective terms (examples include the CYTHERE-ES1 code of Benqué et al. 1982 and TELEMAC as reported by Jankowski et al. 1994). A mobile-bed code driven by a hydrodynamics solver having this feature for momentum advection should logically take advantage of it for the advection of sediment particles in suspension.

For detailed information on numerical-solution techniques for fluid flow equations, the reader may refer to numerous books in this area, such as Fletcher (1991); Hirsch (1991); or Ferziger and Peric (2002).

15.3.5 Coordinate Transformations for Finite-Difference Methods

The structured grids of finite-difference methods are, in their primitive form, inherently ill-suited to the representation of natural bank lines, submerged bars, etc. Early two-dimensional hydrodynamic models of the 1970s used "stair-stepping" to represent boundaries that were not aligned with one or the other orthogonal axes of a Cartesian grid (Benqué et al. 1982). The need to work with curvilinear grids quickly became apparent. However, orthogonal curvilinear grids (i.e., those for which coordinate lines intersect at right angles) still are quite inflexible for representation of local features. Further flexibility can be introduced by relaxing the orthogonality requirement to obtain a nonorthogonal curvilinear grid, in which computational cells can deform in an arbitrary manner to better fit the contour lines of natural features. Even then, it is important to maintain cell aspect

ratios within acceptable limits. Transformation of the governing partial differential equations into the coordinate system of the nonorthogonal curvilinear grid is quite tedious and generates many additional terms that must be discretized and evaluated, further increasing the complexity of the computational engine and required computational time. Most of the two- and three-dimensional codes referenced in Table 15-2 (Section 15.4.2) are based on some level of coordinate transformation.

In unsteady-flow simulation, various grid-adjustment schemes have been developed to cope with the time-dependent position of the free surface and the bed. Perhaps the most common approach is referred to as "sigma stretching," by which the vertical grid structure adapts to changes in the free surface (and changes in the mobile bed elevation) through stretching or compression, the number of grid intervals in the vertical remaining constant.

For detailed information on coordinate transformations, the reader may refer to basic tensor analysis books, such as Simmonds (1994).

15.3.6 Turbulence Closure Models

As mentioned earlier, the Reynolds averaging of the Navier-Stokes equations generates correlations between the fluctuating components of local velocities; these are the so-called Reynolds stress terms shown as effective shear stresses in Eqs. (15-2), (15-3), and (15-4). Evaluation of these terms requires some sort of empirical turbulence closure model. Chapter 16 provides a comprehensive overview of the turbulence-modeling problem in the context of mobile-bed hydraulics. In the simplest approach, the Boussinesq eddy-viscosity model is supplemented with a constant eddy viscosity, either simply assigned by the user based on macroscopic flow properties or derived from a zero-equation mixing-length model or equivalent.

More advanced approaches include the use of a one-equation eddy-viscosity model, or more commonly a two-equation eddy-viscosity model such as the $k-\epsilon$ formulation (see for example Chapter 16 of this manual or Rodi 1993), in which the transport of the turbulence kinetic energy and its dissipation rate are solved in parallel with the flow solution, leading to eddy viscosity coefficients that reflect local shear and bed effects.

More advanced turbulence modeling techniques, such as direct Reynolds stress modeling and large eddy simulation, have been implemented for accurate calculation of internal flows and aerodynamic flows. However, the authors' arguments in Section 15.1.4 notwithstanding, the inherent uncertainties and imprecision of the mobile-bed problem would seem to obviate the need to require more than $k-\epsilon$ turbulence capability in the hydrodynamic computational engine of a mobile-bed model at the current stage of development, unless such advanced techniques

are readily available and implementable in the mobile-bed model.

15.4 OVERVIEW OF MODELS OF SEDIMENT TRANSPORT AND BED EVOLUTION

15.4.1 Introduction

Although the Navier-Stokes equations, along with the continuity equation (usually Reynolds-averaged), represent a generally accepted mathematical description (model) of fluid flow, there is no comparable mathematical formulation for the complete processes of sediment-flow interaction. The most recent attempts to formulate a general mathematical model of sediment-flow interaction are based on the two-phase flow approach (Villaret and Davies 1995; Cao et al. 1995; Ni et al. 1996; Greimann et al. 1999; Liu et al., 1997). The attempts are inspired by the history of two-phase flow models in other fields (Ishii 1975; Drew 1983; Elghobashi 1994; Crowe et al. 1996). The basic idea behind the two-phase flow approach is to formulate governing conservation equations for both phases, which include terms defining interaction between phases such as the stress tensor due to phase interactions, or the interfacial momentum transfer term.

However, even though the two-phase flow approach seems promising, its use and even the formulation of the governing equations in flow-sediment problems are still in their infancy. Certain terms in the governing equations that are typically neglected in other fields may require quite a different treatment in the flow-sediment field. The stress between fluid and sediment particles is usually neglected under the assumption that it is much smaller than the turbulent stress between fluid particles. The stress coming from interactions among sediment particles is neglected under the assumption that sediment particles do not contact each other. Both of these assumptions are questionable in the case of high sediment concentrations, especially near the bed. This probably explains a lingering doubt about the use of the two-phase flow approach in the near-bed areas. Furthermore, certain terms in the two-phase flow governing equations, such as the interfacial momentum transfer, require additional modeling to achieve system closure. Such modeling has to be based on a detailed knowledge of turbulence and requires currently unavailable experimental data. Finally, the two-phase flow solution of practical sediment problems, which routinely require long-term simulations, is likely to be CPU-time-prohibitive even in the not-so-near future.

Therefore, virtually all two-dimensional and three-dimensional flow and sediment models used for solving practical problems are based on a simplified concept. The basic idea classifies sediment transport as either suspended load or bed load and defines a set of equations describing suspended-sediment transport, bed-load transport, and bed evolution. Thus, the concept requires artificially partitioning the otherwise single

Table 15-2 Typical Simplifications Used in Flow and Sediment Modeling

Model and/or references	Flow	Bed-load transport	Bed-elevation changes	Suspended-sediment transport	Sediment-exchange processes	Sediment mixtures	Base numerical method
SUTRENCH-2D, van Rijn (1987)	Quasi unsteady two-dimensional (width-averaged)	Bed-load-layer concept	Total-load concept	Quasi-unsteady two-dimensional (width-averaged)	Entrainment and deposition	No	Finite-volume with structured grid
Brors (1999)	Unsteady two-dimensional (vertical plane)	Yes	One-dimensional Exner equation	Unsteady two-dimensional (vertical plane)	Entrainment and deposition	No	Finite-element
Argos modeling system, Usseglio-Polatera and Cunge (1985)	Unsteady two-dimensional (depth-averaged)	No	Exner equation	Unsteady two-dimensional (depth-averaged)	Entrainment and deposition	No	Finite-difference with Lagrangian advection
TABS-2, Thomas and McAnally (1985)	Unsteady two-dimensional (depth-averaged)	No	Exner equation, empirical total-load formula	No	No	No	Finite-element
CCHE2D Jia and Wang (1999)	Unsteady two (depth-averaged)	Yes	Exner equation	No	No	No	Finite-element
Nagata et al. (2000)	Unsteady two (depth-averaged)	Yes	Exner equation with deposition and pickup terms	No	No	No	Finite-volume with structured grid
MOBED2, Spasojevic and Holly (1990a; 1990b)	Unsteady two (depth-averaged)	Active-layer concept	Active-layer and active-stratum concept	Unsteady two-dimensional depth-averaged)	Entrainment and deposition	Unlimited number of sediment size classes	Finite-difference with Lagrangian advection
FAST2D with sediment processes, Minh Duc et al. (1998)	Unsteady two-dimensional (depth-averaged)	Bed-load-layer concept	Total-load concept	Unsteady two-dimensional (depth-averaged)	Entrainment and deposition	No	Finite-volume with structured grid
Olsen (1999)	Unsteady two-dimensional (depth-averaged)	Yes	Discrepancy in sediment continuity for bed cells	Unsteady three-dimensional, near-bed concentration as boundary condition	No	A budget method for computing the change in bed grain size distribution	Finite-volume with structured grid

MIKE 21	Unsteady two-dimensional	Included in total load	No?	Sand and fine sediment	?	Yes?	Finite-difference
Shimizu et al. (1990)	Steady-state quasi-three-dimensional, hydrostatic pressure assumption, and an empirical longitudinal velocity component profile	Yes	Exner equation	Steady two-dimensional (depth-averaged)	Entrainment and deposition	No	Finite-difference
Demuren (1991)	Steady-state three-dimensional	Bed-load-layer concept	Algebraic equation and iterative procedure	Steady-state three-dimensional	Entrainment and deposition	No	Finite-difference/volume on structured grid
Olsen et al. (1999)	Steady-state three-dimensional	No	No	Steady-state three-dimensional, near-bed concentration as boundary condition	No	No	Finite-volume with structured grid
Olsen and Melaaen (1993); Olsen and Skoglund (1994)	Steady-state three-dimensional	Yes	Discrepancy in sediment continuity for the bed cells	Steady-state three-dimensional, near-bed concentration as boundary condition	No	No	Finite-volume with structured grid
TELEMAC-3D with sediment processes, Jankowski et al. (1994); Hervouet and Bates (2000)	Unsteady three-dimensional, hydrostatic pressure assumption	No	No	Unsteady three-dimensional	Deposition	No	Finite-element
Sheng (1983)	Unsteady three-dimensional, hydrostatic pressure assumption	No	No	Unsteady three-dimensional, without the fall-velocity term	No	No	Finite-difference
FLESCOT, Onishi and Trent (1982), Onishi and Thompson (1984), Onishi and Trent (1985)	Unsteady three-dimensional, hydrostatic pressure assumption	No	Exner equation	Unsteady three-dimensional	Entrainment and deposition	Silt, clay, and sand	Finite-difference
SUTRENCHE-3D, van Rijn (1987)	Quasi-unsteady two-dimensional (depth averaged) with a vertical logarithmic velocity profile	Yes	Layer-layer approach and total-load approach as alternatives	Unsteady three-dimensional	Entrainment and deposition	No	Finite-volume with structured grid

(Continued)

Table 15-2 Typical Simplifications Used in Flow and Sediment Modeling (*Continued*)

Model and/or references	Flow	Bed-load transport	Bed-elevation changes	Suspended-sediment transport	Sediment-exchange processes	Sediment mixtures	Base numerical method
Olsen and Kjellesvig (1998)	Unsteady three-dimensional	Yes	Discrepancy in sediment continuity for the bed cells	Unsteady three-dimensional, near-bed concentration as boundary condition	No	No	Finite-volume with structured grid
Lin and Falconer (1996)	Unsteady three-dimensional, hydrostatic pressure assumption	Yes	No	Unsteady three-dimensional	Entrainment and deposition	No	Finite-difference
Wang and Adeff (1986)	Unsteady three-dimensional, hydrostatic pressure assumption	Yes	Total load concept	Unsteady three-dimensional, near-bed concentration as boundary condition	No	No	Finite-element
CH3D-SED Spasojevic and Holly (1993); Gessler et al. (1999)	Unsteady three-dimensional, hydrostatic pressure assumption	Active-layer concept	Active-layer and active-stratum concept	Unsteady three-dimensional	Entrainment and deposition	Unlimited number of sediment size classes	Finite-volume with structured grid
RMA-10	Unsteady three-dimensional, hydrostatic pressure assumption?	No	?	Unsteady three-dimensional?	Entrainment and deposition of cohesive sediment	No?	Finite-element
MIKE 3	Unsteady three-dimensional, hydrostatic pressure assumption?	No	?	Unsteady three-dimensional, fine-sediment	Deposition of cohesive sediment	No?	Finite-difference
RMA-10	Unsteady three-dimensional, hydrostatic pressure assumption?	No	?	Unsteady three-dimensional?	Entrainment and deposition of cohesive sediment	No?	Finite-element
FAST3D with sediment processes Rodi (2000); Wu et al. (2000)	Unsteady three-dimensional	Layer-layer concept	Total load concept	Unsteady three-dimensional	Entrainment and deposition	No	Finite-volume with structured grid
Delft 3D	Unsteady two- and three-dimensional	No?	No	Unsteady two- and three-dimensional	Entrainment and deposition	Yes	?

and continuous domain of sediment processes into a bed and/or near-bed layer on the one hand, and the rest of the domain on the other. Then the governing equations for the bed and near-bed processes are associated with the bed and near-bed layer, whereas the governing equations for the suspended-material processes are associated with the rest of the domain.

15.4.2 Overview of Conceptual Models of Mobile-Bed Processes

There are several conceptualizations of the bed and near-bed layer, such as the mixing layer proposed by Karim and Kennedy (1982), the bed load layer proposed by van Rijn (1987), and the active layer proposed by Spasojevic and Holly (1990b). Similarly, there is no generally accepted set of governing equations for the bed and near-bed processes. The equations' formulations, even though not so different, may still vary depending on the bed and near-bed layer concept, or simply depending on the approach. More details on the governing equations for the bed and near-bed processes are presented in Section 15.5.

In contrast to the bed and near-bed processes, modeling of suspended-material processes is practically always based on the sediment-transport or advection-diffusion equation with an additional fall-velocity advection term. The suspended-sediment advection-diffusion equation can be derived either from the two-phase flow equations (Greimann et al. 1999) or directly, using the continuum approach, and the assumptions are that the sediment particles' horizontal velocity components are the same as the corresponding fluid velocities and that the sediment particles' vertical-velocity components are equal to those of the appropriate fluid velocity adjusted by the fall velocity. In either case, the result is the familiar suspended-sediment advection-diffusion equation with a special model for particle settling, characterized by a settling velocity. Details on suspended-material modeling are presented in Section 15.6.

The simplified model can only account for the sediment-flow interaction in an indirect way. The flow-sediment interaction in such models is achieved through the flow acting as the driving force for sediment processes and the associated sediment-process feedback to the flow. This sediment-process feedback comprises changes in bed elevation, changes in the flow and the suspended-sediment mixture density, and, possibly, changes in the bed friction coefficient.

This concept of sediment-process modeling based on separation of suspended-material and bed and near-bed processes inevitably requires formulation of sediment-exchange mechanisms. Sediment-exchange processes are commonly formulated as bed and near-bed material entrainment into suspension and suspended-material deposition onto the bed. The same exchange terms, with opposite signs, provide the coupling between equations for near-bed and suspended-material processes. Details on

modeling of sediment-exchange processes are presented in Section 15.7.

Even when these simplifications are made, the development of two-dimensional and three-dimensional flow and sediment models is constrained by the available computing resources. Due to the complexity of the problem and the typical need for long-term simulations, flow and sediment modeling can be prohibitive in terms of CPU time. Therefore, many flow and sediment models adopt further simplification. Table 15-2 summarizes typical simplifications used in flow and sediment modeling. Although the list of models in the table is surely incomplete, the authors hope that the listed models reflect the general scope of current developments in two-dimensional and three-dimensional flow and sediment modeling.

15.4.3 Assessment of Conceptual Bases of Mobile-Bed Models

Because the bed-load flux is a vector parallel to the bed surface, the bed-load transport is essentially two-dimensional. But the flow and the suspended-sediment transport are fully three-dimensional processes. Therefore, two-dimensional flow and suspended-sediment transport models may have restricted applicability, as has been described earlier. On the other hand, use of the two-dimensional equations for flow and suspended-sediment transport is far less demanding of CPU time than use of three-dimensional models, as discussed earlier. The two-dimensional simplification was used extensively during the 1980s, when the available computing resources were typically insufficient for any practically meaningful three-dimensional flow and sediment modeling. The two-dimensional depth-averaged approach was used in the Argos Modeling System (as described by Usseglio-Polatera and Cunge 1985), and MOBED2 (Spasojevic and Holly 1990a; 1990b). TABS-2, as described by Thomas and McAnally (1985), is based on the depth-averaged flow equations, with the bed-load and suspended-sediment transport modeling replaced by the total load concept. Van Rijn (1987) developed the SUTRENCH-2D model in which the flow and suspended-sediment transport are modeled using the two-dimensional width-averaged equations. van Rijn (1987) also developed the SUTRENCH-3D model, in which the flow is modeled using the two-dimensional depth-averaged equations in combination with the assumption of a vertical logarithmic velocity profile, whereas the suspended-sediment transport is modeled using the three-dimensional equations. Shimizu et al. (1990) developed a model based on the depth-averaged suspended-sediment transport equations and quasi-three-dimensional flow equations, assuming a hydrostatic-pressure distribution and using an empirical longitudinal velocity component distribution along the depth.

After being neglected for a few years, during which time a number of three-dimensional flow and sediment

models have been developed and successfully applied, the two-dimensional approach seems to be enjoying renewed popularity. It appears that the price for the sophistication and generality of three-dimensional flow and sediment models is still the often-prohibitive CPU time. Thus, a number of two-dimensional models, often including corrections for three-dimensional effects, have recently been developed to be used for specific applications, perhaps even in combination with three-dimensional models. Minh Duc et al. (1998) presented the FAST2D model with sediment processes, based on the depth-averaged equations for the flow and the suspended-sediment transport, which can be used for relatively long simulations. The CCHE2D model (Jia and Wang 1999), including the depth-averaged flow equations, bed-load transport, and bed-elevation changes, has been developed for cost- and time-effective long-term simulations. Nagata et al. (2000) also developed a model based on the depth-averaged flow equations, bed-load transport, and bed-elevation changes, including the rarely modeled bank erosion. All three models include some kind of correction for three-dimensional flow effects. Brors (1999) reported a three-dimensional model of flow and sediment processes around a submerged pipeline, but its application was limited to consideration of conditions in a two-dimensional vertical plane. Olsen (1999) developed a model based on a combination of the depth-averaged flow equations and three-dimensional suspended-sediment transport, using an empirical expression for the vertical profile of eddy viscosity.

The development of three-dimensional flow and sediment models started in the early 1980s. The simplifications used in three-dimensional models involve both flow-modeling simplifications and the level of complexity included in the sediment equations. One of the typical three-dimensional flow modeling simplifications is the use of the steady-state equations for both flow and suspended-sediment transport (Demuren 1991; Olsen and Melaaen 1993; Olsen and Skoglund 1994; Olsen et al. 1999). Use of this simplification restricts the model's range of applicability, because the sediment processes are naturally unsteady and their effects accumulate in time, eventually affecting the flow computations. Another typical three-dimensional flow modeling simplification is the assumption of a hydrostatic-pressure distribution over the depth as described in Section 15.3.3 above (Sheng 1983; FLESCOT as reported by Onishi and Trent 1985; Wang and Adeff 1986; TELEMAC-3D with sediment processes as reported by Jankowski et al. 1994; Lin and Falconer 1996; CH3D-SED as reported by Gessler et al. 1999). The hydrostatic-pressure assumption is easily violated wherever streamline curvature is significant (e.g., in the vicinity of river-training structures, close to rapidly changing bed surface conditions, in river bends). However, this simplification is still commonly used because it provides for significant CPU time-saving and

thus enables simulations over some significant period of prototype time.

In terms of complexity of sediment-processes modeling, both two- and three-dimensional models in use span quite a wide range. Some models concentrate on bed-load transport and associated bed elevation changes (e.g., the CCHE2D of Jia and Wang 1999 and two-dimensional models of Nagata et al. 2000). Others concentrate on suspended-sediment transport, some including the associated bed elevation changes (e.g., the two-dimensional Argos Modeling System as described by Usseglio-Polatera and Cunge 1985; the three-dimensional FLESCOT model of Onishi and Trent 1985), and some not including bed changes (e.g., the three-dimensional models of Sheng, 1983; Olsen et al. 1999; TELEMAC-3D with sediment processes as described by Jankowski et al. 1994). The three-dimensional model of Lin and Falconer (1996) includes both bed-load and suspended-sediment transport, but does not include bed elevation changes. Models concentrating only on certain aspects of sediment processes are obviously applicable to flow and sediment situations where the corresponding aspects dominate. Examples of such specific flow and sediment situations may include settling tanks or reservoir-sedimentation problems, where suspended-sediment transport and deposition are dominant processes.

More general models recognize that the same sediment particle can remain at the bed surface or move either in suspension or as bed load, all depending on local flow conditions, and attempt to include all relevant sediment processes. Examples of the more general approach among two-dimensional models include SUTRENCH-2D, van Rijn (1987); MOBED2 as reported by Spasojevic and Holly (1990a; 1990b); FAST2D with sediment processes, Minh Duc et al. (1998); and models of Shimizu et al. (1990); Brors (1999); Olsen (1999). Examples among three-dimensional models include SUTRENCH-3D, van Rijn (1987); models of Wang and Adeff (1986); Demuren (1991); Olsen and Melaaen (1993); Olsen and Skoglund (1994); Olsen and Kjellesvig (1998); CH3D-SED as reported by Spasojevic and Holly (1993) or Gessler et al. (1999); and FAST3D with sediment processes as reported by Rodi (2000) or Wu et al. (2000).

Finally, only a few models attempt to include the behavior of nonuniform sediment or sediment mixtures. Spasojevic and Holly (1990a; 1990b) introduced a relatively general approach to the treatment of sediment mixtures with an unlimited number of sediment size classes, as initially developed for the two-dimensional model MOBED2. The approach was subsequently generalized and built into the three-dimensional CH3D-SED model (Spasojevic and Holly 1993). The combined two-dimensional depth-averaged flow and three-dimensional suspended-sediment transport model reported by Olsen (1999) uses a budget method for computing the change in bed grain-size

distribution. The three-dimensional FLESCOT model, as reported by Onishi and Trent (1985), treats three distinct sediment components (clay, silt, sand). Modeling the behavior of sediment mixtures allows accounting for natural phenomena such as differential settling, hydraulic sorting, and armoring.

15.5 BED AND NEAR-BED PROCESSES

15.5.1 Introduction and Overview

One of the major differences among various two-dimensional or three-dimensional flow and sediment models is the treatment of bed and near-bed processes, including bed-load transport, bed elevation changes, and the exchange between the suspended material and the bed and near-bed material.

Demuren (1991) introduced a simplified model for bed-elevation changes in meandering channels using algebraic equations based on perturbations to equilibrium between bed elevations and bedload transport. Olsen and Melaaen (1993), Olsen and Skoglund (1994), Olsen and Kjellesvig (1998), and Olsen (1999) presented models that solve the three-dimensional mass-conservation (advection-diffusion) equation for suspended sediment using an empirical near-bed concentration as a boundary condition. The near-bed concentration is assigned to computational cells next to the bed surface, but the mass-conservation equation for these cells is not solved. In a somewhat arbitrary manner, the discrepancy in the sediment continuity for computational cells next to the bed surface is used to compute bed-surface elevation changes.

Modeling bed-surface elevation changes is often based on an intuitive sediment mass-conservation equation, usually referred to as the Exner equation, written for the sediment resting on the bed or moving as a bed load. The full form of the Exner equation is

$$\rho_s (1 - p_b) \frac{\partial z_b}{\partial t} + \nabla \cdot \vec{q}_b + E - D = 0 \quad (15-16)$$

where

- ρ_s = density of sediment, assumed to be constant;
- p_b = porosity of the bed material, assumed to be constant;
- z_b = bed-surface elevation;
- \vec{q}_b = bed-load flux;
- E = upward bed-sediment entrainment flux, representing the entrainment of sediment particles from the bed into suspension; and
- D = downward suspended-sediment deposition flux, representing gravitational settling of suspended sediment particles onto the bed.

The Exner equation is essentially two-dimensional in the plane parallel to the bed surface.

The models of Shimizu et al. (1990) and Brors (1999) include both bed load and suspended-sediment transport and use a complete form of the Exner equation. The Argos Modeling System, as described by Usseglio-Polatera and Cunge (1985), and the FLESCOT model, as described by Onishi and Trent (1985), both of which include only suspended-sediment transport, use the Exner equation without the bed-load flux-divergence term. The CCHE2D model of Jia and Wang (1999) and the model of Nagata et al. (2000), both of which include only bed-load transport, use the Exner equation without entrainment and deposition sources. Nagata et al. (2000) also use the bed-load deposition and pickup functions instead of the bed-load flux-divergence term. TABS-2, as described by Thomas and McAnally (1985), which does not distinguish between the bed load and the suspended-sediment transport, uses the Exner equation with an empirical total load flux.

Van Rijn (1987) introduced the bed-load-layer concept and proposed two methods for computing the bed-surface elevation changes. One method is based on the sediment mass-conservation equation for the bed-load-layer control volume, and it is called here the bed-load-layer approach. The other is based on the sediment mass-conservation equation for the control volume spanning the entire flow depth and thus comprising the bed-load-layer control volume and the entire water column with suspended sediment above it. This second method requires combining the bed-load flux and the depth-integrated suspended-sediment flux into the total-load flux, so it is called here the total-load approach. The SUTRENCH-2D and SUTRENCH-3D models of van Rijn (1987) have both the bed-load-layer approach and the total-load approach built in as alternatives. The total-load approach was used in the model of Wang and Adeff (1986), in FAST2D with sediment processes (Minh Duc et al. 1998), and in FAST3D with sediment processes (Wu et al. 2000). Both FAST2D and FAST3D with sediment processes also adapted the bed-load-layer approach to compute the nonequilibrium bed-load flux.

Spasojevic and Holly (1990a; 1990b) introduced an active-layer and active-stratum concept and proposed a method to compute the bed-surface elevation and the active-layer size-class distribution changes in the case of nonuniform sediment, i.e., for natural sediment mixtures. The method, initially implemented in the two-dimensional (depth averaged) MOBED2 model (Spasojevic and Holly 1990a; 1990b), and subsequently generalized and built into the three-dimensional CH3D-SED model (Spasojevic and Holly 1993), is called here the active-layer and active-stratum approach.

15.5.2 The Bed-Load-Layer and the Total-Load Approach

Figure 15-1 shows a vertical schematization of the sediment-processes domain, as introduced by van Rijn (1987) and applied by Wu et al. (2000).

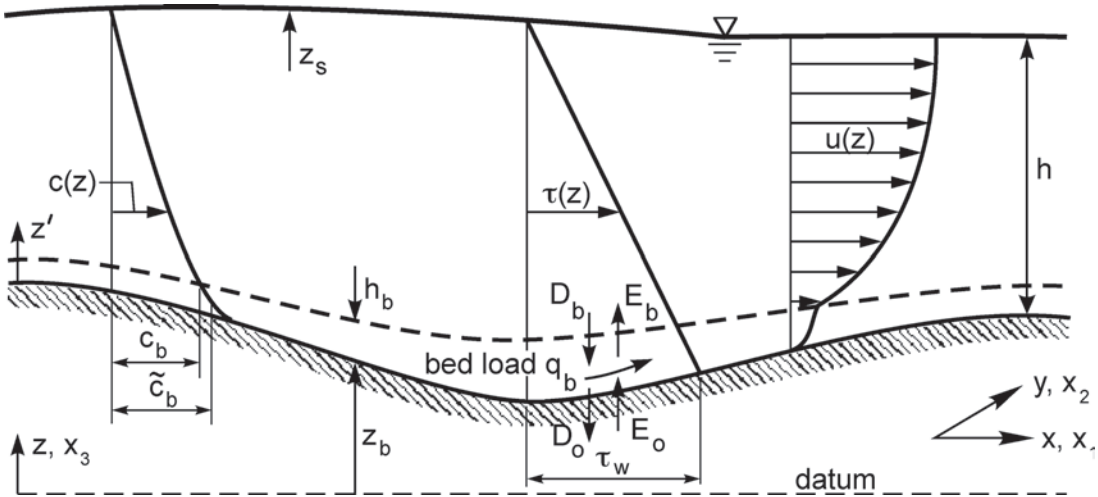


Fig. 15-1. Vertical schematization of the sediment-processes domain (van Rijn 1987; Wu et al. 2000).

According to van Rijn (1987), the mass-conservation equation for the bed-load-layer control volume reads

$$\frac{\partial}{\partial t}(h_b \tilde{c}_b) + \nabla \cdot \vec{q}_b + E_b - D_b - E_0 + D_0 = 0 \quad (15-17)$$

where

- h_b = bed-load-layer thickness;
- \tilde{c}_b = bed-load-layer sediment volumetric concentration averaged over the bed-load-layer thickness;
- \vec{q}_b = bed-load flux;
- E_b = upward sediment entrainment flux at $z = z_b + h_b$;
- D_b = downward sediment deposition flux at $z = z_b + h_b$;
- E_0 = upward sediment entrainment flux at $z = z_b$; and
- D_0 = a downward sediment deposition flux at $z = z_b$.

Entrainment and deposition fluxes E_b and D_b represent the exchange between the bed-load-layer sediment and the suspended sediment through the bed-load-layer control volume ceiling. Entrainment and deposition fluxes E_0 and D_0 represent the exchange between the bed-subsurface sediment and the bed-load-layer sediment through the bed-load-layer control volume floor.

Van Rijn also introduced a similar mass-conservation equation for the bed-subsurface sediment control volume,

$$\rho_s (1 - p_b) \frac{\partial z_b}{\partial t} + E_0 - D_0 = 0 \quad (15-18)$$

where

- z_b = the bed-surface elevation and is the bed-subsurface control volume ceiling.

Because the bed-subsurface control volume floor does not move, its location, i.e., the subsurface control volume thickness, is irrelevant.

Adding Eqs. (15-17) and (15-18) yields the mass-conservation equation for bed-load-layer and bed-subsurface sediment:

$$\rho_s (1 - p_b) \frac{\partial z_b}{\partial t} + \frac{\partial}{\partial t}(h_b \tilde{c}_b) + \nabla \cdot \vec{q}_b + E_b - D_b = 0 \quad (15-19)$$

The mass-conservation equation for the control volume spanning the entire flow depth, including the bed-load layer and the entire water column with suspended sediment above it, reads (van Rijn, 1987)

$$\frac{\partial}{\partial t}(h \tilde{c}) + \nabla \cdot \vec{q}_T - E_0 + D_0 = 0 \quad (15-20)$$

where

h = the entire flow depth;

\tilde{c} = depth-averaged volumetric suspended-sediment concentration ;

$\vec{q}_T = \vec{q}_b + \vec{q}_s$ = total sediment load flux;

q_s = depth-integrated suspended-load flux (advection and diffusion).

Adding Eqs. (15-18) and (15-20) yields the mass-conservation equation for bed-subsurface sediment, bed-load-layer sediment, and suspended sediment in the entire water column above the bed load layer:

$$\rho_s (1 - p_b) \frac{\partial z_b}{\partial t} + \frac{\partial}{\partial t}(h \tilde{c}) + \nabla \cdot \vec{q}_T = 0 \quad (15-21)$$

Van Rijn (1987) states that for steady-flow conditions the storage terms $\frac{\partial}{\partial t}(h_b \tilde{c}_b)$ in Eq. (15-19) and $\frac{\partial}{\partial t}(h \tilde{c})$ in Eq. (15-21)

can be neglected. This assumption may be inappropriate in cases of extensive deposition (such as settling in reservoirs) or extensive entrainment (e.g., erosion behind river-training structures such as chevron dikes). With van Rijn's assumption, Eq. (15-19) reduces to the specific form of the Exner equation (the location of entrainment and deposition fluxes E_b and D_b is well defined)

$$\rho_s(1-p_b)\frac{\partial z_b}{\partial t} + \nabla \cdot \vec{q}_b + E_b - D_b = 0 \quad (15-22)$$

whereas Eq. (15-21) becomes:

$$\rho_s(1-p_b)\frac{\partial z_b}{\partial t} + \nabla \cdot \vec{q}_T = 0 \quad (15-23)$$

Either Eq. (15-22) or Eq. (15-23) can be used to compute bed-surface elevation changes. Wu et al. (2000) state that Eq. (15-23) ensures better mass conservation in numerical procedures.

Equations (15-22) and (15-23) can be written in Cartesian coordinates as follows:

$$\rho_s(1-p_b)\frac{\partial z_b}{\partial t} + \frac{\partial q_{bx}}{\partial x} + \frac{\partial q_{by}}{\partial y} + E_b - D_b = 0 \quad (15-24)$$

and

$$\rho_s(1-p_b)\frac{\partial z_b}{\partial t} + \frac{\partial q_{Tx}}{\partial x} + \frac{\partial q_{Ty}}{\partial y} = 0 \quad (15-25)$$

where

q_{bx} and q_{by} = x - and y -direction components of the bed-load flux and

q_{Tx} and q_{Ty} = x - and y -direction components of the total sediment load flux.

Wu et al. (2000) further modified Eq. (15-24) to account for nonequilibrium effects on the bed-load transport by using the assumption

$$(1-p_b)\frac{\partial z_b}{\partial t} = \frac{1}{L_s}(q_b - q_{be}) \quad (15-26)$$

where L_s is the nonequilibrium adaptation length for bed-load transport, and q_{be} is the bed-load flux under equilibrium conditions. The assumption expressed by Eq. (15-26) was introduced by Wellington (1978), Philips and Sutherland (1989), and Thuc (1991) for the case where the suspended load is negligible (i.e., $E_b - D_b = 0$). With the components of bed-load flux in x - and y -directions expressed as

$$q_{bx} = \alpha_{bx} q_b, \quad q_{by} = \alpha_{by} q_b \quad (15-27)$$

where

α_{bx} and α_{by} = direction cosines,

and with Eqs. (15-26) and (15-27) introduced into Eq. (15-24), one obtains

$$\frac{1}{L_s}(q_b - q_{be}) + \frac{\partial(\alpha_{bx} q_b)}{\partial x} + \frac{\partial(\alpha_{by} q_b)}{\partial y} + E_b - D_b = 0. \quad (15-28)$$

15.5.3 The Active-Layer and Active-Stratum Approach—Sediment Mixtures

Inspired by the mixing-layer concept of Karim and Kennedy (1982), Spasojevic and Holly (1990a; 1990b) introduced the active-layer concept. The active layer (Fig. 15-2) is assumed to comprise sediment moving as a bed load, as well as bed-surface and subsurface sediment already agitated and ready to be set into motion. The active-layer concept is used in conjunction with a modeling approach designed for the treatment of sediment mixtures. Thus, the sediment mixture is represented through a suitable number of sediment size classes.

The active layer is assumed to have a uniform size-class distribution over its thickness h_a . It is assumed that all sediment particles of a given size class inside the active layer are equally exposed to the flow irrespective of their location in the layer. An active-layer control volume ΔV (Fig. 15-2) is defined as having dimension Δl not less than the maximum average saltation length, so that the bed-load flux represents bed-load exchange between two neighboring control volumes.

For a fixed active-layer floor elevation, the mass-conservation equation for size class ks of sediment in the active-layer control volume is written as follows:

$$\rho_s(1-p_b)\frac{\partial(\beta_{ks} h_a)}{\partial t} + \nabla \cdot \vec{q}_{bks} + E_{ks} - D_{ks} = 0 \quad (15-29)$$

where

β_{ks} = active-layer fraction of the size class ks , defined as a ratio of the mass of particles of the size class ks inside the active-layer control volume ΔV to the mass of all sediment particles contained in ΔV ;

\vec{q}_{bks} = bed-load flux for the size class ks ;

E_{ks} = upward sediment entrainment flux for the size class ks ;

D_{ks} = downward sediment deposition flux for the size class ks .

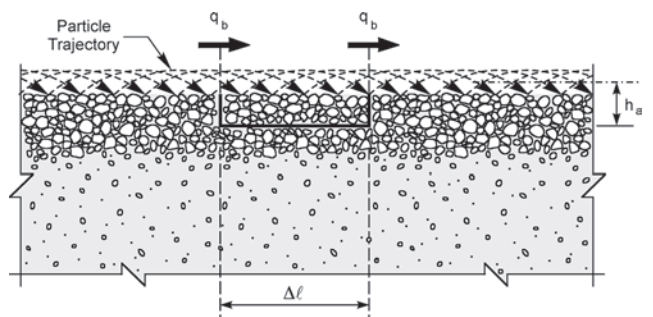


Fig. 15-2. Active-layer definition sketch.

The entrainment and deposition fluxes are evaluated at some distance above the bed surface, and that location is considered to be the near-bed boundary of the suspended material domain.

As Fig. 15-2 indicates, the only bed-load particles changing the mass balance inside the active-layer control volume are the ones entering and leaving the volume. Other bed-load particles start and end their trajectories inside the same active-layer control volume, remaining within the volume and not changing the mass balance within it. To make possible the use of a conventional bed-material porosity p_b , the active-layer thickness h_a in Eq. (15-29) is defined assuming that such bed-load particles are positioned at the bed surface.

Subsurface material below the active-layer control volume is discretized into a sequence of control volumes, one below the other, called here stratum control volumes (Fig. 15-3). Each stratum control volume has the same dimension Δl as the active-layer control volume above it. The bed material inside one stratum control volume is assumed to have uniform size distribution.

The stratum control volume immediately below the active-layer control volume is called the active-stratum control volume. It is possible, indeed likely, that the active-layer and active-stratum elemental volumes have different size distributions. The active-layer floor, which is at the same time an active-stratum ceiling, descends or rises whenever the bed elevation changes due to deposition or erosion occurring in the active-layer control volume. If, for example, the active-layer floor descends, some of the material that belonged to the active-stratum control volume

becomes part of the active-layer control volume, whose homogeneous size distribution thus may change.

In order to represent the exchange of sediment particles between the active-layer and the active-stratum control volumes due to active-layer floor movement, another source term is introduced, called here the active-layer floor source F_{ks} , again specific to the size class ks . The mass-conservation equation for the size class ks of sediment particles in the active-layer control volume then reads

$$\rho_s (1-p_b) \frac{\partial (\beta_{ks} h_a)}{\partial t} + \nabla \cdot \vec{q}_{bks} + E_{ks} - D_{ks} - F_{ks} = 0 \quad (15-30)$$

The mass of a particular size class in the active-stratum control volume may change only due to active-layer floor movement, i.e., due to exchange of material between the active layer and active stratum, whereas the active-stratum floor elevation remains unchanged. This is expressed by a mass-conservation equation written for the size class ks in the active-stratum control volume,

$$\rho_s (1-p_b) \frac{\partial}{\partial t} [\beta_{sks} (z_b - h_a)] + F_{ks} = 0 \quad (15-31)$$

where

β_{sks} = active-stratum fraction of the size class ks ;
and

$(z_b - h_a)$ = active-layer floor elevation, i.e., active-stratum ceiling.

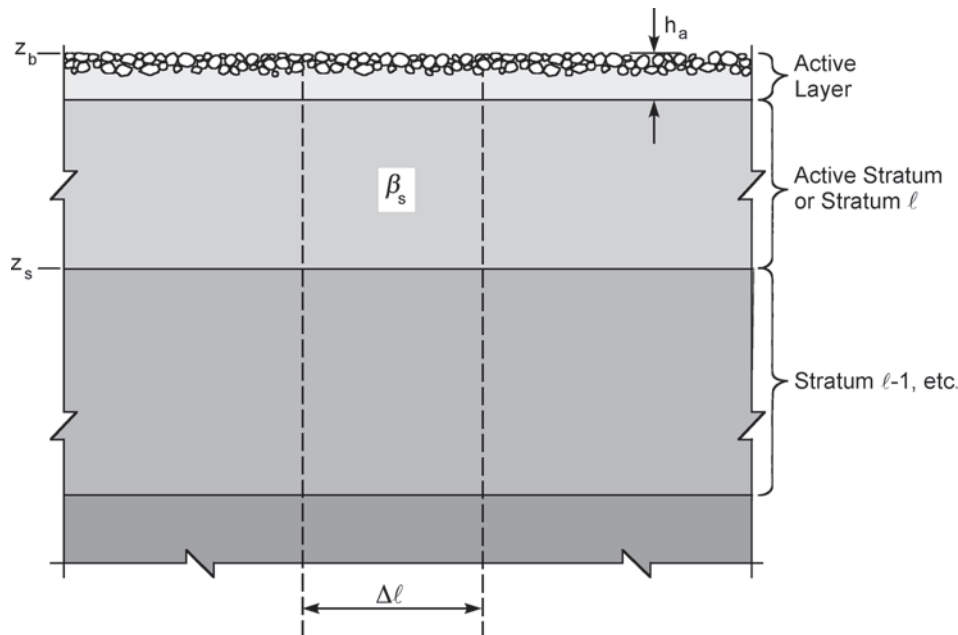


Fig. 15-3. Stratum control volumes below an active-layer control volume.

Summation of the mass-conservation equations for all size classes in the active-layer control volume and use of the basic constraint

$$\sum_{ks=1}^{KS} \beta_{ks} = 1 \quad (15-32)$$

where

KS represents the total number of size classes, leads to the global mass-conservation equation for the active-layer control volume:

$$\rho_s (1-p_b) \frac{\partial h_a}{\partial t} + \sum_{ks=1}^{KS} (\nabla \cdot \vec{q}_{bks} + E_{ks} - D_{ks} - F_{ks}) = 0. \quad (15-33)$$

A similar equation can be obtained for the active-stratum control volume,

$$\rho_s (1-p_b) \frac{\partial (z_b - h_a)}{\partial t} + \sum_{ks=1}^{KS} F_{ks} = 0 \quad (15-34)$$

where again Eq. (15-32) is invoked. Summation of Eqs. (15-33) and (15-34) gives the global mass-conservation equation for bed sediment,

$$\rho_s (1-p_b) \frac{\partial z_b}{\partial t} + \sum_{ks=1}^{KS} (\nabla \cdot \vec{q}_{bks} + E_{ks} - D_{ks}) = 0 \quad (15-35)$$

which can be recognized as the form of the Exner equation written for the summation over all sediment size classes.

One global mass-conservation equation for bed sediment (Eq. (15-35)) written for the bed control volume (comprising active-layer and active-stratum control volumes), and ks mass-conservation equations for active-layer sediment (one Eq. (15-30) for each size class) written for the active-stratum control volume, are used to compute the bed-surface elevation and the active-layer size-class distribution changes. To satisfy the basic constraint (Eq. (15-32)), the equations must be solved simultaneously.

When the overall bed slope is small, the mass-conservation equation for the size class ks of active-layer sediment and the global mass-conservation equation for bed sediment, Eqs. (15-30) and (15-35), can be written in Cartesian coordinates as follows:

$$\begin{aligned} \rho_s (1-p_b) \frac{\partial (\beta_{ks} h_a)}{\partial t} &+ \frac{\partial q_{bxks}}{\partial x} + \frac{\partial q_{byks}}{\partial y} \\ &+ E_{ks} - D_{ks} - F_{ks} = 0 \end{aligned} \quad (15-36)$$

and

$$\rho_s (1-p_b) \frac{\partial z_b}{\partial t} + \sum_{ks=1}^{KS} \left(\frac{\partial q_{bxks}}{\partial x} + \frac{\partial q_{byks}}{\partial y} + E_{ks} - D_{ks} \right) = 0 \quad (15-37)$$

where

q_{bxks} and q_{byks} = x - and y -direction components of the bed-load flux for the size class ks of active-layer sediment.

15.6 SUSPENDED-MATERIAL PROCESSES

15.6.1 General Three-Dimensional Formulation

The majority of two-dimensional and three-dimensional flow and sediment models use the advection-diffusion equation with an additional fall-velocity term to describe the suspended-sediment transport. The three-dimensional mass conservation equation for suspended sediment reads

$$\begin{aligned} \frac{\partial(\rho C)}{\partial t} &+ \frac{\partial}{\partial x}(u\rho C) + \frac{\partial}{\partial y}(v\rho C) \\ &+ \frac{\partial}{\partial z}(w\rho C) - \frac{\partial}{\partial z}(w_f \rho C) \\ &= \frac{\partial}{\partial x}\left(\epsilon_s \frac{\partial(\rho C)}{\partial x}\right) + \frac{\partial}{\partial y}\left(\epsilon_s \frac{\partial(\rho C)}{\partial y}\right) \\ &+ \frac{\partial}{\partial z}\left(\epsilon_s \frac{\partial(\rho C)}{\partial z}\right) \end{aligned} \quad (15-38)$$

where

ρ = density of a mixture of water and suspended sediment;

C = dimensionless concentration, i.e., ratio of the mass of the suspended-sediment particles contained in an elemental volume to the total mass of the elemental volume;

w_f = suspended-sediment particle fall or settling velocity;

u, v , and w = water-velocity components;

ϵ_s = turbulent mass-diffusivity coefficient, i.e., the eddy diffusivity for sediment-particle transport.

When the dimensional or so-called volumetric concentration $c = \rho C$ is used, Eq. (15-38) becomes

$$\begin{aligned} \frac{\partial c}{\partial t} &+ \frac{\partial}{\partial x}(uc) + \frac{\partial}{\partial y}(vc) + \frac{\partial}{\partial z}(wc) - \frac{\partial}{\partial z}(w_f c) \\ &= \frac{\partial}{\partial x}\left(\epsilon_s \frac{\partial c}{\partial x}\right) + \frac{\partial}{\partial y}\left(\epsilon_s \frac{\partial c}{\partial y}\right) + \frac{\partial}{\partial z}\left(\epsilon_s \frac{\partial c}{\partial z}\right) \end{aligned} \quad (15-39)$$

where the volumetric concentration c = the ratio of the mass of the suspended-sediment particles contained in an elemental volume to the elemental volume.

The formulations of Eqs. (15-39) and (15-40), based on the dimensional and dimensionless concentrations, are fully equivalent. Most (but not all) model formulations are based on the dimensional concentration, and field and laboratory data are reported in both forms. There is no inherent advantage in using or the other of the two forms.

At the free surface, the vertical sediment flux is zero. Thus, the simplest free-surface boundary condition for Eqs. (15-38) or (15-39) is to set the vertical diffusion and the fall-velocity advection fluxes to zero at the free surface. The near-bed boundary condition for Eqs. (15-38) or (15-39) can be either the specified concentration, or the specified exchange between the suspended-sediment and the bed- and near-bed processes. The exchange is defined as the difference between the upward sediment entrainment flux E and the downward sediment deposition flux D , having signs opposite to the same terms in the governing equations for the bed- and near-bed processes. The sediment exchange condition is preferred if the model includes both suspended-sediment processes and the bed- and near-bed processes, because it provides the coupling between the two.

15.6.2 Two-Dimensional (Depth-Averaged) Formulation

The depth-averaged form of Eq. (15-39) is:

$$\begin{aligned} \frac{\partial(h\tilde{c})}{\partial t} + \frac{\partial}{\partial x}(\tilde{u}h\tilde{c}) + \frac{\partial}{\partial y}(\tilde{v}h\tilde{c}) \\ = \frac{\partial}{\partial x}\left(\tilde{\varepsilon}_s h \frac{\partial \tilde{c}}{\partial x}\right) + \frac{\partial}{\partial y}\left(\tilde{\varepsilon}_s h \frac{\partial \tilde{c}}{\partial y}\right) + E - D \end{aligned} \quad (15-40)$$

where

h = depth;

\tilde{c} = depth-averaged dimensional (volumetric) concentration;

\tilde{u} and \tilde{v} = depth-averaged water velocity components;

$\tilde{\varepsilon}_s$ = horizontal plane mass-diffusivity coefficient, usually only including the eddy diffusivity and neglecting the dispersion due to depth averaging.

As discussed in Section 15.3.2, model developers have tended to include neither this additional dispersion, nor a tensorial representation to account for the differential effective dispersion parallel and perpendicular to the local flow direction, as described by Holly and Usseglio-Polatera (1984).

15.6.3 Formulations for Sediment Mixtures

When the sediment mixture is considered, Eqs. (15-38) and (15-39) can be written for a particular size class. Equation (15-38) for the size class KS reads

$$\begin{aligned} \frac{\partial(\rho C_{ks})}{\partial t} + \frac{\partial}{\partial x}(u\rho C_{ks}) + \frac{\partial}{\partial y}(v\rho C_{ks}) \\ + \frac{\partial}{\partial z}(w\rho C_{ks}) - \frac{\partial}{\partial z}(w_{fks}\rho C_{ks}) \\ = \frac{\partial}{\partial x}\left(\varepsilon_s \frac{\partial(\rho C_{ks})}{\partial x}\right) + \frac{\partial}{\partial y}\left(\varepsilon_s \frac{\partial(\rho C_{ks})}{\partial y}\right) \\ + \frac{\partial}{\partial z}\left(\varepsilon_s \frac{\partial(\rho C_{ks})}{\partial z}\right) \end{aligned} \quad (15-41)$$

where the dimensionless concentration C_{ks} = the ratio of the mass of the size class ks suspended-sediment particles contained in an elemental volume to the total mass in the elemental volume; and w_{fks} = fall or settling velocity of the size class ks suspended-sediment particles.

Equation (15-39) for the size class reads

$$\begin{aligned} \frac{\partial c_{ks}}{\partial t} + \frac{\partial}{\partial x}(uc_{ks}) + \frac{\partial}{\partial y}(vc_{ks}) \\ + \frac{\partial}{\partial z}(wc_{ks}) - \frac{\partial}{\partial z}(w_{fks}c_{ks}) \\ = \frac{\partial}{\partial x}\left(\varepsilon_s \frac{\partial c_{ks}}{\partial x}\right) + \frac{\partial}{\partial y}\left(\varepsilon_s \frac{\partial c_{ks}}{\partial y}\right) + \frac{\partial}{\partial z}\left(\varepsilon_s \frac{\partial c_{ks}}{\partial z}\right) \end{aligned} \quad (15-42)$$

where the volumetric concentration c_{ks} = the ratio of the mass of the size class ks suspended-sediment particles contained in an elemental volume to the elemental volume.

The depth-averaged Eq. (15-40) for size class ks reads

$$\begin{aligned} \frac{\partial(h\tilde{c}_{ks})}{\partial t} + \frac{\partial}{\partial x}(\tilde{u}h\tilde{c}_{ks}) + \frac{\partial}{\partial y}(\tilde{v}h\tilde{c}_{ks}) \\ = \frac{\partial}{\partial x}\left(\tilde{\varepsilon}_s h \frac{\partial \tilde{c}_{ks}}{\partial x}\right) + \frac{\partial}{\partial y}\left(\tilde{\varepsilon}_s h \frac{\partial \tilde{c}_{ks}}{\partial y}\right) + E_{ks} - D_{ks} \end{aligned} \quad (15-43)$$

where

\tilde{c}_{ks} = depth-averaged dimensional (volumetric) concentration of the size class ks particles;

E_{ks} and D_{ks} = the upward sediment entrainment flux and the downward sediment deposition flux for the size class ks particles, respectively.

15.7 SEDIMENT-EXCHANGE PROCESSES

15.7.1 Introduction

As stated in Section 15.6, the near-bed boundary condition for suspended-sediment computations can be either a specified concentration, or a specified exchange between suspended-sediment and bed and near-bed processes. Prescribing the near-bed boundary condition for suspended-sediment computations, i.e., defining the sediment-exchange processes, has proven to be one of the most challenging problems in mobile modeling.

15.7.2 Imposition of Near-Bed Concentration

A number of researchers use the near-bed concentration as a boundary condition for suspended-sediment computations. Examples include Wang and Adeff (1986); Olsen and Melaaen (1993); Olsen and Skoglund (1994); Olsen and Kjellesvig (1998); Brors (1999); Olsen (1999); or Olsen et al. (1999). The near-bed concentration is typically defined as an equilibrium concentration and evaluated using one of the available empirical relations (see Chapter 2 of this manual).

Celik and Rodi (1988) offer a comprehensive critique of using the equilibrium near-bed concentration in nonequilibrium situations. The two authors analyzed equilibrium and nonequilibrium situations based on two relatively simple experiments, both using a wide rectangular channel with a steady uniform flow. The Jobson and Sayre (1970) experiment had a suspended-sediment load, larger than the transport capacity, introduced at the upstream end of a flume with an initially sediment-starved bed. As a result, the upstream portion of the flume saw a nonequilibrium situation with net deposition and a gradual decrease of the suspended-sediment load along the flume, until the transport capacity was reached. The Ashida and Okabe (1982) experiment had clear water at the upstream end of the flume with a sand source on the fixed bed. As a result, the upstream portion of the flume reflected a nonequilibrium situation with net entrainment and a gradual increase of the suspended-sediment load along the flume, again until the transport capacity was reached. In both experiments, an equilibrium situation was achieved asymptotically in the downstream portion of the flume, characterized by an entrainment-deposition balance and no change in suspended-sediment load along that portion of the flume. Both experiments clearly show a significant difference between the actual near-bed concentration in nonequilibrium situations and the equilibrium near-bed concentration. Therefore, imposition of the exchange between the suspended-sediment and the bed and near-bed processes is a preferable boundary condition for suspended-sediment computations in nonequilibrium situations.

15.7.3 Imposition of Near-Bed Sediment Exchange

Exchange between the suspended-sediment and the bed and near-bed processes is defined as the difference between

the near-bed upward sediment entrainment flux E and the corresponding downward sediment deposition flux D . The governing equations for the bed and near-bed processes contain identical exchange terms, but with opposite signs. Therefore, using sediment entrainment and deposition fluxes E and D as boundary condition for suspended-sediment computations also provides a proper coupling between suspended-sediment processes and bed and near-bed processes.

For an equilibrium situation in a wide rectangular channel with a steady uniform flow, eventually achieved in both the Jobson and Sayre (1970) and Ashida and Okabe (1982) experiments, the classical suspended-sediment transport Eq. (15-39) yields

$$w_f c_e + \varepsilon_s \frac{\partial c_e}{\partial z} = 0 \quad (15-44)$$

where

$$c_e = \text{equilibrium concentration.}$$

Equation (15-44), valid at any depth, describes an equilibrium between a downward advective flux due to fall velocity (gravity effects) and an upward diffusive flux due to turbulence.

At some near-bed location, Eq. (15-44) can be written as

$$w_f c_{be} + \varepsilon_s \left. \frac{\partial c_e}{\partial z} \right|_b = D - E = 0 \quad (15-45)$$

where

$$\begin{aligned} c_{be} &= \text{near-bed equilibrium concentration and} \\ \left. \frac{\partial c_e}{\partial z} \right|_b &= \text{near-bed equilibrium concentration gradient.} \end{aligned}$$

Equation (15-45) is the usual starting point in defining sediment entrainment and deposition fluxes E and D . Assuming that Eq. (15-39) offers an accurate enough description of sediment transport in near-bed regions, the relation can be thought of as representing a zero near-bed net sediment exchange for an equilibrium situation. By analogy, the near-bed net sediment exchange for a nonequilibrium situation is then represented as

$$w_f c_b + \varepsilon_s \left. \frac{\partial c}{\partial z} \right|_b = D - E \neq 0 \quad (15-46)$$

where

$$\begin{aligned} c_b &= \text{near-bed nonequilibrium concentration and} \\ \left. \frac{\partial c}{\partial z} \right|_b &= \text{near-bed nonequilibrium concentration gradient.} \end{aligned}$$

In most models that include sediment exchange processes, the near-bed sediment deposition flux D for nonequilibrium situations is defined as a downward advective flux due to the fall velocity, evaluated for the actual (nonequilibrium) near-bed concentration:

$$D = w_f c_b \quad (15-47)$$

The actual near-bed concentration c_b in Eq. (15-47) is derived from the suspended-sediment computations themselves. This approach was used in models described by Shimizu et al (1990); Spasojevic and Holly (1990a; 1990b); Spasojevic and Holly (1993); Jankowski et al. (1994); Minh Duc et al. (1998); Rodi (2000); and Wu et al. (2000). As an extension to this approach, some researchers (e.g., Jankowski et al. 1994) have proposed introduction of a probability factor into the deposition flux in Eq. (15-47) to account for the possibility that some near-bed sediment particles subjected to downward advection due to their fall velocity may be resuspended without reaching the bed.

Defining the near-bed entrainment flux E for nonequilibrium situations is a far more difficult task. Celik and Rodi (1984) and van Rijn (1986) proposed evaluating the entrainment flux using its equilibrium value. Thus, because the equilibrium entrainment flux is equal to the equilibrium deposition flux (Eq. 15-45), the entrainment flux becomes

$$E = w_f c_{be} \quad (15-48)$$

Equation (15-48) implies that the entrainment always occurs at its maximum rate (Celik and Rodi 1988). This approach was used in models described by Spasojevic and Holly (1990a; 1990b); Lin and Falconer (1996); Minh Duc et al. (1998); Rodi (2000); and Wu et al. (2000).

Brors (1999) specified the entrainment flux, as it appears in the Exner equation, in terms of the near-bed concentration and concentration gradient. Spasojevic and Holly (1993) introduced the entrainment flux evaluated as an upward near-bed mass diffusion flux,

$$E = -\varepsilon_s \frac{\partial c}{\partial z} \Big|_a \quad (15-49)$$

where subscript a denotes that the mass-diffusion flux is evaluated at a near-bed point some distance a above the bed surface. Following the basic definition of the derivative, the entrainment flux in Eq. (15-49) is further modeled as

$$E = -\varepsilon_s \frac{c_{a+\Delta a} - c_a}{\Delta a} \quad (15-50)$$

where

c_a = near-bed concentration reflecting the action of near-bed flow on the bed and bed-load particles, whereas

$c_{a+\Delta a}$ = near-bed concentration at distance $a + \Delta a$ above the bed surface, extrapolated from the suspended-sediment computations.

Equation (15-50) implies that the entrainment varies according to both the near-bed concentration of sediment present on the bed and the concentration of suspended sediment possibly carried by the flow from some upstream location. The concentration c_a is evaluated by using an empirical relation for the near-bed *equilibrium* concentration (see Chapter 2 for different empirical relations).

When applied in the context of sediment mixtures and the active-layer concept (Spasojevic and Holly 1993), the entrainment flux has to be modified by β_{ks} to reflect the availability of the size class ks in the active-layer control volume. Then Eqs. (15-49) and (15-50) become, respectively,

$$E_{ks} = -\beta_{ks} \varepsilon_s \frac{\partial c_{ks}}{\partial z} \Big|_a \quad (15-51)$$

and

$$E_{ks} = -\beta_{ks} \varepsilon_s \frac{(c_{ks})_{a+\Delta a} - (c_{ks})_a}{\Delta a} \quad (15-52)$$

In the same context, the corresponding deposition flux, defined as in Eq. (15-47), becomes

$$D_{ks} = w_{fks} (c_{ks})_{a+\Delta a} \quad (15-53)$$

More information can be found in Chapter 3.

15.8 SYSTEM CLOSURE AND AUXILIARY RELATIONS

15.8.1 Introduction

The mass-conservation principles on which the various governing equation sets described earlier are based do not, in themselves, compose a complete mathematical system. There is a further need for additional closure, or auxiliary, relations, often empirical. System closure for sediment processes is highly dependent on the adopted conceptual sediment model and number of sediment processes included in the model. Thus, these issues are presented here through several examples. For convenience, the governing sediment equations for each example are summarized again here.

Most three-dimensional models use Eq. (15-39) as the governing equation for suspended-sediment processes:

$$\begin{aligned} & \frac{\partial c}{\partial t} + \frac{\partial}{\partial x}(uc) + \frac{\partial}{\partial y}(vc) + \frac{\partial}{\partial z}(wc) - \frac{\partial}{\partial z}(w_f c) \\ &= \frac{\partial}{\partial x}\left(\varepsilon_s \frac{\partial c}{\partial x}\right) + \frac{\partial}{\partial y}\left(\varepsilon_s \frac{\partial c}{\partial y}\right) + \frac{\partial}{\partial z}\left(\varepsilon_s \frac{\partial c}{\partial z}\right) \end{aligned} \quad (15-54)$$

The sediment mass-diffusivity coefficient ε_s is typically related to the turbulent eddy viscosity v_t (Brors 1999; Wu et al. 2000) through

$$\varepsilon_s = \frac{v_t}{\sigma_c} \quad (15-55)$$

where

σ_c = turbulent Schmidt number for sediment (often assumed to be unity).

Major differences among models arise from the treatment of bed and near-bed processes. Different approaches to the

treatment of bed and near-bed processes are classified in Section 15.5 into the bed-load-layer approach; the total-load approach; and the active-layer and active-stratum approach (designed for sediment mixtures).

15.8.2 The Bed-Load-Layer Approach

When the van Rijn bed-load-layer approach described earlier is used, the governing equation for bed and near-bed processes becomes Eq. (15-24) (models described by van Rijn 1987 and Brors 1999):

$$\rho_s (1-p_b) \frac{\partial z_b}{\partial t} + \frac{\partial q_{bx}}{\partial x} + \frac{\partial q_{by}}{\partial y} + E_b - D_b = 0. \quad (15-56)$$

The deposition flux D_b is generally formulated through Eq. (15-47) (models described by Spasojevic and Holly 1993; Brors 1999; and Wu et al. 2000):

$$D_b = w_f c_b. \quad (15-57)$$

The entrainment flux E_b is usually formulated through Eq. (15-48) (models described by Lin and Falconer 1996 and Wu et al. 2000):

$$E_b = w_f c_{be}. \quad (15-58)$$

When the bed-load-layer approach is used, the governing equations for sediment processes are the mass-conservation equation for suspended sediment, Eq. (15-54), and the mass-conservation equation for bed-load-layer and bed-subsurface sediment, Eq. (15-56). Primary sediment unknowns are the volumetric suspended-sediment concentration and the bed-surface elevation z_b . Flow-velocity components u , v , and w are the result of flow computations. The actual near-bed nonequilibrium concentration c_b is the result of suspended-sediment computations. All other sediment-related terms in Eqs. (15-54) and (15-56), such as sediment mass-diffusivity coefficient ε_s (i.e., turbulent Schmidt number σ_c), bed-load flux q_b , fall velocity w_f , and the near-bed equilibrium concentration c_{be} , are in general functions of flow variables and primary sediment unknowns and are treated as auxiliary relations, often empirical. In addition, the near-bed equilibrium concentration c_{be} is evaluated at the top of the bed-load layer, so the bed-load-layer thickness h_b must also be specified on the basis of some empirical or other guidance.

15.8.3 The Total-Load Approach

When the total-load approach is used, the governing equation for computing bed-surface elevation becomes Eq. (15-25) (models described by Wang and Adeff 1986; van Rijn 1987; and Wu et al. 2000):

$$\rho_s (1-p_b) \frac{\partial z_b}{\partial t} + \frac{\partial q_{Tx}}{\partial x} + \frac{\partial q_{Ty}}{\partial y} = 0 \quad (15-59)$$

where

$$q_{Tx} = q_{bx} + \int_{h_b}^h \left(u c - \varepsilon_s \frac{\partial c}{\partial x} \right) dz$$

and

$$q_{Ty} = q_{by} + \int_{h_b}^h \left(v c - \varepsilon_s \frac{\partial c}{\partial y} \right) dz \quad (15-60)$$

represent the total-load components combining the bed load with the suspended-load flux (advection and diffusion) integrated from the top of the bed-load layer h_b to the total depth h .

When the total-load approach is used, the governing equations for sediment processes are the mass-conservation equation for suspended sediment, Eq. (15-54), and the mass-conservation equation for bed-subsurface sediment, bed-load-layer sediment, and suspended sediment in the entire water column above the bed-load layer, Eq. (15-59). The primary sediment unknowns are volumetric suspended-sediment concentration c and bed-surface elevation z_b . The sediment mass-diffusivity coefficient ε_s (i.e., turbulent Schmidt number σ_c), bed-load flux q_b , and fall velocity w_f , are treated as auxiliary relations and evaluated through appropriate empirical relations; see for example Chapter 2.

Wu et al. (2000) introduced a modification to the total-load approach to account for nonequilibrium effects on the bed-load transport using Eq. (15-28):

$$\frac{1}{L_s} (q_b - q_{be}) + \frac{\partial (\alpha_{bx} q_b)}{\partial x} + \frac{\partial (\alpha_{by} q_b)}{\partial x} + E_b - D_b = 0 \quad (15-61)$$

where deposition and entrainment fluxes D_b and E_b are the same as in Eqs. (15-57) and (15-58), respectively. With this modification, nonequilibrium bed-load flux q_b also becomes the primary sediment unknown, computed from an additional governing sediment equation, Eq. (15-61). Because direction cosines α_{bx} and α_{by} are known parameters, additional auxiliary relations include equilibrium bed-load flux q_{be} and near-bed equilibrium concentration c_{be} .

15.8.4 The Active-Layer and Active-Stratum Approach—Sediment Mixtures

The active-layer and active-stratum approach (Spasojevic and Holly 1993) uses the following set of governing equations for sediment processes:

The mass-conservation equations for size class ks of suspended sediment (Eq. 15-42):

$$\begin{aligned} \frac{\partial c_{ks}}{\partial t} + \frac{\partial}{\partial x} (uc_{ks}) + \frac{\partial}{\partial y} (vc_{ks}) + \frac{\partial}{\partial z} (wc_{ks}) - \frac{\partial}{\partial z} (w_{jks} c_{ks}) \\ = \frac{\partial}{\partial x} \left(\varepsilon_s \frac{\partial c_{ks}}{\partial x} \right) + \frac{\partial}{\partial y} \left(\varepsilon_s \frac{\partial c_{ks}}{\partial y} \right) + \frac{\partial}{\partial z} \left(\varepsilon_s \frac{\partial c_{ks}}{\partial z} \right) \end{aligned} \quad (15-62)$$

The mass-conservation equation for the size class ks of active-layer sediment (Eq. 15-36):

$$\rho_s (1 - p_b) \frac{\partial(\beta_{ks} h_a)}{\partial t} + \frac{\partial q_{bxks}}{\partial x} + \frac{\partial q_{byks}}{\partial y} + E_{ks} - D_{ks} = 0 \quad (15-63)$$

The global mass-conservation equation for bed sediment, comprising active-layer and active-stratum sediment (Eq. 15-37):

$$\rho_s (1 - p_b) \frac{\partial z_b}{\partial t} + \sum_{ks=1}^{KS} \left(\frac{\partial q_{bxks}}{\partial x} + \frac{\partial q_{byks}}{\partial y} + E_{ks} - D_{ks} \right) = 0. \quad (15-64)$$

where

$$E_{ks} = -\beta_{ks} \varepsilon_s \frac{(c_{ks})_{a+\Delta a} - (c_{ks})_a}{\Delta a} \quad (15-65)$$

and

$$D_{ks} = w_{fks} (c_{ks})_{a+\Delta a} \quad (15-66)$$

are entrainment and deposition fluxes for size class ks sediment, respectively.

The active-layer floor source F_{ks} , again specific to the size class ks , can be expressed using Eq. (15-31). When the active-layer floor (active-stratum ceiling) descends, then

$$F_{ks} = -\rho_s (1 - p_b) \frac{\partial}{\partial t} [\beta_{sks} (z_b - h_a)] \quad (15-67)$$

gives the mass of the size class ks , formerly comprising size fraction β_{sks} of the active-stratum control volume, which becomes part of the active-layer elemental volume. When the active-layer floor (active-stratum ceiling) rises, then

$$F_{ks} = -\rho_s (1 - p_b) \frac{\partial}{\partial t} [\beta_{ks} (z_b - h_a)] \quad (15-68)$$

gives the mass of the particular size class, formerly comprising size fraction β_{ks} of the active-layer elemental volume, which becomes part of the active stratum control volume.

If the sediment mixture in a natural watercourse is represented by a total of KS sediment size classes, KS mass-conservation equations for suspended sediment (one Eq. (15-62) for each size class) can be written for each

elemental volume in the suspension above the active layer. KS mass-conservation equations for active-layer sediment (one Eq. (15-63) for each size class) can be written for each active-stratum elemental volume, and one global mass-conservation equation for bed sediment, Eq. (15-64), can be written for each bed elemental volume (comprising the active-layer and active-stratum elemental volumes). The global set of sediment equations for all size classes, taken as a whole, describes the behavior of a nonuniform sediment, including natural phenomena such as differential settling, armoring, and hydraulic sorting. The following sediment variables are considered primary sediment unknowns: (1) KS suspended-sediment concentrations c_{ks} for each elemental volume containing a mixture of water and suspended sediment; (2) KS active-layer size fractions β_{ks} for each active-layer elemental volume; and (3) one bed-surface level z_b for each bed elemental volume.

The actual near-bed nonequilibrium concentration $(c_{ks})_{a+\Delta a}$ is extrapolated from the suspended-sediment computations. The equilibrium near-bed concentration $(c_{ks})_a$, bed-load flux q_b , active-layer thickness h_a , fall velocity w_f , and sediment mass-diffusivity coefficient ε_s are in general functions of flow variables and primary sediment unknowns and are treated as auxiliary relations. The location a may be evaluated on the basis of some empirical guidance. However, because the parameter Δa has no direct physical interpretation (being defined only for the purpose of estimating the concentration gradient near the bed), both a and Δa are perhaps best considered calibration parameters as discussed in Section 15.11.

The numerical procedure for solution of the sediment equations is formulated without reference to the specific empirical relations that ultimately must be invoked to evaluate the auxiliary relations. This allows use of any suitable empirical relation to evaluate a particular auxiliary relation and renders the formal numerical procedure independent of any specific empirical relation.

The equilibrium near-bed concentration $(c_{ks})_a$ (for size class ks sediment) generally depends on the near-bed flow characteristics. It is evaluated using an appropriate empirical relation, for example that of van Rijn (1984a).

The net bed-load flux is represented here as

$$q_{bks} = (1 - \gamma) \zeta_h \beta_{ks} q_b^t \quad (15-69)$$

where

q_b^t = theoretical bed-load capacity for a bed containing only sediment of the size class ks , evaluated using an appropriate bed-load predictor such as proposed by van Rijn (1984a).

This load is adjusted by ζ_h , a so-called hiding factor accounting for the reduction or increase in a particular

size class transport rate when it is part of a mixture. Empirical relations such as those proposed by Karim and Kennedy (1982) or Shen and Lu (1983) can be used to evaluate ζ_h . The adjusted load is modified by β_{ks} to reflect the availability of the particular size class in the active-layer elemental volume. Finally, the load is modified by $(1-\gamma)$ to reflect the fact that some fraction γ of the particular size-class particles is expected to be transported only as suspended load, with γ typically related to quantities such as the ratio of fall velocity to shear velocity (Rouse number).

The active-layer thickness h_a is evaluated by an appropriate empirical concept of the depth of bed material that supplies material for bed-load transport and suspended-sediment entrainment. Examples are the concepts of Bennett and Nordin (1977); Borah et al. (1982); or Karim and Kennedy (1982).

Depending on the sediment-particle size, different experimental relations can be used to compute particle fall velocity, as described by van Rijn (1984b).

The sediment mass-diffusivity coefficient ε_s is obtained by modifying the turbulent eddy viscosity v_t coefficient to reflect the difference in the diffusion of a discrete sediment particle and the diffusion of a fluid "particle" (or small coherent fluid structure), and also to reflect possible damping of the fluid turbulence by sediment particles, as suggested by van Rijn (1984b).

The equations presented in this section are the basis for the sediment model incorporated in the CH3D-SED code, used in the examples of Sections 15.11.2 and 15.11.3.

15.8.5 Two-Dimensional Models

Because the governing equations for bed and near-bed processes are two-dimensional in plan parallel to the bed surface, the major difference between two-dimensional and three-dimensional models arises from the governing equation for suspended-sediment processes. For example, depth-averaged models use Eq. (15-40), i.e., the depth-averaged form of the mass-conservation equation for suspended sediment (model described by Minh Duc et al. 1998, etc.),

$$\begin{aligned} \frac{\partial(h\tilde{c})}{\partial t} + \frac{\partial(\tilde{u}h\tilde{c})}{\partial x} + \frac{\partial(\tilde{v}h\tilde{c})}{\partial y} \\ = \frac{\partial}{\partial x}\left(\tilde{\varepsilon}_s h \frac{\partial \tilde{c}}{\partial x}\right) + \frac{\partial}{\partial y}\left(\tilde{\varepsilon}_s h \frac{\partial \tilde{c}}{\partial y}\right) + E_b - D_b \quad (15-70) \end{aligned}$$

or, in the case of sediment mixtures, Eq. (15-43), i.e., the depth-averaged form of the mass-conservation equation written for size class ks of suspended sediment (model described by Spasojevic and Holly (1990a; 1990b)),

$$\begin{aligned} \frac{\partial(h\tilde{c}_{ks})}{\partial t} + \frac{\partial(\tilde{u}h\tilde{c}_{ks})}{\partial x} + \frac{\partial(\tilde{v}h\tilde{c}_{ks})}{\partial y} \\ = \frac{\partial}{\partial x}\left(\tilde{\varepsilon}_s h \frac{\partial \tilde{c}_{ks}}{\partial x}\right) + \frac{\partial}{\partial y}\left(\tilde{\varepsilon}_s h \frac{\partial \tilde{c}_{ks}}{\partial y}\right) + E_{ks} - D_{ks} \quad (15-71) \end{aligned}$$

Thus, instead of computing point concentrations, depth-averaged models compute depth-averaged concentrations. The near-bed concentration in deposition flux is typically evaluated through some kind of theoretical vertical concentration profile, e.g., the Rouse profile. Entrainment flux is usually evaluated as an equilibrium entrainment equal to the equilibrium deposition, which, in case of sediment mixtures, has to be modified by β_{ks} to reflect the availability of the size class in the active-layer control volume (Spasojevic and Holly (1990a; 1990b)):

$$E_{ks} = -\beta_{ks} (c_{ks})_a \quad (15-72)$$

All other system-closure considerations are basically the same as for three-dimensional models, of course depending on the bed and near-bed processes approach. Equations (15-71) and (15-72), together with the governing equations for bed and near-bed sediment processes and other closure auxiliary relations presented in Section 15.8.4, are the basis for the sediment model incorporated into the MOBED2 code, used in the example of Section 15.11.4.

An important issue that has achieved relatively little attention in multidimensional model development as of this writing is the inclusion of flow- and transport-dependent form roughness associated with mobile-bed bed forms such as dunes and ripples. As long as computer time and memory requirements restrict models to plan-view discretizations that are too coarse to resolve individual dune topography and movement, models should incorporate appropriate empirical formulations combining bed-material and bed-form roughness. The authors—always optimistic—expect that as computing resources and turbulence-model development gradually permit plan-view grid refinement that can capture bed-form activity in fully three-dimensional models, it will be necessary only to include bed-material roughness formulations, because the larger-scale bed form "roughness" will be captured within the model's own solution for momentum exchange in nonparallel flow.

15.8.6 Additional Considerations in Auxiliary Relations

Although the auxiliary relations described above are necessary for minimal closure, they do not, in themselves, account for many other possible subtle complexities in the physical processes. Considerable past and present research has been devoted to developing a better understanding, and conceptualizations, of these complex processes.

For example, Nakagawa and Tsujimoto (1980) studied bed instability due to lag system between bed-shear stress and velocity, which is composed of two elements: (1) the phase lag between sediment-transport rate and bed-shear stress; and (2) lag distance between sediment transport and flow field over a wavy bed. They evaluated the lag distance of bed-load transport for bed shear stress based on the model for bed-load transport that is applicable to such nonequilibrium situations as when sand waves are initially formed. In addition, the potential flow model of flow over a wavy bed was modified to take into account the effects of flow convergence and divergence. Using these models for flow and bed-load transport, the lag system in a perturbed sand bed was clarified, and the hydraulic conditions for unstable bed, which may correspond to the regimes for dunes or ripples and antidunes, was predicted. Kovacs and Parker (1994) derived a vectorial bed-load formulation for the transport of coarse sediment for up to the angle of repose both in the streamwise and transverse directions. They developed a mathematical model of the time evolution of straight river channels, focusing on the evolution processes due to the bank erosion in the presence of bed load only. Lau and Engel (1999) studied, using dimensional and theoretical analysis, together with available experimental data, how a combination of flow and stream bed slope affects the beginning of sediment transport. Damgaard et al. (1997) performed experiments on bed-load transport on steep longitudinal slopes and formulated a semiempirical relation that predicts the transport rate on horizontal as well mild and steep slopes. Kitamura et al. (1998) studied the influence of vegetation on sediment transport capability in channels.

These brief examples are intended only to give the reader a sense of the kinds of additional complexities that may need to be included in mobile-bed models.

15.9 MOBILE-BED NUMERICAL SOLUTION CONSIDERATIONS

15.9.1 Numerical Coupling of Flow and Mobile-Bed Processes

As of this writing, the simultaneous solution of all governing equations in three-dimensional or even two-dimensional flow and sediment models is not feasible, due to the prohibitive CPU time requirements. Thus, one of the important issues in flow and sediment modeling is how to provide adequate numerical coupling between and among water and sediment processes. In nature, this coupling is between flow and sediment processes in general, as well as between suspended-sediment and bed and near-bed processes. Numerical coupling or uncoupling of these different processes should reflect the nature and importance of the real physical coupling.

Although the flow is the driving force for sediment-transport and bed-evolution processes, the most important sediment feedback to the flow includes bathymetry changes,

changes in the density of water and suspended-sediment mixture, possibly changes in the bed-surface roughness when sediment mixtures are considered, and flow-dependent form roughness associated with bed forms (dunes, ripples). The bathymetry and the bed-surface roughness changes during a time step appropriate for flow computations are usually too small to change the flow domain and flow field significantly. Only the suspended-sediment transport has the same time scale as fluid flow. In most cases, suspended-sediment concentrations in natural watercourses are relatively small and do not change abruptly with time, which suggests that changes in the density of the water and sediment mixture during a time step appropriate to flow computations are generally insufficient to influence the flow field significantly. Therefore, practically all existing two-dimensional and three-dimensional flow and sediment models uncouple water and sediment computations within one time step. Indeed, the same is true for most one-dimensional mobile-bed models. A notable exception is the SEDICOUP one-dimensional mobile-bed model (Holly and Rahuel 1990), which represented an experiment in complete coupling of all flow and sediment processes in an unsteady, multiple-size-class environment.

On the other hand, the nature of the real physical coupling between different sediment processes may preclude their complete numerical uncoupling, even at a scale of one time step. The entrainment and deposition fluxes (sediment-exchange processes) are the link relating suspended- and bed- and near-bed-sediment processes. It is generally agreed that the deposition flux depends on the actual near-bed concentration evaluated from suspended-sediment computations. The entrainment flux depends on the near-bed equilibrium concentration, associated with the bed surface, bed-load layer, or active layer, depending on the adopted conceptual model. Deposition and entrainment fluxes appearing in the governing equations for bed and near-bed processes are also commonly used as near-bed boundary conditions for suspended-sediment processes.

The active-layer and active-stratum approach associated with sediment mixtures (Spasojevic and Holly (1990a; 1990b; 1993)) emphasizes the need for some level of numerical coupling between suspended-sediment processes and bed and near-bed processes. Whereas the deposition flux in Eq. (15-66) depends on suspended-sediment concentration, the entrainment flux in Eqs. (15-65) and (15-72) depends on the size-class fraction of active-layer sediment. Therefore, models described by Spasojevic and Holly (1990a; 1990b; 1993) are structured to allow for iterative coupling between suspended-sediment and bed and near-bed sediment processes. The mass-conservation equations for bed and near-bed processes are solved by assuming the suspended-sediment concentration, and therefore the deposition flux, to be known from the previous iteration. An improved estimate of active-layer size fractions and the bed-surface elevation is thus obtained. The mass-conservation equations for

suspended-sediment processes are then resolved for the same computational time step, by assuming the active-layer size fractions, i.e., entrainment flux, to be known from the bed and near-bed processes computations. The whole procedure is repeated iteratively until a convergence criterion is satisfied.

Finally, in the case of active-layer and active-stratum concepts associated with sediment mixtures (Spasojevic and Holly 1990a; 1990b; 1993), the governing equations for bed and near-bed sediment processes require simultaneous solution to satisfy the basic requirement that the sum of all size-class fractions is equal to unity. Application of a chosen numerical method to discretize the global mass-conservation equation for bed sediment (Eq. (15-64)) and the mass-conservation equation for active-layer sediment (Eq. (15-63)) yields a system of nonlinear algebraic equations. The discretized (nonlinear algebraic) equations to be solved simultaneously for the same point at the bed are (1) one discretized global mass-conservation equation for bed sediment and (2) K_S discretized mass-conservation equations for active-layer sediment. Solution using, e.g., a Newton-Raphson iterative procedure yields (1) one bed-surface elevation and (2) K_S active-layer size fractions.

15.9.2 Choice of Numerical Method for Mobile-Bed Processes

Because a mobile-bed model is typically built into an already existing hydrodynamic model, the basic choice of numerical method for solving the sediment equations usually follows the choice of numerical method for solving flow equations. In certain cases, this is the only available possibility. For example, if the hydrodynamic model uses the finite-element method with an unstructured grid, it is impossible to use a finite-difference method to solve the sediment equations on the same grid. However, it would appear theoretically possible to allow the numerical method for solving the sediment equations to be different from the one used for solving the flow equations. For example, hybrid or split-operator approaches, which use different numerical methods to solve different parts of the same equation, have proven to yield satisfactory numerical solutions. To the extent that the numerical method for sediment equations can be independent of the method used for the flow equations, one can consider the possibility of developing an independent mobile-bed module, which could be used with different hydrodynamic modules. The numerical method for such an independent mobile-bed module would have to be able to support both structured and unstructured grids, which limits the basic choice to either the finite-element or the finite-volume method.

Existing two-dimensional and three-dimensional flow and sediment models use a variety of numerical methods. The finite-element method is used in models reported by Thomas and McAnally (1985); Wang and Adeff (1986); Brors (1999); Jia and Wang (1999); and the RMA-10

model at the Coastal and Hydraulics Lab, U.S. Army Corps of Engineers. Models reported by Shimizu et al. (1990), Spasojevic and Holly (1990a; 1990b), Spasojevic and Holly (1993), and Lin and Falconer (1996), use the finite-difference method. The model reported by Jankowski et al. (1994), i.e., that in Hervouet and Bates (2000), uses a split-operator approach with the method of characteristics used for advection processes and the finite-element method used for the remaining processes. Models reported by Olsen and Melaaen (1993), Minh Duc et al. (1998), Olsen et al (1999), and Wu et al. (2000) use the finite-volume method associated with a structured grid. As of this writing, no flow and sediment model has been known to use the finite-volume method with an unstructured grid. Advantages and disadvantages of methods associated with structured versus methods associated with unstructured grids have already been discussed in Section 15.3.

It should be noted that the finite-difference method is applied to the governing equations in Cartesian coordinates only in special cases with simple geometry. Models that use the finite-difference method typically require that the governing equations be transformed into curvilinear or body-fitted coordinates to accommodate complex geometries, usually associated with natural watercourses. Models that use the finite-volume method on a structured grid, and thus do not exploit the full potential of the method, also require that the governing equations be cast into in curvilinear coordinates.

Most numerical problems (instability, oscillations, etc.) in solving unsteady flow and sediment equations are caused by advection terms, especially in the case of sharp-front waves. Therefore, the advection terms in the governing flow and sediment equations may require special treatment, usually involving a numerical method that takes into account the hyperbolic nature of advection.

Existing two-dimensional and three-dimensional flow and sediment models typically do not anticipate the existence of bores or moving hydraulic jumps and have no special treatment for advection terms in flow equations. Exceptions include the TELEMAC-3D code, as described by Jankowski et al. (1994) or Hervouet and Bates (2000), which uses the method of characteristics for the momentum advection terms in the flow equations. The bed-load term in the governing equations for bed and near-bed processes, if one considers it as an equivalent advection term, is numerically benign due to the slow nature of the bed-load movement. However, suspended-sediment transport is likely to encounter a sharp-front wave situation. Examples include a postdredging resuspension in the form of a point source, extensive sediment entrainment behind a river-training structure such as a chevron dike, or simply extensive sediment entrainment due to incorrect initial and boundary conditions for sediment.

Several existing two-dimensional and three-dimensional flow and sediment models include special treatment of the advection terms in the suspended-sediment transport equation. For example, the TELEMAC-3D code, as described by

Jankowski et al. (1994), and the MOBED2 code (Spasojevic and Holly 1990a; 1990b), use a split-operator approach combined with the method of characteristics for the advection term in the suspended-sediment transport equation. The CH3D-SED code, as described by Spasojevic and Holly (1993), uses the QUICKEST scheme (Leonard 1979), whereas the model described by Lin and Falconer (1996) uses a modification, called ULTIMATE QUICKEST, of the same scheme, to discretize the suspended-sediment transport equation.

15.9.3 Grid-Generation and Adaptive-Grid Issues in a Mobile-Bed Environment

Grid generation was an important issue in the 1980s and early 1990s, when most two-dimensional and three-dimensional modelers had to develop their own grid-generation programs. Most two-dimensional and three-dimensional sediment modelers now use commercial grid-generation software. As of this writing, the grid-generation software associated with computational fluid dynamics applications (aerodynamics, auto industry, ship hydrodynamics, etc.) is quite sophisticated, but typically accepts geometry input files in specific formats, usually generated by design-support software. The grid-generation software associated with computational hydraulics applications, even though less sophisticated, is generally designed to accept the random geometry data associated with field-data collection for natural watercourses.

On the other hand, adaptive grid technology is currently quite an important issue in mobile-bed modeling. Because mobile-bed modeling typically assumes unsteadiness, both free-surface water elevation and bed-surface elevation are dynamically moving boundaries to which the three-dimensional grid has to adapt at each computational time step. The moving free-surface water elevation, usually being nearly horizontal, poses less of a problem than the moving bed-surface elevation, which presents a real challenge. To begin with, the bed surface has a naturally irregular shape, occasionally modified by man-made hydraulic structures such as river-training structures (weirs, lateral or L-shaped dikes, chevrons, bridge piers, etc.). Furthermore, bed-surface elevation changes may be quite uneven throughout a model domain. Newly installed hydraulic structures may cause extensive and rapid local bed-surface elevation changes, e.g., erosion behind the chevron dike followed by accompanying deposition further downstream. Long-term bed-surface elevation changes, such as river meandering, are slow but can accumulate significantly in time.

As of this writing, general treatment of the adaptive-grid problem in three-dimensional flow and sediment models is in the early stages of development. The most important adaptive grid issue in mobile-bed models arises from bed-elevation changes that require grid adaptation in the vertical direction. Most of the existing three-dimensional flow and

sediment models keep the third coordinate direction straight and vertical, making it relatively easy to deal with bed-related adaptive-grid issues. For example, the CH3D-SED model, as described by Spasojevic and Holly (1993), uses a simple partial coordinate transformation, called σ -stretching, for the vertical coordinate direction. The vertical σ -stretching allows for simple redistribution of a fixed number of computational points along the depth at each time step. Grid adaptation in fully three-dimensional hydrodynamic models that do not rely on a straight vertical coordinate has not been fully addressed, either for hydrodynamic or for mobile-bed applications.

The roles of grid refinement and grid sensitivity in the quality of mobile-bed modeling have gotten rather short shrift, especially compared to the attention devoted to these considerations in computational fluid dynamics and fixed-bed computational hydraulics. D. A. Lyn (personal communication, 2002) has aptly posed a number of relevant questions, to wit,

- Should the grid simply be as fine as the budget allows?
- To what extent is it reasonable to accept a coarse grid in one direction, and a fine grid in the other directions?
- Is a coarse-grid high-dimensional (three-dimensional) model solution always better than a fine-grid low-dimensional (two-dimensional) model with more schematic empirical input?
- Can a coarse grid yield misleading results?
- Can a coarse (horizontal) grid be used for a nonhydrostatic problem where rapidly varied flow prevails?
- Are grid-independence tests necessary and practical?
- Does one just choose a grid and accept the fact that details finer than the grid simply cannot be resolved?
- Can/should one accept calibration as a means of working around a coarse-grid limitation?

The easy answer to all of these questions is “it depends.” As mobile-bed modeling development and practice mature, these issues will surely attract more careful attention and hopefully lead to a body of literature and acquired wisdom that respond at least partly to the above questions.

15.10 FIELD DATA NEEDS FOR MODEL CONSTRUCTION, CALIBRATION, AND VERIFICATION

15.10.1 Field Data for Model Construction

Both two- and three-dimensional models require essentially the same type of bathymetric and geometric data to provide a basic description of the physical domain. An initial bed elevation must be assigned at every grid intersection, node, or spatial element of the plan-view computational mesh of a model, two-dimensional or three-dimensional.

It obviously would not be feasible first to lay out the computational mesh, identify the geographical coordinates of

every point requiring an initial bed elevation, and then visit each location in the field to determine the elevation. In reality, one first obtains the best available “mapping” of the bathymetry through spot elevations, generally taken from a moving vessel with GPS positioning technology, and describing the bed-surface bathymetry at a scale appropriate for the anticipated density of the computational mesh. For example, if it is expected that the mesh will resolve plan-view details at a scale on the order of 10 m, then the density of spot elevations taken in the field should be such that significant bed features of a scale of 10 ms or larger can be captured.

Once the actual computational mesh is laid out, the measured spot bed elevations are projected onto the required grid or nodal points. This is done through two-dimensional curve-fitting techniques, by which a two-dimensional curvilinear surface is appropriately fit to the data points, and then grid elevations are extracted from the fitted surface.

In a mobile-bed modeling context, these bed elevations so painstakingly and expensively obtained are nothing more than the initial conditions set for further evolution during the model simulation runs. In this sense, the initial bed elevations do not have the sacred, absolute character they are given in a fixed-bed model. Indeed, the initial bed-elevation data may reflect the movement of dunes several meters high, and an individual dune elevation is not necessarily representative of the bed area associated with a given computational mesh point. In some sense, the initial bed elevations can even be thought of as subject to calibration, and thus grid-dependent, if not model-dependent. If the bed elevation (and associated initial bed sediment size distribution; see further on) assigned to a grid point does not represent a quasi-equilibrium with the model’s hydrodynamic and sediment equations, then the model will respond with rapid scouring (or deposition) in the first few time steps of the mobile-bed simulation, and the initial elevation may have to be adjusted accordingly. If it were feasible to obtain long-term time-averaged bed elevations on a network of points, thus averaging out the influence of dune movement, this would likely reduce, but probably not eliminate, the need for adjustment of initial elevations.

This approach to obtaining initial bathymetry is somewhat different from the traditional one used for one-dimensional river modeling. For backwater and flood-propagation river modeling, the general practice was to obtain transects, or cross sections, of the river channel, each associated with a single one-dimensional computational point. This historical practice was driven not only by its logical correspondence with one-dimensional model needs, but also by the practical pre-GPS need to identify position on a river with reference to distance along a well-defined transect anchored at surveyed points on the river banks. Multidimensional modeling, in contrast, makes good use of developments such as multibeam technology and GPS positioning for more general, off-transect bathymetric data acquisition.

Bed bathymetry must be complemented by geometric descriptions of any structures in the domain of interest. Such structures might include river-training works (submerged or emerged dikes, etc.), bridge pier bases, or hydraulic structures such as weirs, dams, or intake works. In two-dimensional modeling, a plan-view description of the boundaries of such structures may be sufficient. But for three-dimensional modeling, the complete three-dimensional description of the structural surfaces in contact with the flow domain must be obtained with precision at least consistent with the spatial scale of the computational mesh, especially in the vertical. For example, if the mesh is expected to have 10 vertical elements in the vicinity of the structure, then the details of the structure’s wetted surfaces must be described geometrically in sufficient detail to be resolved at 10 points in the vertical.

15.10.2 Model Initialization

Initial conditions for water and sediment are far more important in mobile-bed modeling than in fixed-bed applications. In a fixed-bed environment, initial discharges and water-surface elevations must be assigned, but they quickly wash out of the model as boundary-condition influence takes over. Fixed-bed initial conditions can be quite arbitrary without affecting the simulations results of interest.

As is illustrated in the examples at the end of this chapter, mobile-bed models are usually started up in a fixed-bed mode. Somewhat arbitrary initial hydrodynamic conditions (water-surface elevations and velocities or unit discharges, often for horizontal, nil flow) are specified. Then the model is run with fixed bed for a sufficiently long period for the arbitrary initial condition to wash out or stabilize under fixed boundary conditions. At the end of this stabilization period the model should have nearly attained a viable steady-state hydrodynamic solution. Sudden imposition of the inflow boundary conditions on a zero-flow situation may cause unacceptable “sloshing,” including bed uncovering, causing the computation to fail. Such a situation may require a more careful initial condition, or perhaps a progressive phasing in of the boundary inflows, as is the case in purely fixed-bed models.

The initial conditions for sediment must be handled with a great deal of care, because the bed elevations themselves are subject to change through interaction with the initial conditions. Initial sediment conditions fall into three categories: suspended-load concentrations, bed-material size distribution, and subsurface-material size distribution. It should be noted that the following guidelines, driven by the authors’ experience with multiple-size-class models, reflect the special challenges of model initialization for nonuniform sediments. Initial-condition specification for a single-size-class model is considerably less challenging.

15.10.2.1 Suspended-Sediment Initial Conditions The initial conditions for suspended sediment comprise

concentration of each size class at each computational point of the two- or three-dimensional grid. These obviously are depth-averaged concentrations in a two-dimensional model, and point concentrations in a three-dimensional model. Because the time scale of movement of suspended sediment is relatively short (as is the time scale of movement of water through the model), a model is generally fairly forgiving of initial suspended-sediment conditions that may not be in equilibrium with the flow, bathymetry, bed-material size distribution, and inflow boundary conditions. The initial suspended-sediment mass advects out of the system fairly quickly, as boundary-condition suspended-sediment inflows progressively influence the model from upstream to downstream.

Of course the suspended sediment does interact with the bed during this washout process, so the initial concentrations must be assigned with reasonable care. For example, if the initial condition specified a grossly exaggerated suspended-sediment load for one or more size classes, that load will tend to be deposited quite quickly and influence the bed elevations in an unrealistic way during the sediment startup period. Similarly, an initial condition of clear water may provoke excessive entrainment from the bed in the sediment startup period as the model seeks to establish a local equilibrium between the water column and the bed material. A reasonable starting procedure is to consider inflow boundary and/or interior suspended-sediment size distributions, vertically and horizontally, and assign them to the model's interior vertical grid lines in a logical fashion. This might involve assigning some sort of average concentration values, based on all available measurements throughout the domain, as initial conditions. An alternative could be to assign average concentrations for subdomains, for example, if there are clear differences in concentration between the main channel and lateral channels. If the boundary inflow concentrations by size class are reasonable to begin with, then the initial suspended-sediment startup period should proceed smoothly, with minimal bed-elevation or bed-composition changes provoked by the suspended-sediment initial condition.

15.10.2.2 Bed-Surface Material Initial Conditions

The initial conditions for bed-material composition comprise the size distribution (fractional representation of each size class in the model) at each computational grid point, or each computational cell, on the bed. It has been the authors' experience that this initial-condition assignment is quite delicate and unforgiving of casual treatment. Indeed, if the assigned initial bed-material size distribution does not reflect an approximate equilibrium condition given the initial hydrodynamics, bathymetry, and initial suspended-suspended concentrations, then the model will tend to adjust toward equilibrium (as defined by its own intrinsic sediment relations) quite rapidly, and this can cause excessive erosion or deposition in the first few time steps. For example, if the initial bed material distribution at a grid point contains a high fraction of fine silt, and yet there is no fine silt in

suspension, but the initial water velocities and shear stresses are relatively large, the model may call for a large entrainment of fine silt into the water column in the first few time steps. Through the bed-sediment conservation laws, this may result in a large, and unrealistic, erosion of the bed at the particular grid point, essentially distorting the user's assigned initial condition for bed elevations and possibly causing subsequent model failure.

Because the initial bed-sediment size distribution is generally based on, if not taken directly from, actual field measurements, one is tempted to expect that as long as the truth as represented by the field data is assigned to the model, the above scenario of excessive bed adjustment should not occur. However, as is brought out in the examples of Section 15.11, field observations of bed-material size distribution are necessarily quite sparse. The bed-material size distribution assigned to a single computational grid point is implicitly assumed to be representative of the bed material on the entire portion of the bed associated with that grid point. On the other hand, an individual field sample may or may not be representative of an equivalent portion of bed surrounding it. The sample may have been taken from the top of a transient dune as it moved through, or from a briefly exposed lens of fine material, or from a local accumulation of gravel exposed only intermittently as dunes move across it. Whereas in nature the water-sediment response to the local bed-material size distribution remains local, in the model "local" is defined by the plan-view of the computational grid around that point, and therein lies the difficulty in assigning sparse field observations to computational grid points.

Field bed-material samples should be used to make an overall assessment of what appears to be the average bed-material composition in the computational domain, or subdomains, if there are clearly distinct geomorphological regions. Initial model response to average bed-material distributions will suggest the possible need to modify the initial bed-material distribution locally to achieve a nearly equilibrium situation in the initial condition. In this sense, one essentially needs to calibrate, or adjust, the initial bed-material distribution to achieve a benign model startup. This approach obviously presumes that the startup situation is not one of major dynamic change; if this were the case, an extremely detailed set of initial bed-material distributions, i.e., at subgrid scale, would be required.

15.10.2.3 Subsurface Strata Initial Conditions

The initial conditions for subsurface bed material comprise specification of the thickness of each subsurface stratum and its sediment size distribution below each bed computational point or cell. This initial condition specification can obviously be quite onerous, and may or may not be important, depending on the problem under study and the nature of the bed material. For example, if it is anticipated that only persistent deposition will occur in the region under study, then

there is no need to specify the subsurface structure, because it will never be susceptible to entrainment through contact with the water column. Similarly, if the anticipated maximum depth of erosion in the region under study is such that the bed material is known to be essentially homogeneous to that depth, a single, infinitely deep subsurface stratum having the same size distribution as the initial bed-surface material may be sufficient. But in a general case in which there may be successive cycles of erosion and deposition, and/or the erosion is expected to progress through multiple strata of differing composition (e.g., historical lenses of deposition), the subsurface structure under each bed computational point or cell must be specified with care. Indeed, if erosion progresses into a layer having a size distribution that is markedly finer than that of the material initially above it, the model may display rapid erosion of this layer, and it is important that this be physically realistic and not the result of a careless assignment of excessively fine material to a subsurface layer. Similarly, a very coarse subsurface layer, physical or otherwise, will have a tendency to arrest further erosion.

15.10.3 Hydrodynamic and Sediment Boundary Conditions

The hydrodynamic boundary conditions for a mobile-bed model are the same as those required for a fixed-bed model, i.e., generally the water-surface elevation at model outflow boundaries, and unit discharges (two-dimensional model) or three velocity components (three-dimensional model) at all model inflow boundaries. Depending on the particular hydrodynamic model framework, additional combinations of levels, local velocities/unit discharges, or relations between them may be imposable.

Suspended-sediment boundary conditions comprise specifications of the suspended-sediment concentrations, by size class, at all model inflow points. For a two-dimensional model, these are depth-averaged concentrations; for a three-dimensional model, these are concentrations at every grid point in the plane of the inflow boundary.

A special consideration here is that in a model having strongly unsteady hydrodynamics, for example, a tidal model with a reversing flow boundary or even a riverine model with possible reversing flow during strong transients, a boundary may be outflow or inflow at different times during the simulation. Whenever inflow occurs at such a boundary, a corresponding suspended-sediment inflow condition must be assigned.

The inflow suspended-sediment concentrations for three-dimensional models, generally simulating a relatively short portion of a hydrograph, are taken from whatever suspended-sediment measurements are available for the discharges under study. For longer-term two-dimensional modeling, the time-varying suspended-sediment inflow concentrations must be generated from presumed suspended-sediment rating curves applied to a time-dependent inflow hydrograph.

As increases in computing speed lead to the opportunity to make truly unsteady three-dimensional simulations (e.g., for one or more hydrographs), it will become important to acquire truly unsteady sediment-inflow boundary conditions.

As of this writing, few attempts have been made to measure the time history of suspended-sediment concentrations during an unsteady-flow event. However, current efforts by the U.S. Agricultural Research Service and others are leading to a better understanding of how suspended-sediment concentrations vary during a flood event, and such improved understanding should play an important role in setting unsteady inflow boundary conditions for suspended sediment.

The nature of bed-sediment boundary conditions depends on the model formulation. For example, in the authors' two- and three-dimensional models, the formulations are such that bed-sediment inflow boundary conditions comprise specification of the bed-material size distribution at each bed computational point or cell at an inflow boundary. In other formulations, the bed-material inflow condition may be bed-load flux by size class or other equivalent quantity. Inflow bed-material size distributions generally can only be deduced from existing field measurements of bed-material size, the same as used for initialization of the bed material as described above. Inflow bed-load fluxes are difficult to measure, and are more likely deduced from one or another empirical bed-load predictor known, or calibrated, to be applicable to the site under study.

Subsurface strata require no boundary conditions per se, because their interactions are limited to exchanges with the strata immediately above and below during deposition and erosion.

15.10.4 Hydrodynamic and Mobile-Bed Calibration and Verification

Mobile-bed model calibration and verification are considerably more challenging and elusive than their fixed-bed counterparts. The complex interactions between hydrodynamic and sediment processes, combined with the highly heterogeneous nature of field observations, make it extremely difficult to isolate, or target, the individual processes and associated empirical coefficients subject to adjustment. This is in contrast to fixed-bed modeling, in which the general reliability and accuracy of the Reynolds averaged-flow equations, combined with appropriate turbulence models, leave characterization of the bed roughness as the primary calibration target. Even the bed-roughness target becomes more elusive in a mobile-bed context, because the roughness comprises the bed composition itself, including flow-dependent bed forms, both intimately coupled with the flow hydrodynamics as well as sediment properties.

For sediment processes, three levels of calibration can be identified. One level is the very discretization of sediment into

appropriate size classes, because model response depends on the degree of resolution, i.e., the number of size classes and the representative particle diameter assigned to each. A second level, having no real counterpart in fixed-bed modeling, is the selection of auxiliary empirical relations most suited to the particular area under study. Such relations can include the bed-load predictor, the suspended-sediment entrainment predictor, the fall velocity predictor, and the bed-roughness characterization, as outlined in previous sections. The third level comprises adjustable parameters within the adopted auxiliary relation. For example, one might choose to use the van Rijn formulation for estimation of near-bed equilibrium concentration, and then be faced with the need to choose an appropriate value of the near-bed distance, which is a critical parameter in that formulation. How does one choose discretizations and relations and parameters at these three levels as part of the calibration process, especially in view of the fact that all three levels interact with each other?

There is no universal answer to this question. A particular size-class discretization and set of auxiliary relations and their associated parameters may not be unique; several different sets may produce equally viable mobile-bed response in a given problem. Ultimately one must simply rely on the not-so-tired notion of good engineering judgment.

The discretization of nonuniform sediment into size classes is driven by the need to achieve resolution as high as possible within the constraints of computational time, and judgment as to the role that the finest and coarsest sediment represented in the field may, or may not, play in the problem under study. Collapsing two or more traditional sediment types (e.g., silt and fine silt) into a single size class with a single representative particle diameter may need to be revisited during the calibration process to ensure that the collapsing and choice of representative diameter does not, in itself, influence the overall mobile-bed response being studied—it is in this sense that the size-class discretization is very much a calibration issue, as is the assignment of initial bed-material composition discussed earlier.

The choice of auxiliary relations should be guided first and foremost by an assessment of the likelihood that a given relation is valid for the particular area under study, based on previous studies and/or similarities between the study site and the conditions under which auxiliary relations were developed. For example, the bed-load predictor adopted for a particular model study ought to be one that might be adopted for general use at that site, based on published information and experience at that site and elsewhere. Still, during the calibration process, it may prove necessary to modify standard parameters in that predictor, or indeed adopt an alternative one based on model response in early trial runs.

Even if one accepts that there is no unique, or best, set of auxiliary relations and their parameters for a given discretization, how does one know that a given set is acceptable in the context of calibration? The situation is quite unlike fixed-bed modeling, in which, for example, measured water-surface

slope, local or global, and perhaps measured local two- or three-dimensional velocities can be used as specific targets for adjusting bed roughness. It is far more difficult to identify individual response indicators in mobile-bed modeling. Imagine that a model's prediction of suspended concentration of a certain size class is an order of magnitude different from available field measurements at a particular location. Is this because of uncertainty arising from the chosen empirical auxiliary relations such as the fall-velocity predictor, suspended-load entrainment formulation, and bed-roughness predictor and their parameters? Or is it perhaps because of the sparseness and natural variability of available field data, which makes it difficult to assign an appropriate initial bed-material composition and/or choose a representative sediment size-class discretization?

Similarly, imagine that a model is showing what appears to be excessive scour at a certain location. What are the roles of the initial bed-material composition, the bed-load predictor, and the suspended entrainment function parameters in these predictors and functions, or the sediment discretization in causing this excessive scour?

These questions point to the need for sensitivity/uncertainty analyses to determine the range of influence of empirical relations on simulation results. They also point to the need for careful engineering judgment in dealing with sparse and stochastic field data, and/or the need for more comprehensive and detailed field data collection efforts.

Regarding calibration/verification of empirical auxiliary relations, it is generally impossible to associate a particular model response with a particular formulation or parameters within it. The only alternative appears to be one of seeking a self-consistent set of relations and parameters, guided by good judgment for the site under study, such that the overall model response conforms to reasonable expectations based on past experience. The overall response indicators most easily observed are bed-elevation changes, changes in bed-material composition, total suspended load concentrations, overall water-surface slopes, etc. A self-consistent set of relations and parameters, with the associated sediment and grid discretization and initial and boundary conditions, is one for which the model persists in a known flow-sediment quasi-equilibrium for some time into the future (if only a few days) with no major changes to bed elevation, total concentrations, bed-material composition, etc.

Another way of looking at this is to say that a self-consistent model, when run some time into the future, will continue to display the same range of variability of observable features (e.g., bed-material composition) that are characteristic of the site from previous observations. Then, when the model is used to study, e.g., structural modifications or long-term response to changes in the hydrologic and sediment-inflow imposed on the area under study, one can have some confidence that the model response is a valid one because it is a self-consistent (but perhaps not unique) representation of the physical site.

15.10.5 Special Considerations Regarding Acoustic-Doppler Current Profiling Velocity Data

Acoustic-Doppler current profiling (ADCP) techniques have become quite popular. They offer a combination of accuracy, ability to measure local velocities in three coordinate directions, and rapid field deployment and use.

However, the authors and their colleagues have found that use of ADCP measurements to provide boundary-condition and calibration/verification velocity fields for three-dimensional mobile-bed models must be cautious and mindful of the error that can be induced when the measurements are taken from a moving boat. The need for this caution is based on the experience and analyses reported by Morlock et al. (2002) and Muste et al. (2004a; 2004b).

15.10.6 Field Data—What Is the Truth?

In the field of computational hydraulics, both developers and users tacitly accept the notion that measured field data represent some sort of “truth” to which model results should aspire. As legitimate as this viewpoint may be in the abstract, in practice it has to be tempered by careful consideration of the temporal and spatial scales that a model is capable of resolving.

A numerical model cannot resolve hydrodynamic or mobile-bed processes at spatial or temporal scales finer than those of the computational grid. The computational grid resolution is constrained by computer memory and time limitations on one hand, and by numerical stability and convergence constraints on the other.

Because solvers of two-dimensional and three-dimensional mobile-bed models generally have both implicit and explicit features, numerical stability generally requires that the time step be constrained by a Courant-type criterion. In most applications a horizontal grid scale on the order of 10 m implies a maximum time step on the order of 10 s. Although one could, in principle, work with much smaller spatial and temporal scales, this is generally impractical due to computer memory and processor limitations.

Therefore mobile-bed codes do not generally resolve turbulent motions of scales smaller than the order of 10 m or 10 s or bed forms smaller than the order of 10 m, for reasons of grid resolution alone. Even if the grid scales were sufficiently small to resolve such features, it is doubtful that the mathematical formulations or numerical procedures of models available as of this writing could resolve the flow separation and turbulent moment exchange associated with such features.

Comparison of suspended-sediment data with model predictions is subject to similar problems of reconciliation of scales. Figure 15-4 shows a comparison of measured and computed fine-sand profiles across a river at a particular transect. Although the suspended-sediment samples necessarily represent a certain time-averaging (on the order of

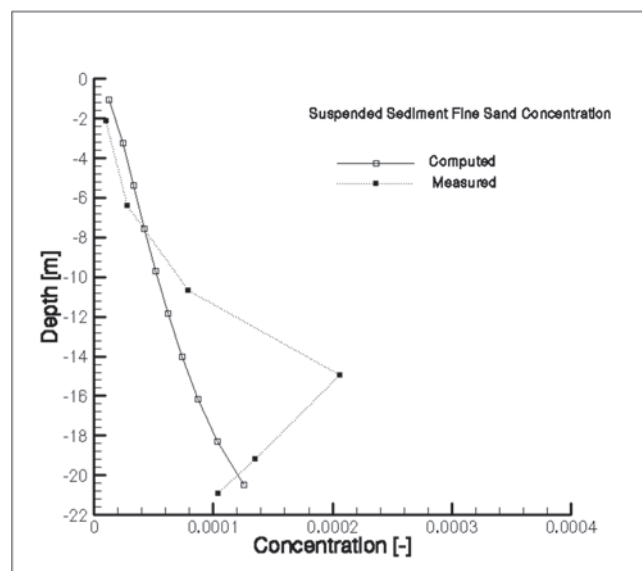


Fig. 15-4. Computed and measured suspended-sediment concentrations (fine sand).

several seconds) at a well-defined stationary vertical profile, one can still observe the kind of nonmonotonic behavior in the measured data that suggests the existence of large-scale variability (probably associated with large eddies or possibly with dune migration) that cannot be resolved by the numerical model. Therefore one cannot conclude, from this comparison alone, that the model’s suspended-sediment profiles are or are not correct in their detailed structure.

Similar attention was focused on the issue of the appropriate initial bed-material size distribution in the model, as has been discussed earlier in Section 15.10.4. In this study, dozens of grab-samples of bed material were available in the study reach, and additional grab-sample thalweg data was available from a previous study.

Clearly several of the measured size distributions, although undoubtedly representative of “the truth” at the time and location they were taken, were not representative of the general area of the river at the spatial scale resolvable by the model. These samples may have been representative of the portion of a dune from which they were taken, or perhaps of lenses of finer material moving through the system, but were clearly not representative of a quasi-equilibrium bed condition representative of most of the width of the river over several hundred meters of length. This conclusion was driven by the fact that the mobile-bed model generates excessive and unrealistic scour in the first few time steps if the initially imposed bed-material distribution is unrealistic, or not nearly in equilibrium, with the hydraulic characteristics of the river in that vicinity.

Of course the “satisfactory” or “true” initial bed-material size distribution is also dependent on the particular bed-sediment entrainment algorithm in the model. Does this

suggest that the “truth” in field data must also be interpreted in light of the model’s sediment-mechanics formulations?

The problem of reconciling the needs of field data collection with the needs of numerical models is not a new one. Even in one-dimensional modeling, the need for measurements of time-varying stages and discharges is still too seldom recognized when field data programs are designed and executed. Now that three-dimensional modeling has entered the realm of engineering practice, study managers and modelers must work together to ensure that data-collection efforts are aimed at collecting and/or processing data resolved at temporal and spatial scales that are meaningful to the model’s grid resolution. Judgments as to the validity and accuracy of numerical predictions must be conditioned by a realistic view of the scales and processes that a model can and cannot be expected to resolve, given its mathematical formulation and grid constraints. The “truth” is relative in this context: relative to the model’s framework, and to the accuracy of the field-data. With regard to the latter, it is important to keep in mind that just like model results, field data are also subject to errors in collection, analysis, and reporting, and thus must also be interpreted and assessed carefully in the context of their use in an overall modeling effort.

15.11 EXAMPLES

15.11.1 Introduction

The purpose of this section is to present a few examples of multidimensional mobile-bed modeling. These are necessarily based on the authors’ own experiences and are intended to illustrate the scope, challenges, and possibilities of such modeling and to give the reader a sense of the kinds of problems to be anticipated. Section 15.11.2 describes application of the three-dimensional mobile bed model CH3D-SED to an analysis of sediment dynamics at the Old River Control Complex on the lower Mississippi River. Section 15.11.3 describes the application of CH3D-SED to the study of river habitat restoration measures on the Leavenworth Bend of the Missouri River. Section 15.11.4 describes application of the two-dimensional mobile-bed model MOBED2 to the prediction of reservoir sedimentation in three flood-control reservoirs in Iowa.

15.11.2 Old River Control Complex, Mississippi River

15.11.2.1 Background The Old River Control Complex is located on the lower Mississippi River about 300 km upstream of New Orleans, in the state of Louisiana and adjacent to the state of Mississippi. Figure 15-5 shows the general layout of the site, which has an interesting and complex history as described by Tuttle (unpublished manuscript, 1998).

Prior to the fifteenth century, the Red River flowed generally parallel to the Mississippi, continuing independently

to the Gulf of Mexico. In the fifteenth century a westward meandering loop of the Mississippi broke into the basin of the Red River and captured it, also intersecting a south-flowing distributary of the Red currently known as the Atchafalaya River. Through time, and in response to both artificial cut-off construction and log-raft clearing, the Red came to flow directly into the Atchafalaya and henceforth to the Gulf of Mexico, but with a connecting channel to the Mississippi known as the Old River. Bidirectional flow occurred in the Old River according to hydrological and hydraulic conditions in the adjacent river systems.

After World War II, it became apparent that the increasing natural diversion of the Mississippi flow into the Atchafalaya channel through the Old River would begin to threaten the geomorphic viability of New Orleans as a deep-water port. Therefore, after extensive study and analysis involving Professor Hans Albert Einstein and others, it was agreed to seek a long-term flow distribution such that 30% of the “latitudinal” flow (i.e., the sum of the Red River and Mississippi River flows at the latitude of the Old River complex) would flow to the gulf through the Atchafalaya. This was to ensure the long-term geomorphic stability and navigational viability of both the Mississippi and Atchafalaya.

In 1959 the low sill structure and outflow channel (see Fig. 15-5) were constructed to achieve the 30 to 70% targeted flow split. However, during the Lower Mississippi flood of 1973, this structure was severely threatened and nearly failed due to scour and associated loss of a wing wall. Consequently, in 1986, the auxiliary structure (see Fig. 15-5) was constructed to obviate total reliance on the low sill structure to achieve the targeted flow diversion.

Recognizing the hydropower potential of the average 6-m head difference between the Mississippi and Atchafalaya, in 1977 a group of investors proposed construction of the Sidney A. Murray, Jr. Hydroelectric Station 2 km above the low sill structure (see Fig. 15-5). This 192-MW bulb-turbine facility was constructed in a New Orleans shipyard and towed up the Mississippi to the site, where it was sunk into place and completed in 1990. Since that time it has been operated successfully by the Louisiana Hydroelectric Corporation, in close coordination with the U.S. Army Corps of Engineers, to achieve the 30 to 70% target flow distribution in concert with the auxiliary and low sill structures. The facility passes an average discharge of about 2,800 m³/s.

Although the turbines were designed to pass a significant sand and silt load, the hydroelectric facility is located on a relatively sediment-poor location of the right descending bank of the Mississippi. Because long-term geomorphic stability of the lower Atchafalaya River requires a continuing supply of sediment from upstream, Louisiana Hydroelectric and the U.S. Army Corps of Engineers have been exploring ways of increasing the diversion of sands and silts from the Mississippi to the Atchafalaya in and around the Old River Control complex. The purpose of the study was to develop an understanding of the short- and long-term sediment dynamics

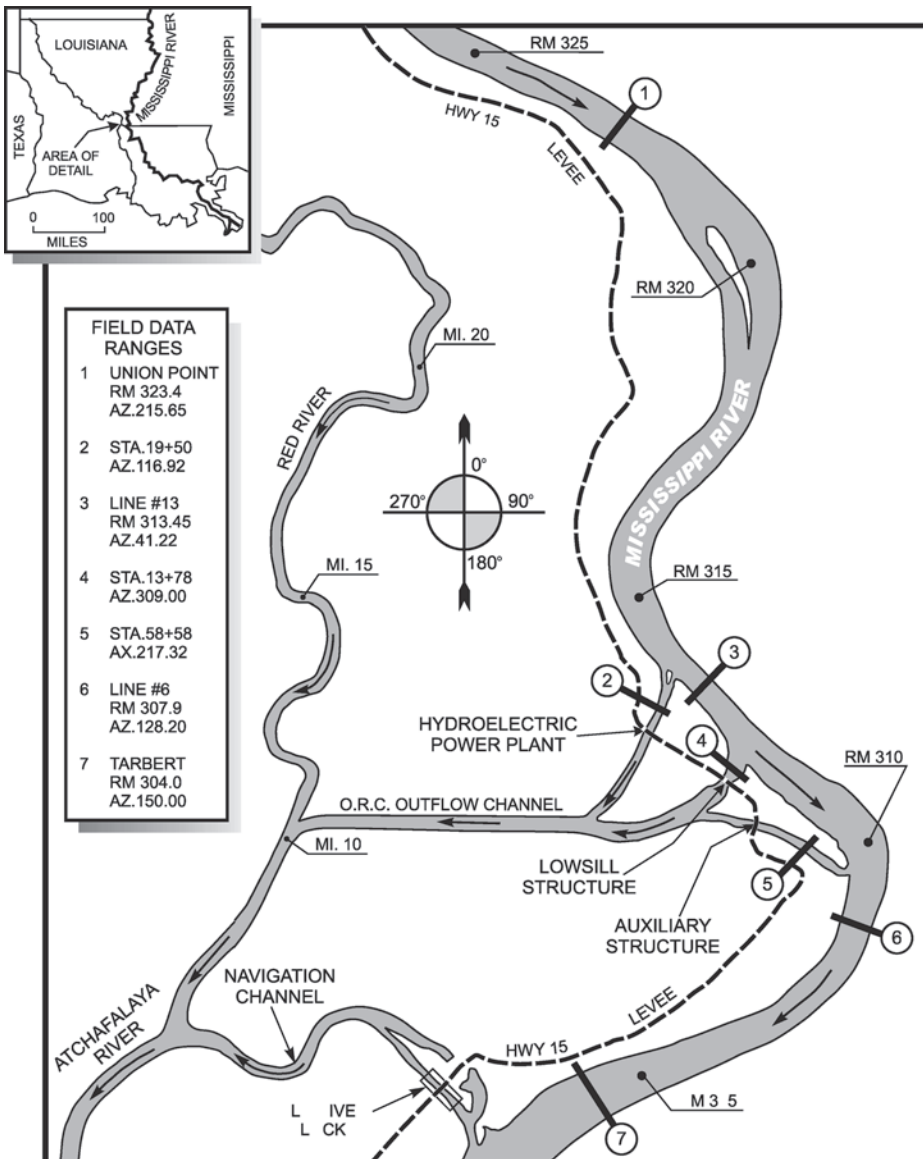


Fig. 15-5. Old River Control Complex, lower Mississippi River.

of the system, both locally and along extended downstream reaches of the Mississippi and Atchafalaya rivers.

Supported by extensive analysis of historical data and dedicated field campaigns to collect new hydraulic and sediment data, the project involved a detailed and comprehensive geomorphic study, the use of one-dimensional mobile-bed modeling for the study of long-term stability of the downstream reaches (see Chapter 14), and three-dimensional mobile modeling for the study of short-term sediment dynamics in the immediate vicinity of the complex. The overall objectives were to quantify the present diversion rate of Mississippi River sediment into the Atchafalaya River and identify possible structural or sediment-management strategies that could increase the diversion of suspended

and bed-load sediments through the hydroelectric complex into the Atchafalaya. The overall study is the subject of a comprehensive report (Catalyst-Old River Hydroelectric Limited Partnership d.b.a. Louisiana Hydroelectric Limited Partnership 1999).

15.11.2.2 CH3D Modeling System The CH3D modeling system has been described in some detail by Gessler et al. (1999). The code simulates unsteady free-surface three-dimensional (hydrostatic) hydrodynamics, constituent and sediment transport, and mobile-bed dynamics in natural waterways. In one time step, the code sequentially solves the hydrodynamic, constituent, and mobile-bed equations.

In the hydrodynamic solution, CH3D first solves the depth-averaged Reynolds approximation of the momentum

equations (Eqs. (15-14) and (15-15)) coupled with the depth-averaged mass-conservation equation (Eq. (15-9)) to yield the depth-averaged velocity and water-surface elevation on a two-dimensional grid. This solution is based on finite-difference approximations applied to a boundary-fitted, nonorthogonal curvilinear grid in the horizontal plane. The deviations from the depth-averaged velocity are then computed for each computational cell through solution of the momentum-conservation equations (Eqs. (15-12) and (15-13)), whereas the vertical-velocity component is obtained by solving the mass-conservation equation (Eq. (15-1)), all coupled with a $k-\epsilon$ closure for vertical momentum diffusion on a sigma-stretched vertical grid. These procedures for the hydrodynamic solution are described in more detail by Chapman and Johnson (1996) and Sheng (1983).

The mobile-bed algorithms have been described in detail by Spasojevic and Holly (1993). In the mobile-bed solution within one time step, the computations are based on a two-dimensional solution of the mass conservation equations for the channel bed (Eqs. (15-63) and (15-64)) and the three-dimensional advection-diffusion equation for suspended-sediment transport (Eq. (15-62)), both for any number of distinct sediment size classes. Auxiliary relations used for the system closure are discussed in Section 15.8.4 of this chapter. The sediment transport algorithms autonomously account for the movement of multiple size classes as either bed load or suspended load, with the exchange between these modes of transport and the bed being governed by local hydrodynamic conditions interacting with sediment properties.

15.11.2.3 Field Data Campaign and Model Construction In the ORCC study, an initial CH3D model data was constructed to the prototype dimensions of an existing coal-bed 1:120 scale undistorted outdoor hydraulic model at the Waterways Experiment Station, Vicksburg, Miss. This preliminary study was used to verify the overall behavior of the CH3D model for a range of prototype discharges and support design of the actual ORCC model data set.

During the 1998 hydrologic cycle seven field-data collection campaigns were organized. A morphology survey was conducted during January 1998. Field sediment and flow data were collected on (1) February 27 (reported Mississippi River discharge at Union Point was $Q = 1,059,000 \text{ cfs}$; $29,989 \text{ m}^3/\text{s}$); (2) March 23 ($Q = 1,082,000 \text{ cfs}$; $30,640 \text{ m}^3/\text{s}$); (3) April 10 ($Q = 1,224,000 \text{ cfs}$; $34,661 \text{ m}^3/\text{s}$); (4) April 17 ($Q = 1,178,000 \text{ cfs}$; $33,358 \text{ m}^3/\text{s}$); (5) May 8 ($Q = 1,445,000 \text{ cfs}$; $40,919 \text{ m}^3/\text{s}$); (6) June 9 ($Q = 739,000 \text{ cfs}$; $20,927 \text{ m}^3/\text{s}$); and (7) August 3 ($Q = 573,000 \text{ cfs}$; $16,226 \text{ m}^3/\text{s}$). The collected data were used in conjunction with data available from other sources, to formulate the initial and boundary conditions for the three-dimensional Old River Control Complex model, to calibrate the model, and to verify the model results.

Detailed calibration and verification of the three-dimensional Old River Control Complex model is presented here, as well as a critical assessment of the model's simulation

results for the February 27, 1998, data set. Established calibration procedures and experience gained through simulations based on February 27 data were successfully used to make simulations of flow and sediment diversions for other data sets.

On February 27, 1998, field sediment and flow data were collected at six field-data ranges (Fig. 15-5): Range 1, the Mississippi River at Union Point; Range 2, the hydroelectric power plant (HPP) channel some distance upstream from the hydroelectric power plant; Range 3, the Mississippi River at Line 13; Range 5, the auxiliary structure channel some distance upstream from the auxiliary structure; Range 6, the Mississippi River at Line 6; and Range 7, the Mississippi River at Tarbert. The field data were not measured at Range 4, in the low sill structure channel, because the low sill structure was closed.

To obtain sediment data in a particular range, four verticals were chosen along the range. Twenty-four suspended-sediment samples were taken at the range, six point samples along each of the four chosen verticals. Also, four bed-sediment samples were collected at bed-surface locations corresponding to the same four chosen verticals. Suspended-sediment samples were processed to obtain vertical suspended-sediment concentration profiles by size class for each of the chosen verticals. Bed-sediment samples were processed to obtain bed-sediment size distribution at the bed-surface location of each vertical.

Flow data at a particular data range were obtained using an acoustic Doppler current profiler to measure the distribution of horizontal velocity vector intensities and directions across the range. The total water discharge at the range was obtained by integrating measured velocities across the range. To be consistent with sediment data, the distribution of horizontal velocity vector intensities and directions was reported only along the four chosen verticals, the same ones that were used for collecting suspended-sediment samples. Furthermore, reported vertical profiles of velocity vector intensities and directions were the result of ensemble averaging (Fagerburg 1998). Each velocity vector intensity and direction value, reported for a particular point on a particular vertical, is the average of the value at that particular point and five or eight surrounding points. Ensemble averaging, instead of time averaging, was introduced to eliminate significant randomness in measured velocities caused by ADCP high-frequency sampling (1–3 s per vertical).

All field sediment and flow data collected during the seven field data collection campaigns in 1998, including the February 27 data, can be found in the report of the Catalyst-Old River Hydroelectric Limited Partnership d.b.a. Louisiana wHydroelectric Limited Partnership (1999).

Certain data relevant to the Old River Control Complex model are available on a daily basis from sources other than the 1998 field-data collection effort. The Mississippi River discharges at Union Point and Tarbert, as well as the free-surface elevation at the Tarbert Landing gauge, are reported

daily. At the hydroelectric power plant, the low sill structure, and the auxiliary structure, free-surface elevations are measured and discharges computed on daily basis.

On February 27, 1998, the reported Mississippi River discharges at Union Point and Tarbert were 1,059,000 cfs (29,988 m³/s) and 870,000 cfs (24,636 m³/s), respectively. The calculated discharges at the hydroelectric power plant and the auxiliary structure were 162,000 cfs (4,587 m³/s) and 27,000 cfs (765 m³/s), respectively. The low sill structure was closed.

The three-dimensional model domain comprises (1) the Mississippi River between Union Point and Tarbert; (2) the channel between the Mississippi River and the hydroelectric power plant (HPP channel); (3) the channel between the Mississippi River and the low sill structure (low sill structure channel); and (4) the channel between the Mississippi River and the auxiliary structure (auxiliary structure channel) (Fig. 15-16).

The computational grid for the February 27 data has 344×49 points that lie in a horizontal plane and 10 points in a vertical direction, i.e., along the depth. However, for a complex domain such as the Old River Control Complex, the CH3D-SED computational grid covers an area larger than the actual model domain. In this case, the number of active computational points inside the model domain is 7,200 in the horizontal plane, with 10 points along the depth.

15.11.2.4 Hydrodynamic Boundary and Initial Conditions Hydrodynamic computations require either free-surface elevations or unit discharges as boundary conditions at all open boundaries. For the February 27 data, the open boundaries of the Old River Control Complex model are (1) the Mississippi River at Union Point as an upstream inflow boundary; (2) the Mississippi River at Tarbert as a downstream outflow boundary; (3) the hydroelectric power plant as an outflow boundary; and (4) the auxiliary structure as an outflow boundary. All other boundaries, including the closed low sill structure, are treated as impermeable boundaries.

It should be noted that available measured-velocity data did not support the imposition of measured unit discharges as a boundary condition at open boundaries, which would have been the ideal situation. For the Mississippi River at Union Point and Tarbert, measured velocities were reported only for four verticals along each of the respective data ranges, whereas there are 20 computational-grid verticals at each range. It was practically impossible to extrapolate data measured at four locations to 20 computational points, and still satisfy the total-discharge requirement, without using unfounded assumptions. Furthermore, in the HPP and auxiliary structure channels, velocities were not even measured at model boundaries, but rather at some distance upstream from the hydroelectric power plant and the auxiliary structure. Thus, when unit discharges were used as a boundary condition for the Mississippi River at Union, the total measured discharge was distributed across the flow so that the ratio

between total discharge and the particular unit discharge through a computational-cell face was the same as the ratio between the total cross-section area and the appropriate cell-face unit area. This commonly used approximation amounts to assigning constant depth-averaged velocities across the flow. The measured free-surface elevation was assigned as a downstream boundary condition for the Mississippi River at Tarbert, horizontal across the section.

A measured free-surface elevation seemed to be the logical choice for the outflow boundary condition at the hydroelectric power plant and the auxiliary structure. The alternative, unit outflow discharges, required using the constant depth-averaged velocity approximation to distribute the total discharge across the channel. However, using the free-surface elevation as an outflow boundary condition at the hydroelectric power plant and the auxiliary structure would have made modeling the proper flow diversion at these two locations very difficult. It would have required almost perfect bed morphology and bed-surface friction data, as well as a very advanced flow model, to reproduce the complex flow pattern caused by the flow diversion through the HPP and the auxiliary structure channels. Assignment of unit discharges as boundary conditions at the hydroelectric power plant and the auxiliary structure automatically achieved the desired flow diversion, but the model still needed to be calibrated to reproduce the proper free-surface elevations in respective channels. This task was also difficult, because the free surface in the HPP and the auxiliary channels is dictated by specific rating curves at the hydroelectric power plant and the auxiliary structure. The CH3D hydrodynamic computations do not include a rating-curve boundary condition. Thus, final runs of the model, with calibrated parameters for the HPP channel, were made with unit discharges as the HPP boundary condition, ensuring the exact HPP discharge.

For the auxiliary structure, approximated unit discharges, providing the proper flow distribution, were assigned as a boundary condition. The discharge through the auxiliary structure on February 27 was small as compared to other discharges throughout the model. Thus, velocities and free-surface elevation slope at the auxiliary channel were small, leading to a relatively simple calibration of free-surface computations.

Zero-flow initial conditions (i.e., horizontal free-surface elevation and zero-velocity field) were used for the hydrodynamic computations. The chosen combination of initial and boundary conditions (realistic discharges and/or free-surface elevations imposed on initially still water) is known to produce a disturbance (wave) that propagates back and forth throughout the flow domain. A stabilization period is required to allow the disturbance to eventually die out. Avoidance of transient dry-bed conditions and high Courant numbers associated with the arbitrary initial condition required careful treatment, and is not discussed further here. At the end of the flow-stabilization period, the flow approached a steady-state condition.

15.11.2.5 Hydrodynamic Model Calibration and Verification

For the purpose of model calibration and verification, the results of the steady-state flow solution for the February 27 discharge were compared to available field data.

A flow-stabilization period of 10 h (2,400 15-s computational time steps) proved to be sufficient for the dissipation of the initially severe wave propagation in the domain. At the end of the flow-stabilization period, a steady-state flow solution was achieved.

The first series of calibration and verification runs was made with measured free-surface elevation as a boundary condition for the Mississippi River at Tarbert, and unit discharges (obtained by using the constant depth-averaged velocity assumption to distribute known total discharges across appropriate boundaries) as a boundary condition for the hydroelectric power plant, the auxiliary structure, and the Mississippi River at Union Point. The low sill structure was closed on February 27, 1998.

The goal of these runs was to achieve generally good agreement between the computed and measured data throughout the domain by globally calibrating the friction coefficient. The agreement between computed and known free-surface elevations was checked throughout the model domain (the Mississippi River at Union Point, the hydroelectric power plant, the low sill structure, and the auxiliary structure). Also, the agreement between computed and measured horizontal velocity vector intensities and directions was checked for all verticals at all data ranges.

The CH3D hydrodynamic-computations program module has two major physical parameters that can be determined through the calibration process: (1) the bed-surface friction coefficient and (2) the horizontal eddy-viscosity coefficient, used in conjunction with the boussinesq approximation for horizontal turbulent-diffusion terms. For both coefficients only an expected range of values can be estimated, because the exact values are unknown *a priori*.

Initially, a number of runs with different values for the eddy-viscosity coefficient were made. Changing the horizontal eddy-viscosity coefficient within the expected range of values, from 10 to 10,000 cm²/s, did not significantly

affect the computed hydrodynamic results. Thus, all subsequent hydrodynamic computations were made with an eddy-viscosity coefficient of 1,000 cm²/s. Considerably more effort was devoted to the spatial variability of the absolute roughness and consequent friction and manning coefficients in the model. This is described in detail in Catalyst-Old River Hydroelectric Limited Partnership d.b.a. Louisiana Hydroelectric Limited Partnership (1999).

Through the calibration process, it became apparent that the present CH3D hydrodynamics model could not fully reproduce the complex flow pattern in the HPP channel, especially in the channel's upstream portion. In general, the existing CH3D hydrodynamic model cannot fully reproduce strong secondary currents, due to the simplified horizontal turbulence model, but even more to the vertical hydrostatic pressure assumption, which implies parallel streamlines in a vertical direction. Thus, even with carefully calibrated friction and a corrected cross-section area, the model could not reproduce the exact flow diversion through the HPP channel when the measured free-surface elevation was used as the HPP boundary. However, the calibrated friction and the corrected morphology could still be used to improve HPP free-surface computations in the case when unit discharges were used as a HPP boundary condition. HPP unit discharges were obtained by using the constant depth-averaged velocity assumption to distribute known total discharge across the HPP boundary. The described unit-discharge boundary condition amounts to assigning known total discharges at the hydroelectric power plant, thus forcing the correct HPP flow diversion. Using the previously calibrated friction coefficient and adjusted cross-section area in the HPP channel, resulted in a computed HPP surface elevation that was only 9 cm lower than the measured one.

Table 15-3 shows the final comparison between computed and known free-surface elevations throughout the model domain. This should be indicative of reasonable expectations for the water-surface elevation calibration in a three-dimensional hydrodynamic model of this type. As previously stated, after each calibration run the agreement between computed and measured horizontal velocity-vector

Table 15-3 Computed and Measured (or estimated) Free-Surface Elevations

	Measured (or estimated) free-surface elevations	Computed free-surface elevations
Mississippi River at Union Point	15.58 m asl (51.1 ft) (estimated)	15.60 m asl (51.18 ft)
Hydroelectric power plant	14.82 m asl (48.6 ft)	14.73 m asl (48.33 ft)
Low-sill structure	14.91 m asl (48.9 ft)	14.95 m asl (49.05 ft)
Auxiliary structure	14.69 m asl (48.2 ft)	14.66 m asl (48.10 ft)
Mississippi River at Tarbert	14.38 m asl (47.17 ft)	14.38 m asl (47.17 ft) assigned boundary condition

intensities and directions was checked for all data verticals in all data ranges. Fig. 15-6 shows a sample of computed (at the end of the calibration process) and measured horizontal velocity-vector intensities and directions for the Mississippi River at Line 13.

The computation of velocities at Line 13 (Fig. 15-6) required additional calibration of the local Mississippi River model area immediately downstream from the HPP channel. Specifically, the Mississippi River navigation charts show the presence of a clay shelf next to the Mississippi River's right bank immediately downstream from the HPP channel. In that location, the Mississippi River's main flow leaves the right bank and crosses toward the left bank. This is reflected in velocities measured at line 13. Evidently, the present CH3D hydrodynamic model cannot properly reproduce the flow over and around the clay shelf, due to an oversimplified horizontal turbulence model. Thus, an engineering approximation was used. At the clay shelf area, the wall-shear stress was significantly increased to compensate for the poorly modeled flow around the shelf and the associated drag. An absolute roughness of 3 cm, corresponding to a friction coefficient C_d of 0.02, i.e., a Manning coefficient n of 0.066, for $H = 10$ m, proved to be sufficient to achieve satisfactory agreement

between computed and measured velocities at line 13 (Fig. 15-6).

Fagerburg (1998) reported the existence of a strong reverse flow area along the right bank of the auxiliary structure channel. Fig. 15-7 shows the computed mid-depth velocity vector intensities and streamlines at the auxiliary structure channel, featuring the predicted reverse flow. However, although it is known that the turbulence model based on constant eddy viscosity can predict the strong reverse flow, it cannot correctly predict the size of the reverse flow area. This was confirmed when computed and measured horizontal velocity-vector intensities and directions in the auxiliary structure channel were compared. Range 4 (Fig. 15-6) in the auxiliary structure channel is located slightly upstream from the predicted reverse flow area shown in Fig. 15-7. However, measured horizontal velocity-vector directions show that, whereas velocities at verticals 2, 3, and 4 are generally oriented toward the auxiliary structure, velocities at vertical 1 (next to the right bank) are still generally oriented away from the structure. Thus, the model underestimates the size of the reverse-flow area.

At locations other than the Mississippi River at line 13 and the auxiliary structure channel, similar calibration procedures

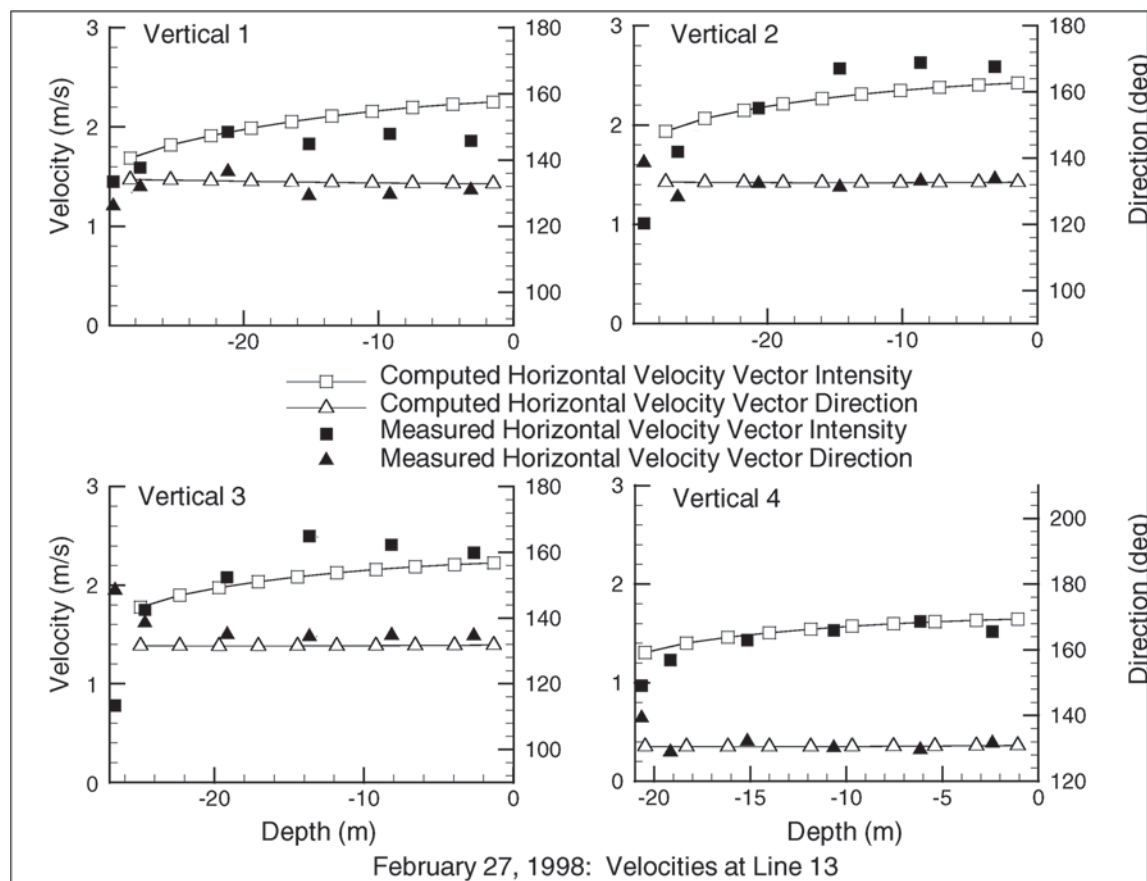


Fig. 15-6. A sample of computed and measured velocities at line 13.

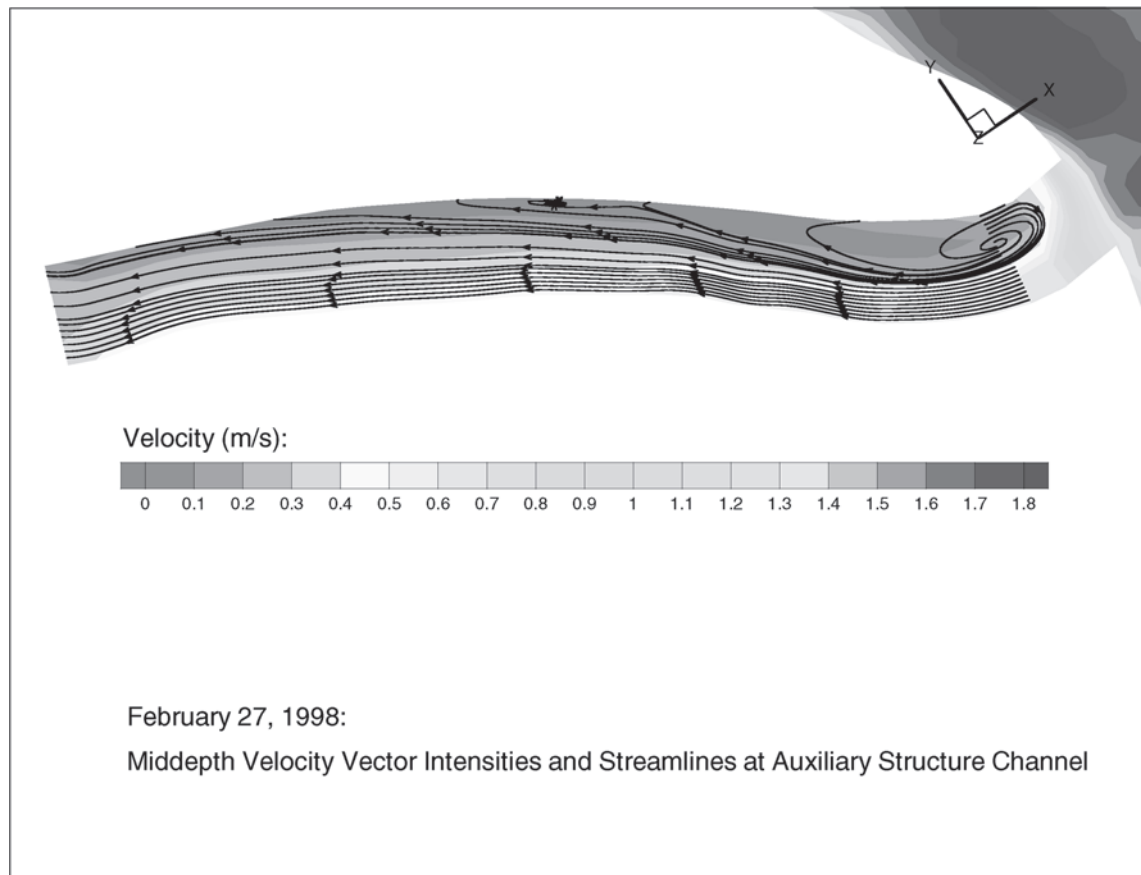


Fig. 15-7. Middepth velocity vector intensities and streamlines in the auxiliary structure channel.

produced generally good agreement between computed and measured horizontal velocity-vector intensities and directions.

It should be noted that the hydrodynamic-computations results were checked again after the sediment-model calibration and the sediment simulation runs. Results of the hydrodynamic computations at the end of the 10-h flow-stabilization period and at the end of the total flow and sediment simulation period of 34 h were virtually identical. The difference in free-surface elevations was 1 cm at Union Point and smaller everywhere else. The difference in velocity magnitudes at field-data verticals was less than 0.5%, and the difference in velocity angles at field-data verticals was around 0.1%.

15.11.2.6 Model Sediment Size Classes Suspended-sediment samples, collected on February 27, 1998, were processed to obtain suspended-sediment concentrations by size class. Grain-size analysis for suspended sediment showed the five size classes. These suspended-sediment samples generally contained a significant amount of silt and clay and fine sand (suspended-sediment size classes 1 and 2), some amount of very fine and medium sand (size classes 3 and 4), and very little coarse sand (size class 5).

Bed-sediment samples, collected on February 27, were also processed to obtain bed-sediment size distribution at the bed-surface. Grain-size analysis for bed sediment

featured the 18 size classes. These bed-sediment samples generally contained a significant amount of sediment with diameter smaller than 1 mm (bed-sediment size classes 1 to 9), and only a small percentage of sediment with diameter larger than 1 mm.

In addition, it is known that the HPP channel bed is covered with very coarse material (essentially cobbles), and that revetments along the Mississippi River near the Old River Control Complex comprise very coarse material.

Based on the above observations, the six size classes in Table 15-4 were chosen to represent the totality of natural sediment mixtures relevant to the Old River Control Complex model.

Size class 6 (referred to as gravel) was used to model the coarse material found in small amounts at the bed surface, and also the coarse material at the HPP channel bed and the revetment material. The characteristic sizes for the silt and clay and the gravel were not known in advance, and were determined during the model calibration. Characteristic sizes for sand size classes were obtained as geometric means of the diameter-range limits.

15.11.2.7 Sediment Boundary Conditions Sediment computations in CH3D-SED recognize three boundary types: sediment-inflow, sediment-outflow, and impermeable

Table 15-4 Representative Size Classes for the Old River Control Complex Model

Model size class	Diameter range (mm)	Characteristic diameter (mm)(geometric mean of diameter-range limits)	Corresponds to suspended-sediment size class	Corresponds to bed-sediment size class
1(silt and clay)	$D < 0.062$		1	1
2(very fine sand)	$0.062 < D < 0.125$	0.088	2	2–4
3(fine sand)	$0.125 < D < 0.250$	0.177	3	5–6
4(medium sand)	$0.250 < D < 0.500$	0.326	4	7–8
5(coarse sand)	$0.500 < D < 1.00$	0.707	5	9
6(gravel)	$D > 1.00$			10–18

boundaries. Boundary conditions are required only along sediment-inflow boundaries.

Boundary conditions for suspended-sediment computations are known vertical suspended-sediment concentration profiles for all size classes, assigned at each vertical along all sediment-inflow boundaries. For bed load, the formulations of CH3D-SED require assignment of a size-fraction distribution (featuring size fractions for all size classes) to each bed point along all sediment inflow boundaries. The assigned size-fraction distribution at each particular bed point must satisfy the basic requirement that the sum of all fractions must be equal to unity. This requirement, in conjunction with other sediment boundary conditions, determines the proper total number of sediment boundary conditions, because the bed-surface elevation computations do not require a boundary condition in the formulation of CH3D-SED. Boundary conditions for both suspended- and bed-sediment computations can be either constant or time-dependent.

Sediment computations also require declaring a potential reverse-flow boundary (a boundary where the flow could potentially change direction during the simulation) as a sediment-inflow boundary, and assigning the appropriate boundary conditions along it. Assigned boundary conditions are used only when the potential reverse-flow boundary becomes an actual inflow boundary and are ignored otherwise.

The only real potential reverse-flow boundary is a tidal boundary. However, any flow boundary with an imposed free-surface elevation as a boundary condition can theoretically become a reverse-flow boundary, depending on the variations in the imposed water level. When CH3D-SED code is used to model river flow, transitory waves at the beginning of the flow-stabilization period may actually cause reverse flow for a short period of time at such boundaries.

For the Mississippi River at Union Point, initial suspended-sediment data, obtained as described later, were also used as the suspended-sediment inflow boundary condition. The Mississippi River at Union Point is the only real sediment inflow boundary. The Mississippi River at Tarbert and the hydroelectric power plant with free-surface

elevation as a hydrodynamic boundary condition were identified as potential reverse-flow boundaries, and therefore declared as sediment-inflow boundaries. However, for the two potential reverse-flow boundaries, zero-concentration profiles were assigned as suspended-sediment boundary conditions, so that if momentary reverse flow occurred during the stabilization period, no suspended sediment would be advected into the domain through those normally outflow boundaries. The described suspended-sediment boundary conditions were kept constant for the duration of the simulation.

15.11.2.8 Suspended-Sediment Initial Conditions As an initial condition for suspended-sediment computations, vertical concentration profiles for all size classes must be defined for all verticals throughout the model domain, including outflow boundaries. Sediment data collected on February 27, 1998, were used to extract vertical suspended-sediment concentration profiles for all representative model size classes at all data-collection ranges and appropriate verticals.

Fig. 15-8(a) through 15-8(f) show a sample of measured suspended-sediment concentrations along four data verticals at Line 13. More specifically, Figs. 15-8(a) through 15-8(e) contain measured suspended silt and clay, very fine sand, fine sand, medium sand, and coarse sand concentrations, respectively. Fig. 15-8(f) contains measured total suspended-sediment concentrations.

Simultaneous inspection of measured suspended silt and clay concentrations for all data verticals in all data ranges shows a relatively modest variation in measured values. Similarly, measured vertical concentration profiles for suspended very fine sand do not show significant variation between different vertical locations. The same observations apply to measured vertical concentration profiles for suspended medium sand, as well as measured vertical concentration profiles for suspended coarse sand. Measured vertical concentration profiles for suspended fine sand are the only profiles showing relatively significant changes from one location to another.

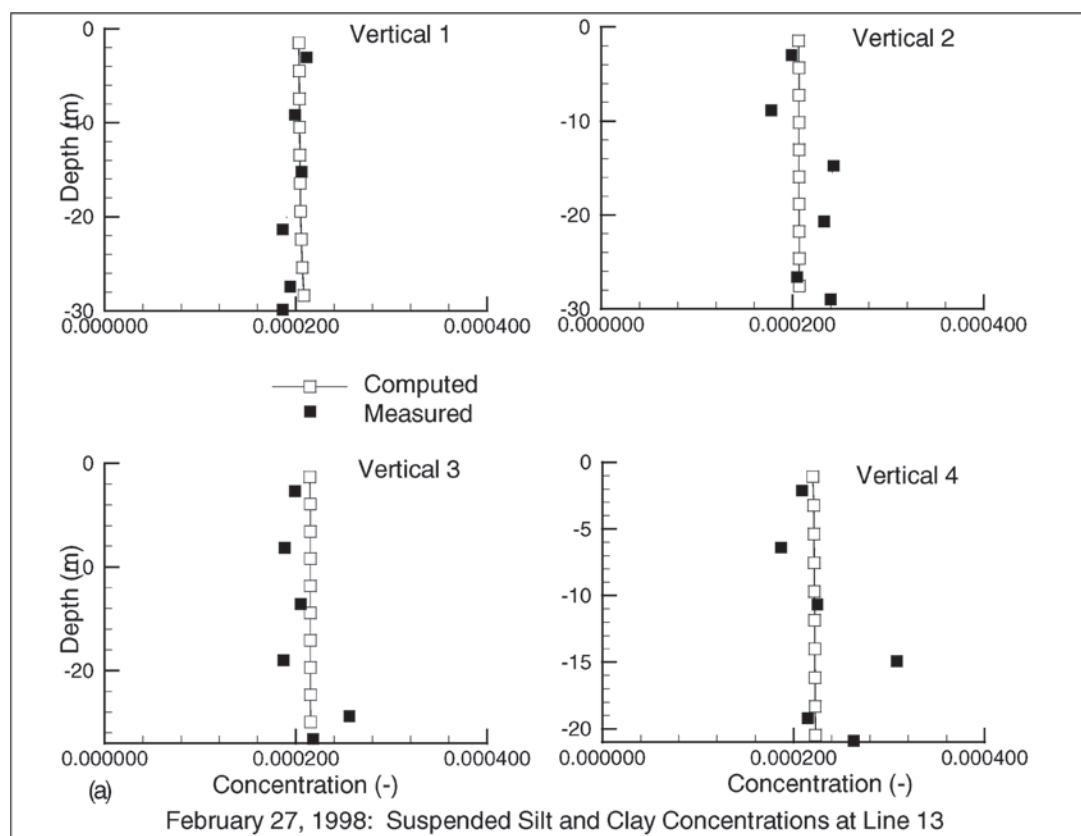


Fig. 15-8(a). Computed and measured suspended silt and clay.

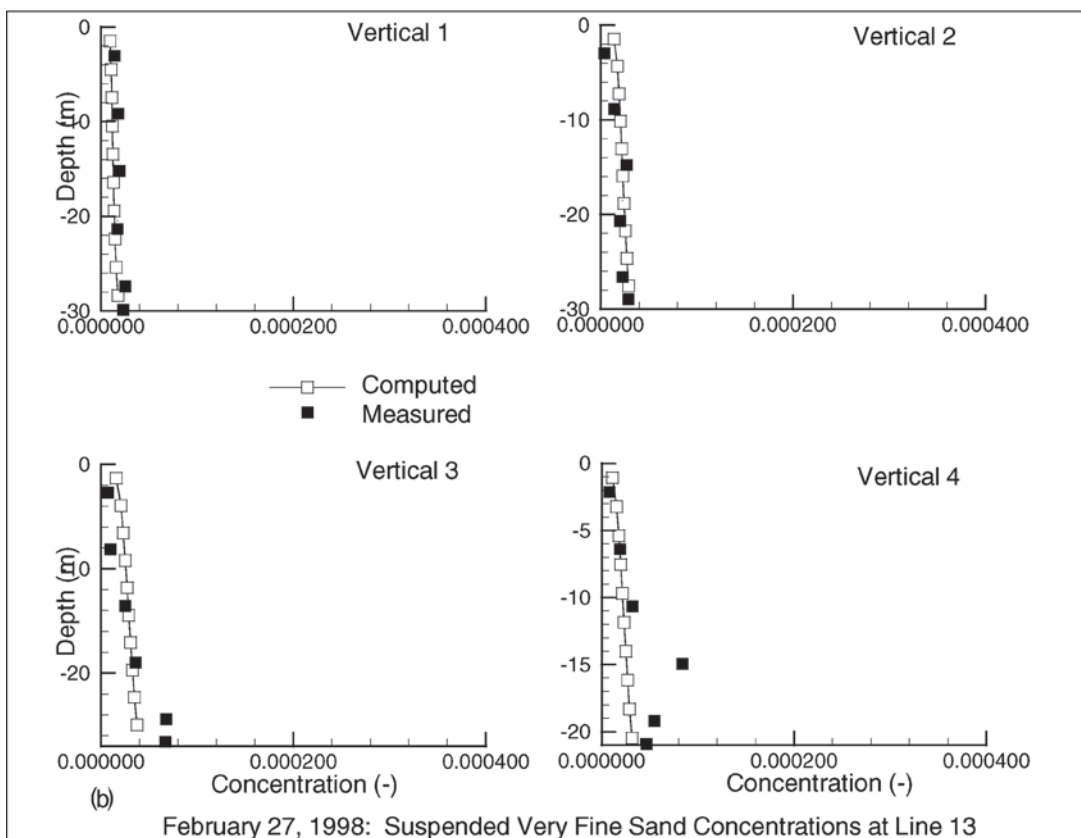


Fig. 15-8(b). Computed and measured suspended very fine sand.

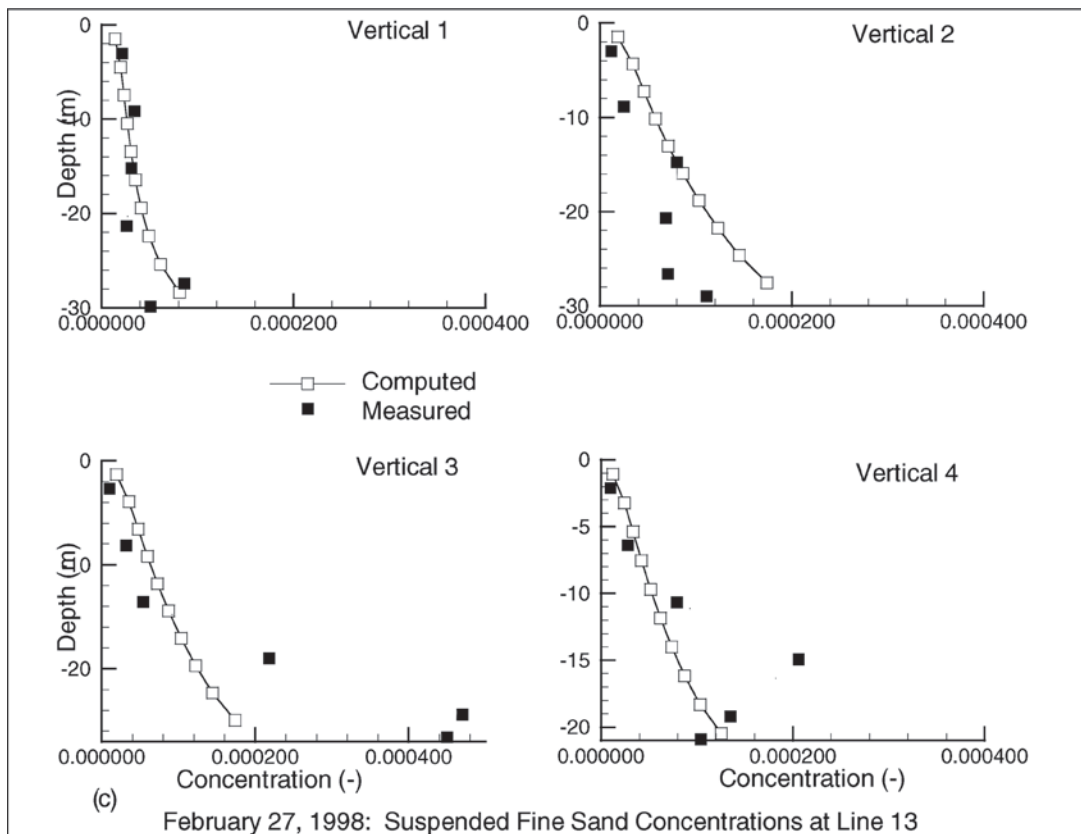


Fig. 15-8(c). Computed and measured suspended fine sand.

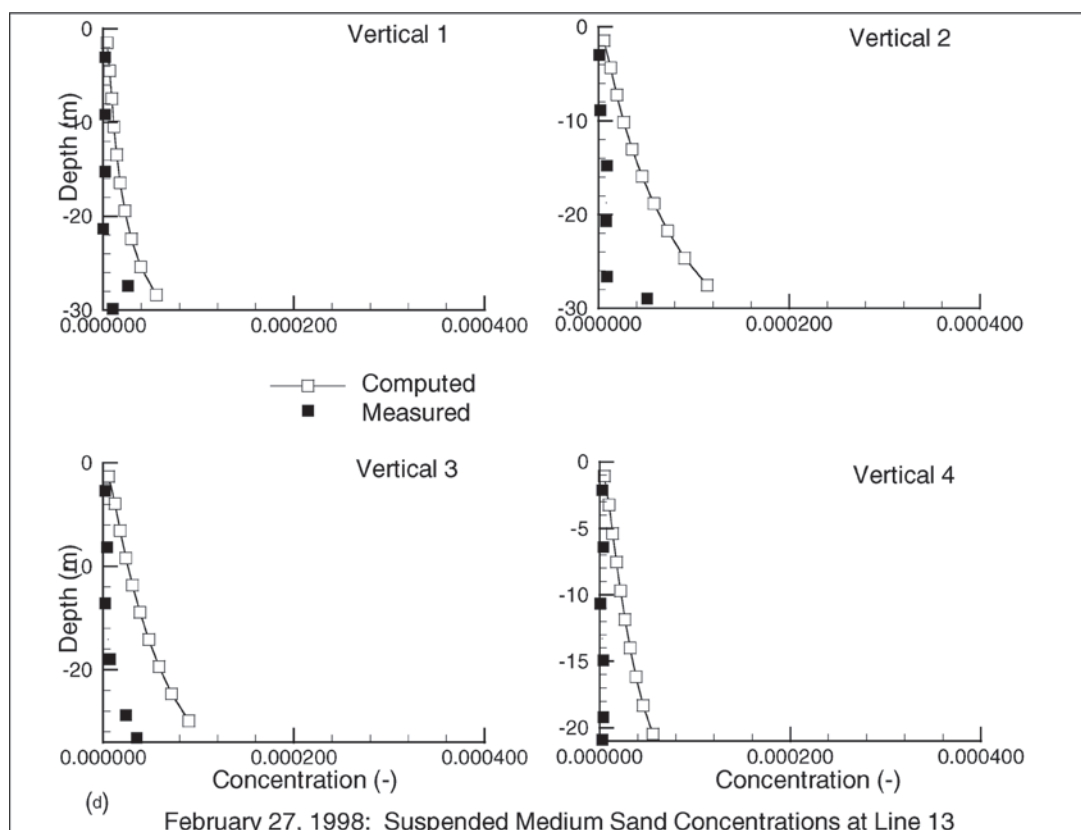


Fig. 15-8(d). Computed and measured suspended medium sand.

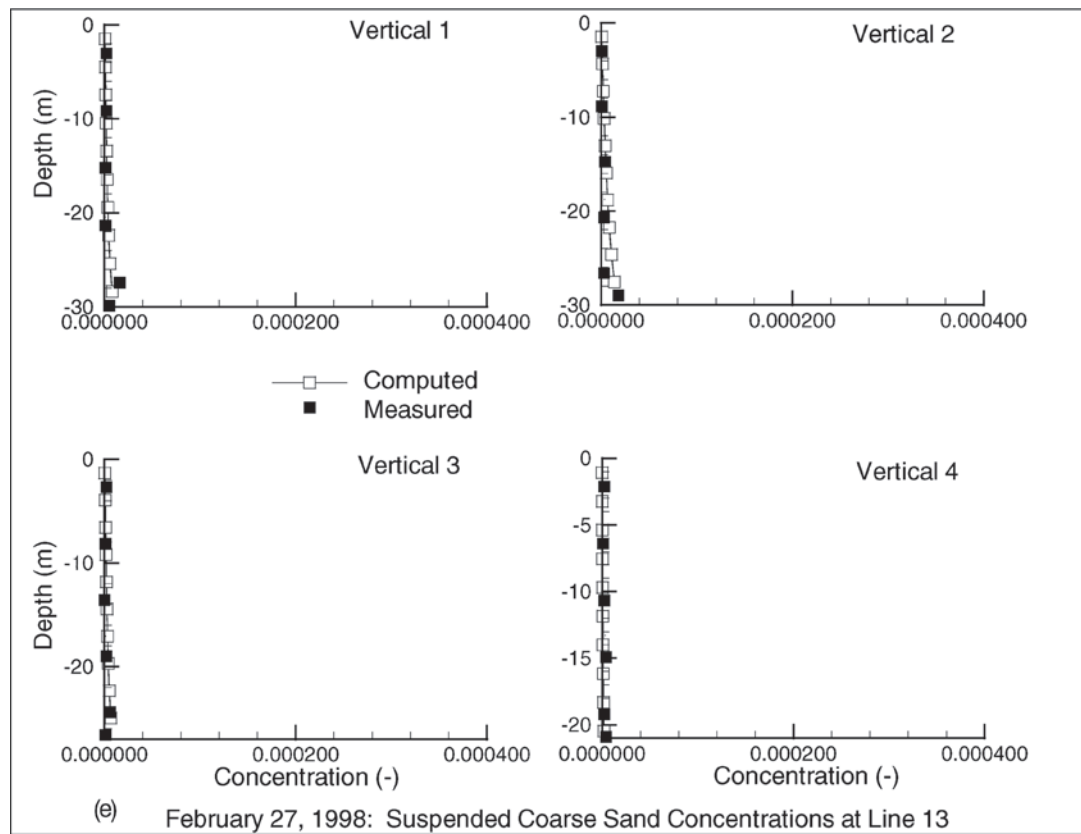


Fig. 15-8(e). Computed and measured suspended coarse sand.

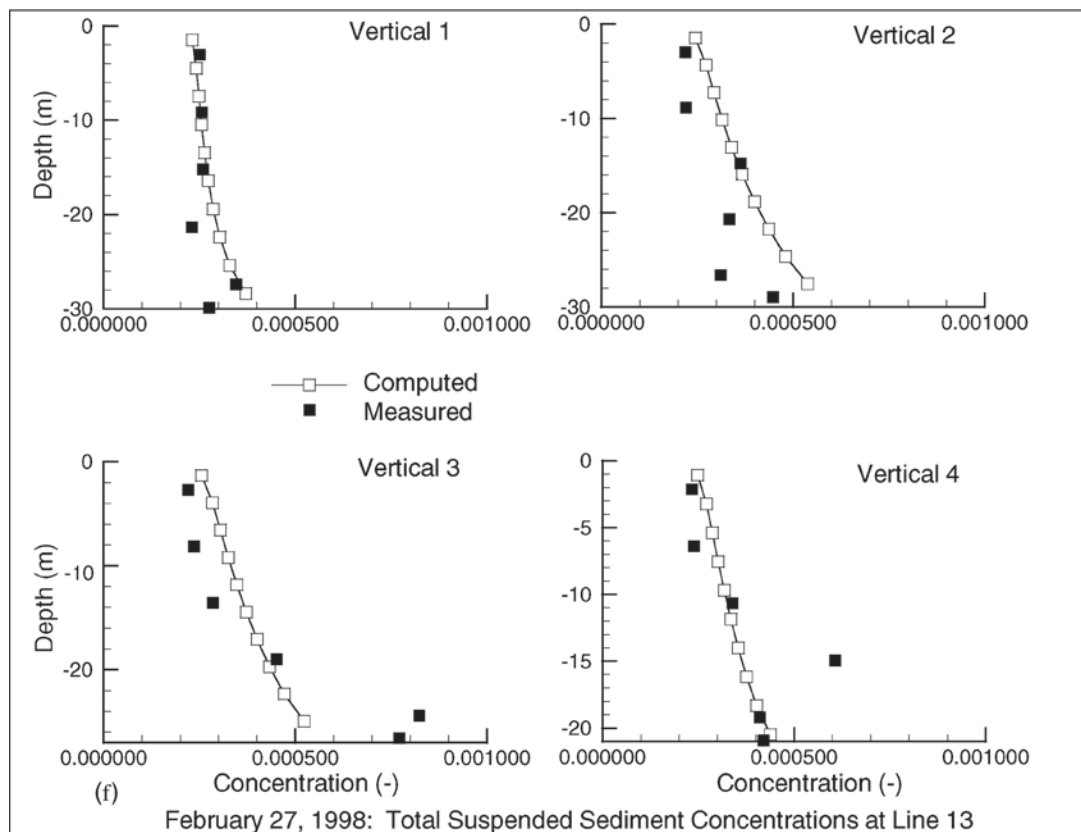


Fig. 15-8(f). Computed and measured suspended total concentrations at line 13.

The preceding observations supported the use of simple extrapolation to construct the initial condition for suspended-sediment computations. First, six suspended-sediment concentrations measured along a particular data vertical were used to construct a set of measured concentration profiles, one for each size class, corresponding to the appropriate computational grid vertical with ten computational points. Each constructed set of vertical concentration profiles was then assigned not only to the corresponding computational-grid vertical, but also to neighboring left and right grid verticals across the flow and grid verticals upstream and downstream from the corresponding grid vertical, until all computational verticals were assigned initial suspended-sediment data. The initial suspended-sediment distribution thus determined at the upstream model boundary, Union Point, was also assigned as a constant suspended-sediment boundary condition.

15.11.2.9 Bed-Sediment Initial Conditions As an initial condition for bed-sediment computations in CH3D-SED, initial size-fraction distributions and bed-surface elevations have to be defined for all bed-surface points throughout the domain, including outflow boundaries. In addition, bed-sediment computations in CH3D-SED require definition of initial bed-material characteristics below each bed-surface point in the model domain: (1) the initial active-layer (bed-surface layer) depth at a particular bed point; (2) the initial number of bed-sediment strata below a particular bed-surface point; and (3) the initial depth and size-fraction distribution for each stratum below a particular bed-surface point.

Flow-stabilization hydrodynamic computations, assuming a nonmovable bed, can successfully start up using exact but unrealistic zero-flow initial conditions (e.g., horizontal free-surface elevation and zero-velocity field). Fixed-bed hydrodynamic computations with simple zero-flow initial conditions and proper boundary conditions kept constant over a period of time yield an observed steady-state flow solution at the end of the flow-stabilization period.

Sediment computations, by contrast, initiated from the steady-flow hydrodynamic condition at the end of the flow-stabilization period, require initial conditions to be as close to reality as possible. With boundary conditions held constant over time, flow and sediment will eventually reach a balance, or state of equilibrium. But if the initial sediment conditions are unrealistic, then so will be the achieved solution. For example, if sediment computations are initiated in a flow with relatively high velocities (as observed on February 27, 1998), and if the assigned initial sediment condition assumes an unrealistically fine bed sediment for this flow rate, flow and sediment balance will still be achieved, but only after unrealistically excessive bed erosion (just as if one introduced a sudden large discharge into a channel with very fine material on the bed—the fine material would be removed very quickly). Thus determination of the appropriate initial bed-sediment size distribution comprises part of the model calibration process, as described below.

Sediment data collected on February 27, 1998, were initially used to extract size-fraction distributions at bed-surface

points corresponding to locations of data-collection verticals at all data-collection ranges.

Bed-material samples were not collected in the HPP channel, where the bed is predominantly covered with large cobbles. Thus, the initial size-fraction distribution for the HPP channel was assumed to comprise 100% of the model size class 6 (gravel), and 0% of all other size classes.

Table 15-5 shows measured size-fraction distributions at bed-surface points corresponding to four data verticals in the auxiliary structure channel. Bed material in the auxiliary structure channel does not contain sediment coarser than fine sand. The reason is probably a combination of generally small velocities in the auxiliary structure channel (due to the relatively small average discharge through the auxiliary structure) and the reverse flow in the upstream portion of the auxiliary structure channel. Measured size-fraction distributions (Table 15-6) were extrapolated and assigned as an initial condition throughout the auxiliary structure channel area.

Table 15-6 shows measured size-fraction distributions at bed-surface points corresponding to all data verticals at four data ranges along the Mississippi River. Silt and clay were virtually nonexistent on the bed throughout the domain, except for the bed-surface point corresponding to Vertical 1 at Line 13, where silt and clay make up one-half of the bed-surface sediment mixture. Bed-material samples generally contain less than 5% of very fine sand, but again there are a few exceptions where very fine sand makes up one-third of the bed-surface sediment mixture (bed-material samples corresponding to Vertical 1 at Line 13 and Vertical 4 at Line 6). Fine sand and medium sand were found in virtually all bed-sediment samples, but their percentage in the bed-surface sediment mixture varies from 0% to 89% for the fine sand, and from 0% to 77% for medium sand. Coarse sand was not found in six bed-material samples, but for the remaining ten samples its percentage in the bed-surface sediment mixture varies from 0 to 43%. Gravel was found only in the bed-material sample corresponding to Vertical 1 at Union Point. Vertical 1 at Union Point is the vertical closest to the right bank, and it is also close to the island next to the upstream boundary.

Based on bed-material samples collected on February 27, 1998, it could be generally concluded that the bed-material composition varies significantly within the studied portion of the Mississippi River. Experience showed that the assumption that a particular measured size fraction distribution is representative of a large surrounding area (as was done successfully with measured suspended-sediment concentrations) lead to unrealistic initial conditions for bed-sediment computations. For example, the assignment of the measured size-fraction distribution corresponding to Vertical 1 at Line 13 (with a large silt and clay fraction) to a large model domain lead to excessive erosion in the first few hours of the mobile-bed simulation.

This conclusion is supported by consideration of the Nordin and Queen (1989) study, which presents particle size distributions for several hundred bed-sediment samples collected along the Mississippi River thalweg

Table 15-5 Measured Size-Fraction Distributions at the Auxiliary Structure Channel

Data range	Data verticals	Size fractions					
		Silt and clay	Very fine sand	Fine sand	Medium sand	Coarse sand	Gravel
Auxiliary structure channel	1	0.31	0.45	0.24	0.00	0.00	0.00
	2	0.34	0.41	0.25	0.00	0.00	0.00
	3	0.01	0.23	0.74	0.02	0.00	0.00
	4	0.42	0.31	0.27	0.00	0.00	0.00

Table 15-6 Measured Size-Fraction Distributions along the Mississippi River

Data ranges	Data verticals	Size fractions					
		Silt and clay	Very fine sand	Fine sand	Medium sand	Coarse sand	Gravel
Union Point	1	0.00	0.00	0.00	0.00	0.30	0.70
	2	0.00	0.00	0.34	0.55	0.11	0.00
	3	0.00	0.01	0.57	0.39	0.03	0.00
	4	0.00	0.01	0.78	0.21	0.00	0.00
Line 13	1	0.51	0.32	0.17	0.00	0.00	0.00
	2	0.00	0.00	0.15	0.64	0.21	0.00
	3	0.00	0.02	0.61	0.33	0.04	0.00
	4	0.00	0.01	0.73	0.26	0.00	0.00
Line 6	1	0.00	0.01	0.24	0.60	0.15	0.00
	2	0.00	0.01	0.44	0.41	0.14	0.00
	3	0.00	0.02	0.37	0.54	0.07	0.00
	4	0.04	0.30	0.65	0.01	0.00	0.00
Tarbert	1	0.00	0.04	0.89	0.07	0.00	0.00
	2	0.00	0.01	0.76	0.23	0.00	0.00
	3	0.00	0.00	0.19	0.77	0.04	0.00
	4	0.00	0.00	0.01	0.56	0.43	0.0

Table 15-7 Default Size-Fraction Distribution for the Mississippi River

Size fractions					
Silt and clay	Very fine sand	Fine sand	Medium sand	Coarse sand	Gravel
0.00	0.01	0.45	0.45	0.08	0.01

between Head of Passes and Cairo, Illinois. It includes 15 bed-material samples within the Old River Control Complex model domain. Relevant particle size distributions show similar variations in bed-material composition to those of the February 27, 1998, data. Samples containing a significant amount of silt and clay were also found, but seem to have been local phenomena, not representative of larger areas.

Thus, for the Old River Control Complex model, an average size-fraction distribution (Table 15-7), obtained by combining February 27, 1998, data and relevant Nordin and Queen (1989) data, was chosen to be representative of the default size-class distribution for the Mississippi River.

Initial size-fraction distributions for the Mississippi River were then obtained by assigning the default size-fraction distribution to all Mississippi River bed points, except for the local areas at and around the data-vertical locations, where measured (February 27, 1998) size-fraction distributions were assigned.

The initial thickness of the active (bed-surface) layer was assumed to be 5 cm throughout the model domain. Because no other information was available, a single very

thick stratum below the bed surface was initially assumed. The Mississippi River's default size-fraction distribution was initially assigned to all subsurface sediment below the Mississippi River's bed surface. The initial subsurface size-fraction distribution for the HPP and the auxiliary structure channels was assumed to be the same as the appropriate bed-surface size-class distribution.

Furthermore, measured size-fraction distributions at four union point verticals were extrapolated to neighboring points left and right across the flow and used as the bed-sediment boundary condition for the Mississippi River at Union Point. For the two potential reverse-flow boundaries (the Mississippi River at Tarbert and the hydroelectric power plant with free-surface elevation as the hydrodynamic boundary condition) the boundary size-fraction distribution was assumed to be 100% of the model size class 6 (gravel) and 0% of all other size classes. The described bed-sediment boundary conditions were held constant for the duration of the simulation.

15.11.2.10 Physical Calibration Parameters Calibration of the mobile-bed model comprised not only adjustment of the boundary and (especially) initial conditions, but also the adjustment of certain physical parameters associated with various terms in the auxiliary sediment equations used in CH3D-SED. For the sediment size classes that showed a significant presence in both suspension and at the bed surface (such as sand size classes), the bed-sediment erosion source and the near-bed concentration contain physical parameters that can be calibrated.

The sediment model uses an empirical relation to compute the concentration of near-bed sediment particles, detached from the bed and available either to be entrained into suspension, or to be moved near the bed (sliding, rolling, or saltating) as bed load. This near-bed concentration is evaluated at a certain distance a above the bed. The bed-sediment erosion source describes the entrainment of near-bed sediment particles into suspension. It is modeled as an upward mass-diffusion flux featuring a vertical-concentration gradient. The vertical-concentration gradient is computed using the difference between near-bed concentration, evaluated at distance a above the bed, and the suspended-sediment concentration, evaluated at distance $a + \Delta a$ above the bed. The suspended-sediment concentration at distance $a + \Delta a$ above the bed is obtained by extrapolating suspended-sediment concentrations computed at the two nearest computational points in suspension above the bed as described in Section 15.7.

Both near-bed distances a and $a + \Delta a$ are input data calibration parameters. Their proper assignment ensures proper values for the near-bed concentration and erosion source terms. The near-bed distances a and $a + \Delta a$ with assigned values of 8 and 2 cm, respectively, provided the most satisfactory computed concentrations for suspended very fine, fine, medium, and coarse sand.

For silt and clay (the size class that is present mainly in suspension as wash load and that has little contact with the bed

surface) adjustment of the bed-sediment erosion source and the near-bed concentration term has virtually no effect on the sediment model. For this finest size class, the fall-velocity term decisively influences the final suspended-sediment model results. The fall velocity appears in the advection-diffusion equation governing suspended-sediment transport, but also in the bed-sediment governing equations throughout the suspended-sediment deposition source term. The calibration of the fall-velocity term was based on the proper choice of the previously unknown characteristic grain diameter for the silt and clay size class. A characteristic silt and clay diameter of 0.01 mm proved to provide satisfactory suspended silt and clay concentrations throughout the model domain, except in the auxiliary structure channel.

15.11.2.11 Model Calibration and Verification The three-dimensional model was used to simulate sediment fate and behavior at the Old River Control Complex on February 27, 1998. The sediment simulation period was 1 day. Sediment computations were initiated after a 10-h flow-stabilization period. Thus, the total flow and sediment simulation period was 34 h. Sediment computations were performed using a computational time step of 15 s.

Model calibration included choosing physical calibration parameters as well as choosing initial and boundary conditions as described earlier. To verify the model, computed suspended-sediment concentrations, at the end of the sediment simulation period, were compared to suspended-sediment concentrations measured on February 27. Also, computed bed-sediment size-fractions distributions, at the end of the sediment simulation period, were analyzed and compared to the February 27, 1998, data as well as to the Nordin and Queen (1989) data. Finally, computed changes in bed-surface elevations were analyzed to ensure that the January 1998 morphology data were not severely distorted during the sediment simulation period.

Figures 15-8(a–f) show the comparison between the computed (at the end of a 1-day simulation period) and the measured suspended-sediment concentrations along four data verticals at Line 13. More specifically, Figs. 15-8(a–e) contain computed and measured suspended silt and clay, very fine sand, fine sand, medium sand, and coarse sand concentrations, respectively, whereas Fig. 15-8(f) contains computed and measured total suspended-sediment concentrations. For silt and clay (Fig. 15-8(a)), the model correctly reproduces the total depth-averaged concentration. For very fine sand and coarse sand (Figs. 15-8(b and e)) the model correctly reproduces both total depth-integrated concentration and concentration-profile shape. For fine sand (Fig. 15-8(c)) the model slightly overestimates the total depth-integrated concentration along Vertical 2 and underestimates the total depth-integrated concentration along Verticals 3 and 4. Medium-sand concentrations (Fig. 15-8(d)) are generally overestimated, but small when compared to fine sand concentrations, and do not significantly influence the total suspended-sediment concentrations at Line 13. Thus, the computed total

suspended-sediment concentration (Fig. 15-8(f)) is mainly influenced by the computed fine-sand concentration. The model slightly overestimates the total depth-integrated concentration along vertical 2 and underestimates the total depth-integrated concentration along verticals 3 and 4 at line 13. At locations other than the Mississippi River at line 13, same calibration procedures produced similar agreement between computed and measured suspended-sediment concentrations.

Model calibration and verification consisted primarily of detailed analysis of changes that the bed-surface elevations and bed-sediment size-fraction distributions underwent during the 1-day sediment simulation period.

Except for a few local spots, the total deposition and erosion varied between +10 cm and -10 cm throughout the model domain. This relatively moderate bed-elevation change indicates that the assigned initial sediment conditions were appropriate. Somewhat higher erosion, up to -20 cm, is observed in the Mississippi River close to the HPP channel, and may be attributed either to the local flow pattern or to the fine material assigned to the bed surface next to the right bank at line 13. Large deposition values, up to +50 cm, were observed within the local area next to the upstream boundary at Union Point. This large amount of deposition can be attributed to the high fine-sand concentration assigned as a boundary condition at Union Point.

The silt and clay fraction was initially assigned a zero value everywhere throughout the domain, except for the small area next to the right bank at line 13, and the auxiliary structure channel. The computed silt and clay fraction at the end of the 1-day simulation period is below 0.05 (or 5%) throughout the domain. The initially assigned fine material at line 13 was eroded, whereas the initially assigned fine material at the auxiliary structure channel remained.

The very fine-sand fraction was initially assigned a value of 0.01 (1%) everywhere throughout the domain, except at the Mississippi River areas where collected bed-sediment samples dictate different values. The very fine-sand fraction at the auxiliary structure channel was also assigned according to the measured data. The computed very fine-sand fraction at the end of the 1-day simulation period shows almost no change as compared to initial data, except that the very fine-sand was eroded from the Mississippi River bed at those few spots where the initial very fine-sand fraction was assigned a larger value.

The fine-sand fraction was initially assigned a default value of 0.45 (45%) everywhere throughout the domain except at the Mississippi River data ranges, in the HPP and the auxiliary structure channels, and at the location of revetments along riverbanks. In the auxiliary structure channel and at the Mississippi River data ranges, the fine-sand fraction was initially assigned measured values. In the HPP channel and at the locations of revetments along the riverbanks, the fine-sand fraction was initially assigned a zero value. The computed fine-sand fraction after the 1-day simulation varied between 0 and 0.9 (90%) throughout

the domain, depending on the location. A similar range of variation in the fine-sand fraction was also found in the February 27, 1998, data and the Nordin and Queen (1989) data. Small computed values of the fine-sand fraction generally coincide with the computed erosion areas. The largest computed values of the fine-sand fraction are found at and downstream of the Union Point area with the largest computed amount of deposition, and can be attributed to the high fine-sand concentration assigned as a boundary condition at Union Point. A slight computed increase of the initially zero fine-sand fraction in the HPP channel indicates a small computed amount of deposition of fine sand in the HPP channel. A computed increase in the fine-sand fraction along the left bank in the upstream portion of the auxiliary structure channel indicates the computed erosion of the initially assigned larger fractions of silt and clay and very fine sand.

The medium-sand fraction was initially assigned a default value of 0.45 (45%) everywhere throughout the domain except in the Mississippi River data ranges, in the HPP and the auxiliary structure channels, and at the location of revetments along riverbanks. In the auxiliary structure channel and in the Mississippi River data ranges, the medium-sand fraction was initially assigned measured values. In the HPP channel and at the locations of revetments along the riverbanks, the medium-sand fraction was initially assigned a zero value. The computed medium-sand fraction varies between 0 and 0.7 (70%) throughout the domain, depending on the location. A similar range of variation in the medium-sand fraction was also found in the February 27, 1998, data and the Nordin and Queen (1989) data. Small computed values of the medium-sand fraction coincide with the computed erosion areas. Small computed values of the medium-sand fraction are also found at and downstream of the Union Point area with largest amount of deposition, and can be attributed to the large amount of fine-sand deposition which is related to the high fine sand concentration values assigned as a boundary condition at Union Point. Large computed values of the medium-sand fraction at the mid- and downstream portions of the model domain are attributed to the fine-sand erosion in those areas. The slight increase of the initially zero medium-sand fraction in the HPP channel indicates a small amount of medium-sand deposition in the HPP channel.

The coarse-sand fraction was initially assigned a default value of 0.08 (8%) everywhere throughout the domain, except in the Mississippi River data ranges, in the HPP and the auxiliary structure channels, and at the location of revetments along riverbanks. In the auxiliary structure channel and at the Mississippi River data ranges, the coarse-sand fraction was initially assigned measured values. In the HPP channel and at the locations of revetments along the riverbanks, the coarse-sand fraction was initially assigned a zero value. The computed coarse-sand fraction varies between 0 and 0.4 (40%) throughout the domain, depending on the location. A similar range of variation in the coarse-sand fraction was also found in the February 27, 1998, data and the Nordin

and Queen (1989) data. Computed values of the coarse-sand fraction that are larger than the initially assigned values are generally attributed to the erosion of fine and medium sand.

Finally, the gravel fraction was initially assigned a default value of 0.01 (1%) everywhere throughout the domain, except in the Mississippi River data ranges, in the HPP and the auxiliary structure channels, and at the location of revetments along riverbanks. In the auxiliary structure channel and in the Mississippi River data ranges, the gravel fraction was initially assigned measured values. In the HPP channel and at the locations of revetments along the riverbanks, the gravel fraction was initially assigned a value of 1.0 (100%). The computed gravel fraction at the HPP channel is 10 to 15% below the initially assigned value, reflecting the small amount of fine and medium sand deposition in the HPP channel. The large computed gravel fraction (up to 80%) can also be found in the large-erosion areas. Evidently, in the large-erosion areas, all finer-than-gravel-size classes were gradually eroded, leading to the bed-surface armoring with gravel and preventing further erosion.

15.11.2.12 Use of Calibrated Model One of the primary objectives of the use of CH3D-SED in this study was to provide sediment rating curves, by size class, for flow in the ORCC structure channels and at Tarbert Landing. This was needed for study of the long-term stability of the Mississippi and Atchafalaya rivers below the ORCC with the hydropower facility in operation, using one-dimensional mobile-bed sediment transport simulation (HEC-6 model). An associated secondary objective was to determine the expected size distribution of sediment diverted from the Mississippi into the Atchafalaya through the various outlet structures.

For these purposes, the model as calibrated for the February 27 conditions as described above was first validated through application to three other flow events for which field data campaigns had been conducted; this resulted in no further adjustment of the bed roughness, eddy viscosity, or sediment parameters.

For each of these additional flows, which ranged from 573,000 to 1,178,000 cfs (16,226 to 33,358 m³/s), the CH3D-SED model was run to a short-term water and sediment steady state, and the amount and size distribution of sediment transport, both bed load and suspended load, through the hydropower installation and auxiliary structure and downstream of Tarbert Landing were determined from model results. The limited number of discharges tested were marginally sufficient to establish rating curves for the one-dimensional models, yet the flows that were tested provided invaluable and heretofore unavailable information on sediment dynamics in the vicinity of the structures. In the end, the overall study, based on three-dimensional modeling, one-dimensional modeling, geomorphic analysis, and direct analysis of field data, concluded that operation of the hydropower installation did not have a detectable or measurable effect on the long-term stability of the Mississippi and Atchafalaya rivers downstream of the complex.

As is invariably the case in application of computational hydraulics to prototype situations, an extremely valuable secondary benefit of the three-dimensional modeling effort was the understanding of, and insight into, the interaction among flow, sediment, bathymetry, and structures in the Old River Control Complex. A detailed modeling effort such as this one can be thought of as a magnifying glass that draws the attention of the investigators to the fine details of mobile-bed hydraulics in the system, forcing them to reconcile model response with field data observations in a way that sharpens and deepens their overall understanding of the system.

15.11.3 Leavenworth Bend, Missouri River

15.11.3.1 Introduction As part of the Missouri River Mitigation Program, the U.S. Congress has mandated 48,000 acres of habitat mitigation in Iowa, Nebraska, Missouri, and Kansas. As of this writing, this mandate was being significantly expanded to well over 100,000 acres. The Omaha and Kansas City Districts of the U.S. Army Corps of Engineers are seeking guidance as to how to achieve bendway mitigation with minimal adverse affect on the stability and viability of the navigation channel. The study is presented in detail in Spasojevic et al. (2001).

The objective of this work was to perform a three-dimensional mathematical-model study of free-surface hydrodynamics, sediment transport, and bed evolution, in order to analyze the Missouri River habitat restoration measures. The chosen sample location was Leavenworth Bend on the Missouri River between Omaha and Kansas City. The CH3D-SED code was used as the basis of the mathematical model. The model's domain includes the Missouri River from river mile 399.4 to river mile 405. Fig. 15-9 shows the overall layout of Leavenworth Bend.

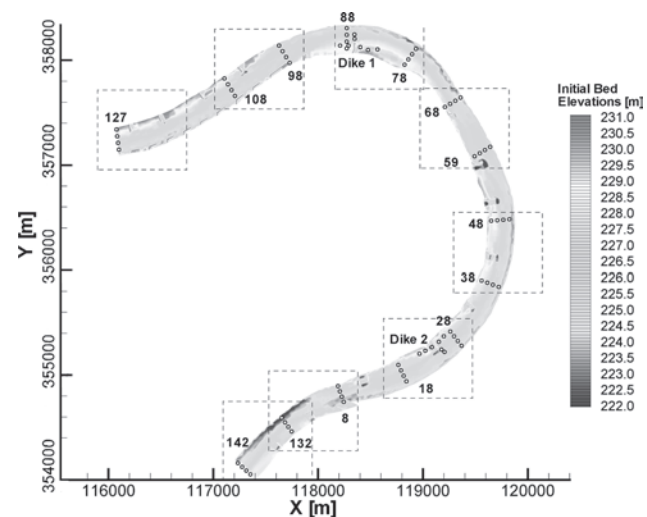


Fig. 15-9. General layout of Leavenworth Bend, Missouri River.

15.11.3.2 Field Data Campaigns Two field data sets were used for model calibration and verification to ensure that model results reproduce as closely as possible the available prototype data. One field sediment and flow data set was collected within the study area during October 5 to 7, 1999, the other during June 9 to 10, 2000. Both October 1999 and June 2000 data sets contained ADCP (Acoustic Doppler Current Profiler) discharge and velocity measurements, water free-surface elevation measurements, suspended- and bed-sediment data, and bathymetry survey data. However, the conventional techniques used during the October 1999 data set collection revealed a need for improvements, which were implemented during the June 2000 data collection effort (see Spasojevic et al. 2001). Therefore, the October 1999 data set was used for initial model calibration and verification, whereas the improved June 2000 data were used for the final model calibration and verification.

The upstream model domain boundary was chosen to approximately coincide with Line 127 (Fig. 15-9). The downstream model domain boundary was chosen to approximately coincide with Line 142. All other boundaries were treated as impermeable. Because sufficiently detailed bathymetry data around both perpendicular and L-shaped dikes were difficult to obtain, the exact dike shapes and crest elevations were recovered from the COE 1994 Hydrographic Survey maps.

15.11.3.3 Model Construction Once the exact location of model-domain boundaries and the dike geometry had been established, the computational grid was generated. Following experimentation with several levels of the grid refinement, a relatively uniform grid was constructed throughout the domain, with an average computational cell chosen to be about 10×10 m.

In the end, the computational grid had 22,947 so-called active points in a horizontal plane and 10 points in the vertical direction, i.e., along the depth. CH3D-SED uses a single-block computational grid, which, for a complex domain, covers an area larger than the actual model domain. The computational grid points inside the actual model domain are labeled “active,” whereas the rest of the points are labeled “inactive.” The size of the entire computational grid block was 823×33 points in the horizontal plane, again with 10 points along the depth.

The model construction, revisited as part of the calibration process, included choosing the proper representation of dikes within CH3D-SED limitations. The code offers two possibilities for dike modeling. One is to use an internal boundary condition called a thin barrier, which applies to the computational-cell face. The cell face is assumed to be a thin membrane with zero flow in the perpendicular direction. Because the thin barrier must extend all the way to the free surface, this condition can apply to nonsubmerged dikes or portions of dikes. For submerged dikes or portions of dikes, the dike crest elevation can be directly assigned as input data.

Eventually, a combination of the two possibilities for dike representation was used. For clearly submerged portions of dikes, the crest elevation was directly assigned, which also provided the dike-volume representation. For nonsubmerged portions of dikes, the thin-barrier condition was used in combination with an assigned crest elevation. To avoid the potential small-depth problem, the assigned crest elevation was chosen to be clearly submerged, although still providing a correct representation of the dike volume.

15.11.3.4 Boundary and Initial Conditions—October 1999 Event Hydrodynamic computations require either a free-surface elevation or an elemental-discharge distribution across the flow as a boundary condition at an open boundary. The elemental-discharge distribution across the flow can be extracted from the ADCP velocity measurements. However, the October 1999 velocity data, collected with the moving-vessel ADCP, are not fully reliable, as discussed by Spasojevic et al. (2001). The more reliable June 2000 velocity data were only collected at four verticals across the flow, which is insufficient for extraction of the elemental-discharge distribution across the width of the channel. Furthermore, measured velocities are generally not available for the model’s prediction of future scenarios, such as the analysis of proposed habitat-restoration measures.

Thus, when an elemental-discharge distribution was used as a boundary condition, the total measured discharge was distributed across the flow using the assumption that the ratio between an elemental discharge and the maximum elemental discharge was the same as the ratio between the appropriate elemental area and the maximum elemental area, assuming that the maximum discharge corresponds to the maximum elemental area. This assumption amounts to forcing the depth-integrated velocities to be proportional to the corresponding flow depths. The assumption has been already tested elsewhere using ADCP velocity data and has proven to yield reasonable results.

The approximated elemental-discharge distribution was used as a boundary condition for the upstream inflow boundary at Line 127 (Fig. 15-9). The horizontal free-surface elevation was used as the boundary condition for the downstream outflow boundary at Line 142.

Suspended-sediment samples collected on October 5 to 7, 1999 were processed to obtain suspended-sediment concentrations by size class. Bed-sediment samples collected on October 5 to 7, 1999 were also processed to obtain bed-sediment size-class distributions at the bed surface.

Because of CPU time restrictions, it proved impractical to have more than three size classes in the model. Following considerable analysis, and based on early calibration runs, the three size classes in Table 15-8 were chosen to represent the natural sediment mixture in the model of the Missouri River at Leavenworth Bend.

Table 15-8 Representative Size Classes for the Model of the Missouri River at Leavenworth Bend

Model sediment size class	Diameter range (mm)	Characteristic diameter (mm)
Size class 1 (SC1)	$D < 0.074$	Determined in calibration
Size class 2 (SC2)	$0.074 < D < 0.420$	0.176
Size class 3 (SC3)	$0.420 < D < 3.360$	1.188

Even though it was obvious from field observation that there was appreciable sand content in suspension in Leavenworth Bend, the October 1999 suspended sediment data showed no sand size classes in suspension, even though the general shape of some of the fine-sediment vertical distributions bore a strong resemblance to the shape one would have expected for suspended sand. (Suspended fine-sediment concentrations are typically more or less constant over the flow depth. Suspended-sand concentration profiles typically resemble the theoretical profile (e.g., the Rouse profile), with highest concentrations close to the bed.)

After thorough analysis, it was concluded that the suspended-sediment sample measurements required double sampling, with one sample providing the proper total suspended-sediment concentration, and the other sample providing the proper size-class distribution. Double sampling was then used to collect the June 2000 suspended-sediment data.

Based on analysis of the field data, an approximate set of boundary and initial conditions for the October 1999 sediment computations was constructed. An average size class 1 concentration profile, with a concentration of 160 ppm constant over the flow depth, was assigned as the size class 1 initial condition throughout the domain. Zero-concentration profiles were assigned as an initial condition for size classes 2 and 3, again throughout the domain.

The measured suspended-sediment concentrations were also used to construct a set of vertical concentration profiles, one for each size class, at the location of each data vertical at the inflow sediment boundary (Line 127). Size class 1 profiles were constant over the depth, with average concentration values of 100, 175, 155, and 100 ppm, corresponding to verticals 1, 2, 3, and 4, respectively. Zero-concentration profiles were constructed for size classes 2 and 3. Each constructed set of vertical concentration profiles was then assigned not only to the corresponding computational-grid vertical, but also to neighboring grid verticals across the flow, until all computational verticals across the inflow sediment boundary were assigned a boundary suspended-sediment condition.

Because the free-surface elevation was used as a downstream boundary condition for flow computations, Line 142 was identified as a potential reverse-flow boundary and also defined as a sediment inflow boundary if the flow should reverse, which of course should not occur once initial-condition transients have settled down.

Bed-sediment data collected on October 5 to 7, 1999 were used to extract size-class percentage (or fraction) distributions at bed-surface points corresponding to locations of sediment data collection verticals at all sediment data collection lines (Fig. 15-9).

Size class 1 was seldom found at the bed surface. In addition, bed-sediment samples that contained size class 1 typically showed a very small amount of fine sediment (1–5%). Exceptions were a few samples with quite significant amounts (40–60%) of size class 1, such as Vertical 4 at Line 8, vertical 1 at Line 28, or Vertical 1 at Line 108. Such samples suggest the movement of fine-sediment lenses traveling through the system, typically close to the bank. The amount of size class 2 at the bed surface varied between 10 and 100%, whereas the amount of size class 3 at the bed surface varied between 0 and 90%. Except for its large variability, the bed-material data did not offer any specific clues on the spatial distribution of size classes 2 and 3, as related to different bathymetry or flow features.

Therefore, an average size-class fraction distribution, based on all the field data, was assigned as an initial condition for bed-sediment computations. This approach ensures the correct amount of bed material in the system, and allows for comparison between the computed and the measured spatial variation ranges for each size-class fraction. An average size-class fraction distribution, based on the data for four verticals at Line 127, was assigned as an inflow boundary condition for bed-sediment computations in CH3D-SED. The inflow bed-sediment boundary conditions were kept constant for the duration of the simulation.

The initial thickness of the active (bed-surface) layer was assumed to be 5 cm throughout the model domain. Because no other information was available, a single very thick stratum below the bed surface was initially assumed. The initial subsurface size-class percentage distribution was assumed to be the same as the appropriate bed-surface distribution.

15.11.3.5 Model Calibration—October 1999 Event The flow model was first built and calibrated without sediment. The computational time step for the flow computations was 5 s; this choice was dictated by the familiar Courant-number-related numerical stability criterion. Zero-flow initial conditions (i.e., horizontal free-surface elevation and zero-velocity field) were used to begin the flow computations. The chosen combination of initial and boundary conditions (realistic discharges and/or free-surface elevations imposed on initially still water) is known to produce a disturbance (wave) that propagates back and fourth throughout the flow domain. A stabilization period is required to allow the disturbance to eventually die out. At the end of the

flow-stabilization period, a steady-state flow solution was achieved. A flow-simulation period of 12 h (8,640 f5-s computational time steps) proved to be sufficient to achieve a steady-state flow solution for a given set of boundary and initial conditions.

The major physical parameter in the CH3D hydrodynamic computations, to be determined through the calibration process, is the bed-surface friction coefficient. The CH3D flow-computations program module requires the absolute roughness as input data. The absolute roughness k determined through calibration runs had a value of 0.7 cm throughout the model domain. The appropriate friction coefficient C_d varied from 0.0124 for depth $H = 5$ m to 0.0414 for $H = 1$ m. The high absolute roughness and corresponding friction coefficients probably compensated for the simplifications in the CH3D hydrodynamic computations module, most of all the hydrostatic-pressure assumption. This assumption is ill suited for the strong secondary currents associated with almost 180° bend flow at Leavenworth Bend. Furthermore, the hydrostatic-pressure assumption does not allow for a detailed simulation of the near-field flow around dikes, which is mainly responsible for the formation of large turbulent structures and associated energy losses.

Analysis of the computed discharges showed that the model was capable of reproducing the steady-state flow condition, as defined by the average ADCP discharge, to an accuracy of 0.5%. also, as shown in Table 15-9, the

Table 15-9 Measured and Computed Free-Surface Elevations for the October 1999 Event

River mile	Free-surface elevation [m]	
	Measured	Computed
399.4	230.50	230.50 (b/c)
400.6	230.80	230.83
402.1 (d/s)	231.22	231.20
402.1 (u/s)	231.26	231.25
404.0	231.81	231.82
405.0	232.09	232.05

computed free-surface elevations showed good agreement with the measured ones.

However, computed velocities for the October 1999 event showed a fairly random pattern of agreement/disagreement with ADCP velocity measurements throughout the model domain. Fig. 15-10 presents a sample comparison of computed and measured velocities, in which significant data scattering is apparent.

The shift between measured and computed velocities in the figure appears randomly at other locations throughout the domain. As described in Spasojevic et al. (2001), the data scattering, associated with the moving-vessel ADCP velocity

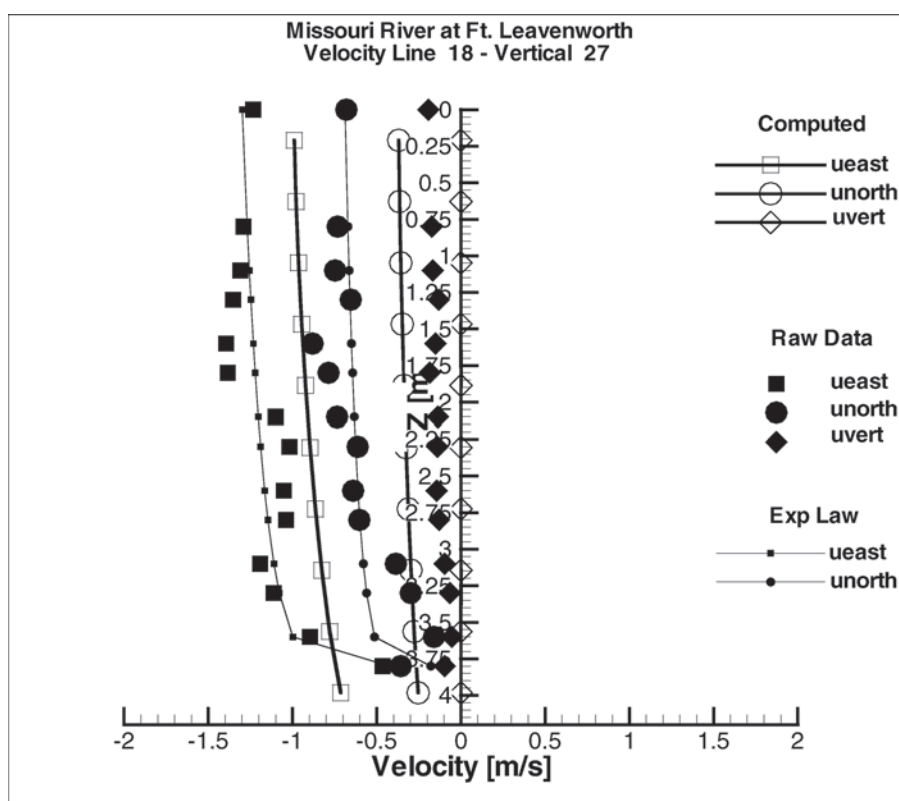


Fig. 15-10. Sample of computed and measured velocities for October 1999 event.

measurements, is caused by small-scale turbulence. Also, as shown in Spasojevic et al. (2001), the large-scale turbulence produces a random shift between the moving-vessel ADCP measurements and the proper mean-flow velocity profile. Thus, the disagreement between the computed and measured velocities in Fig. 15-10 can be attributed to the moving-vessel ADCP velocity measurements. This conclusion is further supported by the consistently fair agreement between computed and measured velocities for the June 2000 event as seen further on, when the stationary ADCP was used for collecting velocity data.

Sediment computations were initiated after a 12-h flow-stabilization period. A flow and sediment simulation period of one full day proved to be sufficient to achieve a quasi-equilibrium state between the flow and the sediment. The combined flow and sediment computations were made using a computational time step of 5 s, which was small enough to satisfy the stability condition associated with the suspended-sediment computations.

During the combined flow and sediment computations, the flow-model boundary conditions and physical parameters were kept the same as for the flow-only computations.

For the fine sediment of size class 1, the fall-velocity term had a decisive influence on the final suspended-sediment model results. The fall velocity appears in the advection-diffusion equation governing suspended-sediment transport, but also in the bed-sediment governing equations throughout the suspended-sediment deposition flux term. The calibration of the fall-velocity term was based on the proper choice of the previously unknown characteristic grain diameter for the fine sediment size class. A characteristic fine-sediment diameter of 0.015 mm proved to provide satisfactory suspended fine-sediment concentrations, but only for cases when the measured concentration profiles did not indicate the presence of sand in suspension.

Fig. 15-11 presents a sample of computed and measured suspended-sediment concentrations for the October 1999 event. Shown is a comparison between measured and computed suspended fine-sediment (size class 1) concentrations for all four sediment-data verticals at sediment data line 59. The measured size class 1 concentrations shown are also the total measured concentrations in suspension as described earlier.

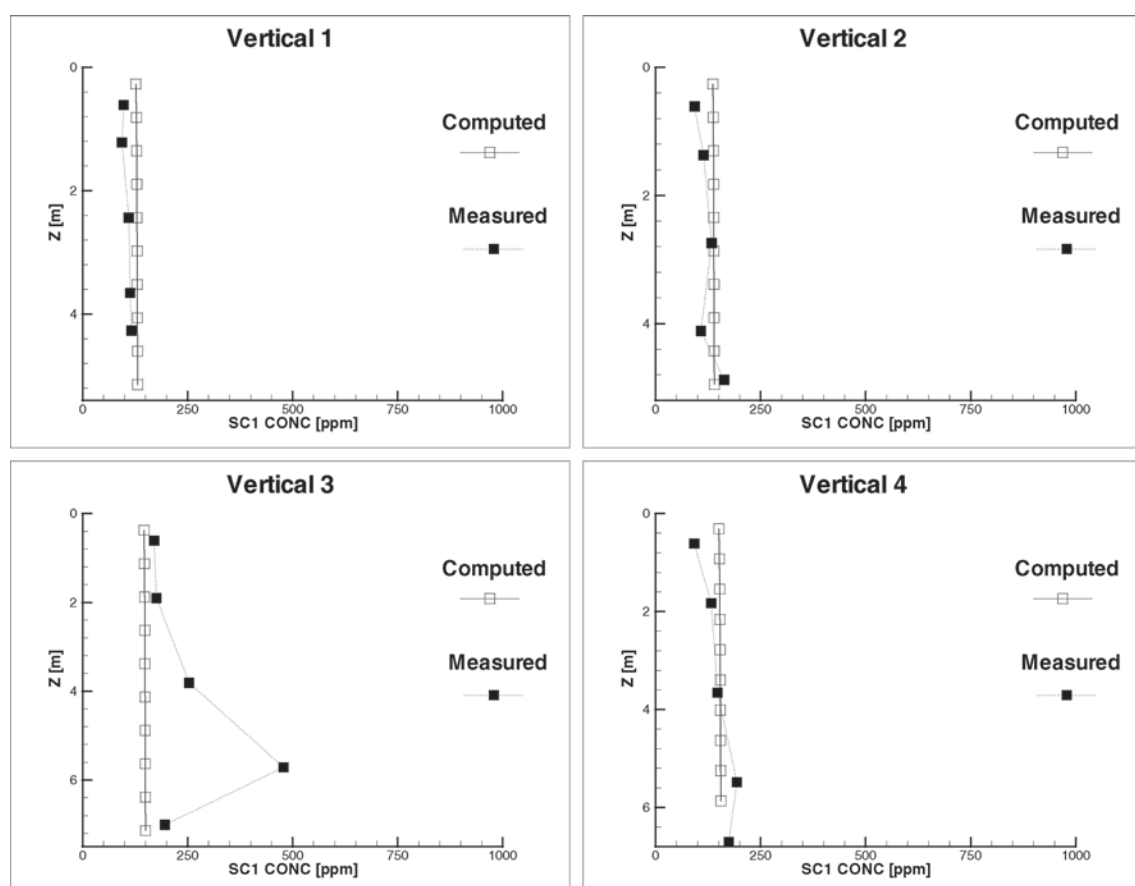


Fig. 15-11. Sample of computed and measured suspended-sediment concentrations for October 1999 event.

Satisfactory agreement between measured and computed size class 1 concentrations was achieved only when measured concentration profiles had the usual fine-sediment profile characteristics (verticals 1, 2, and 3 in Fig. 15-10). The shape of the measured concentration profile for vertical 4 in the figure clearly suggests the presence of sand in suspension.

At the end of the 1-day flow and sediment simulation period, preceded by the 12-h flow-stabilization period, the flow and the sediment reached a quasi-equilibrium state. Except for some local spots, the total (cumulative) deposition and erosion at the end of the simulation period varied between +5 and -10 cm throughout the model domain. This moderate bed-elevation change indicated a reasonable choice of initial sediment conditions.

15.11.3.6 Model Calibration—June 2000 Event The June 2000 data set was used for the detailed model calibration. This data set includes ADCP discharge and velocity measurements, free-surface elevation data, suspended- and bed-sediment data, and bathymetry. The model domain boundaries and the computational grid were the same as for the October 1999 event.

15.11.3.6.1 Flow Computations All discharges computed from the June 2000 velocity data were within $\pm 5\%$ of an average value. In addition, partial averages for multiple transect discharge measurements were within $\pm 3\%$ of the average value. Therefore, an average discharge of 37,500 cfs, or approximately $1,060 \text{ m}^3/\text{s}$, was used to represent the quasi-steady-state flow situation observed during June 9 to 10, 2000.

The choice of the initial and boundary conditions, as well as the representation of dikes, was the same as defined during the October 1999 event modeling. The June 2000 flow-model calibration comprised further refining the friction coefficient.

Table 15-9 shows that the longitudinal free-surface elevation slope was fairly uniform during October 5 to 7, 1999 (about 1 ft/mi, or about 20 cm/km). However, the free-surface elevation data collected during June 9 to 10, 2000 showed a significant longitudinal-slope variation from one portion of the domain to another. Therefore, the absolute roughness k determined through calibration runs also had different values along the domain: 0.8 cm between river miles 399.4 and 400.6, 0.05 cm between river miles 400.6 and 402.1, 0.4 cm between river miles 402.1 and 404, and 0.8 cm between river miles 404 and 405. Again, the high absolute roughness in certain areas and corresponding friction coefficients probably compensated for the simplifications in the CH3D hydrodynamic module, in particular the hydrostatic-pressure assumption.

The computed discharges reproduced the steady-state flow condition, as defined by the average ADCP discharge, within 0.5%. Also, as shown in Table 15-10, the computed free-surface elevations showed good agreement with the measured ones, with somewhat larger discrepancies at river mile 402.1.

Computed velocities for the June 2000 event showed fairly good agreement with ADCP velocity measurements throughout the model domain. Fig. 15-12 presents a sample comparison of computed and measured velocities.

15.11.3.6.2 Sediment Computations The representative sediment size classes were the same as those chosen during the October 1999 event modeling (Table 15-8); the characteristic fine-sediment diameter was also taken to be the same as determined for the October 1999 event. Sediment initial and boundary conditions were also constructed following the procedure established during the October 1999 event modeling and discussed in the previous section. The model calibration included defining the physical parameters that were not calibrated during the October 1999 event modeling, notably due to the incomplete suspended-sediment data.

Measured suspended fine sediment (size class 1) concentrations were more or less constant over the depth. Furthermore, with only two or three exceptions, depth-averaged values of measured fine sediment concentrations varied between 90 and 120 ppm throughout the domain. Therefore, a concentration profile with a depth-constant value of 105 ppm was assigned as an initial condition for the fine-sediment concentrations at all computational points.

Measured suspended size class 2 concentrations showed rather large variation throughout the domain. The near-bed concentration generally varied between 0 and 300 to 400 ppm, but some data points showed concentrations an order of magnitude larger (up to 3,000 ppm). Furthermore, even though the measured size class 2 concentration profiles generally resembled the theoretical sand concentration profiles, several of them showed distinctly nonmonotonic behavior. An occasional spike in a measured sand-concentration profile could be attributed to the large turbulent structures (boils) carrying the high concentrations away from the bed. However, the two-spike profiles with maximum concentration about 3,000 ppm (dike 2, vertical 7) are more difficult to explain. This difficulty was obviated by simply assigning an average size class 2 profile with a near-bed concentration of

Table 15-10 Measured and Computed Free-Surface Elevations for the June 2000 Event

River mile	Free-surface elevation [m]	
	Measured	Computed
399.4	229.55	229.55 (b/c)
400.6	230.04	230.05
402.1 (d/s)	230.13	230.26
402.1 (u/s)	230.24	230.31
404.0	230.90	230.92
405.0	231.23	231.24

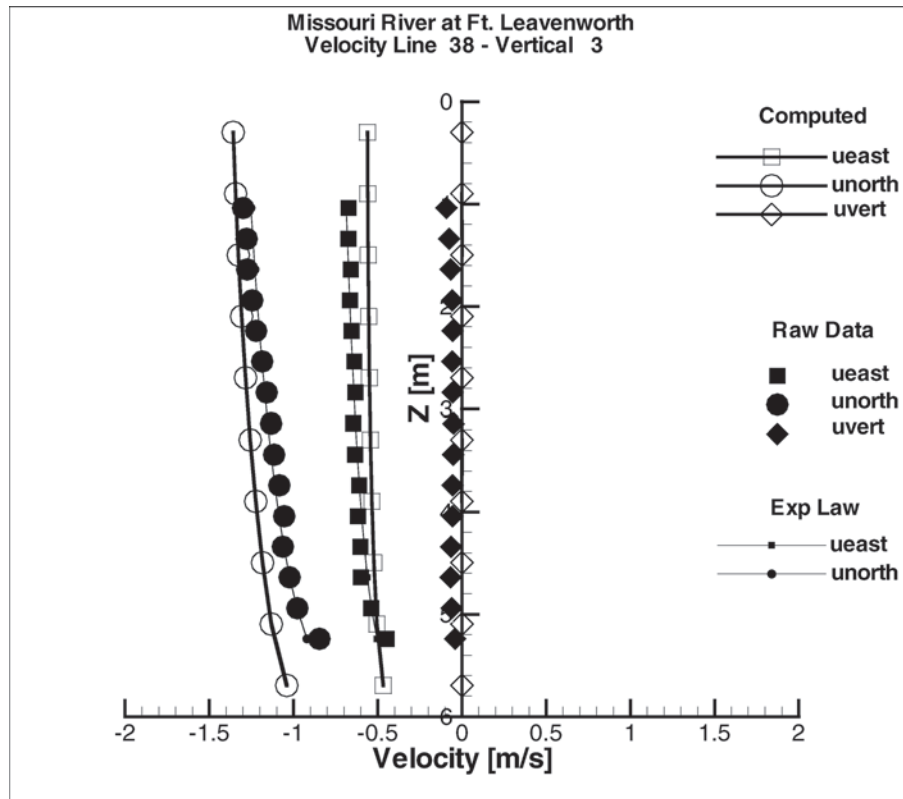


Fig. 15-12. Sample of computed and measured velocities for June 2000 event.

100 ppm as the initial condition for all computations points. This approach succeeded in initially introducing enough size class 2 sediment into suspension to let the sediment-flow interaction converge to the final computed size class 2 profiles.

Measured suspended size class 3 concentrations were generally close to zero, again with typically excessive exceptions, such as the near-bed concentration of 1,600 ppm at vertical 2 of Line 28. Neglecting these isolated exceptionally large measured concentrations, an average size class 3 profile with a near-bed concentration of 10 ppm was assigned as the initial condition to all computational points.

The actual measured suspended-sediment concentrations at Line 127 were used to construct a set of vertical concentration profiles, one for each size class, at the location of each data vertical at the inflow sediment boundary. Each constructed set of vertical concentration profiles was then assigned not only to the corresponding computational-grid vertical, but also to neighboring grid verticals across the flow, until all computational verticals across the inflow sediment boundary were assigned a boundary suspended-sediment condition.

It should be noted that the measured size class 2 concentrations at Line 127 in some cases contained excessive values. As a result of using the measured excessive concentrations

as the sediment inflow boundary, computations showed corresponding excessive deposition at and immediately downstream from the boundary. Thus, it was concluded that the excessive measured concentrations are probably a short-lived phenomena associated with transitory turbulent structures, and not characteristic of longer periods of time as resolved by the model. Consequently, the excessive concentrations at the boundary were replaced by average values, which led to moderate computed bed elevation changes in the first few hours of mobile-bed simulation.

Most bed-sediment samples did not contain size class 1. Those samples that did contain size class 1 typically showed a small amount of fine sediment (1–4%). Two bed-sediment samples that contained somewhat larger amounts of the fine sediment (around 15%) were collected next to the right bank at Line 8 (vertical 1) and behind Dike 1 (vertical 6). The data did not offer clear evidence of a fine-sediment lens traveling through the system. The amount of size class 2 at the bed surface varied between 3 and 96%, whereas the amount of size class 3 at the bed surface varied between 3 and 97%. Again, the bed-material data did not offer any specific clues on the spatial distribution of size classes 2 and 3, as related to different bathymetry or flow features, other than the inherent large variability and nonhomogeneity of the bed material. As an example, whereas the data shows a significant amount of

size class 2 upstream from Dike 1, the amount of the same size class upstream from Dike 2 is quite small.

Therefore, an average size-class fraction distribution, based on all collected data, was assigned as an initial condition for bed-sediment computations. Furthermore, because the June 2000 data did not contain any bed-sediment samples at Line 127 (the closest bed-sediment samples were collected at Line 108), the same average size-class fraction distribution was used as an inflow boundary condition for bed-sediment computations. Table 15-11 shows the size-class fraction distribution used as both initial and boundary conditions. The inflow bed-sediment boundary conditions were kept constant for the duration of the simulation.

Table 15-11 The Size-Class Fraction Distribution Used as Initial and Boundary Conditions, June 2000

Size-class fractions [-]			
	Size class 1	Size class 2	Size class 3
I/C and B/C	0.01	0.53	0.46

The initial thickness of the active (bed-surface) layer was assumed to be 5 cm throughout the model domain. Because no other information was available, a single very thick stratum below the bed surface was initially assumed. The initial subsurface size-class percentage distribution was assumed to be the same as the appropriate bed-surface distribution.

The near-bed distances a and $a+\Delta a$ with assigned values of 1 and 3 cm, respectively, provided the most satisfactory computed suspended-sediment concentrations. Fig. 15-13 presents an example of computed and measured suspended-sediment concentrations for the June 2000 event. Shown is a comparison between measured and computed suspended size class 1 concentrations for all four sediment-data verticals at Line 28.

The agreement between the computed and measured fine sediment concentrations is quite good throughout the domain. Because the model cannot reproduce the large variation and sudden discontinuities of the size class 2 sediment concentration data, the calibration goal was to achieve an agreement between computations and measurements in an average sense. As shown in Fig. 15-13, computed size class 2 concentrations were occasionally overestimated at one and underestimated at another vertical, whereas the excessive

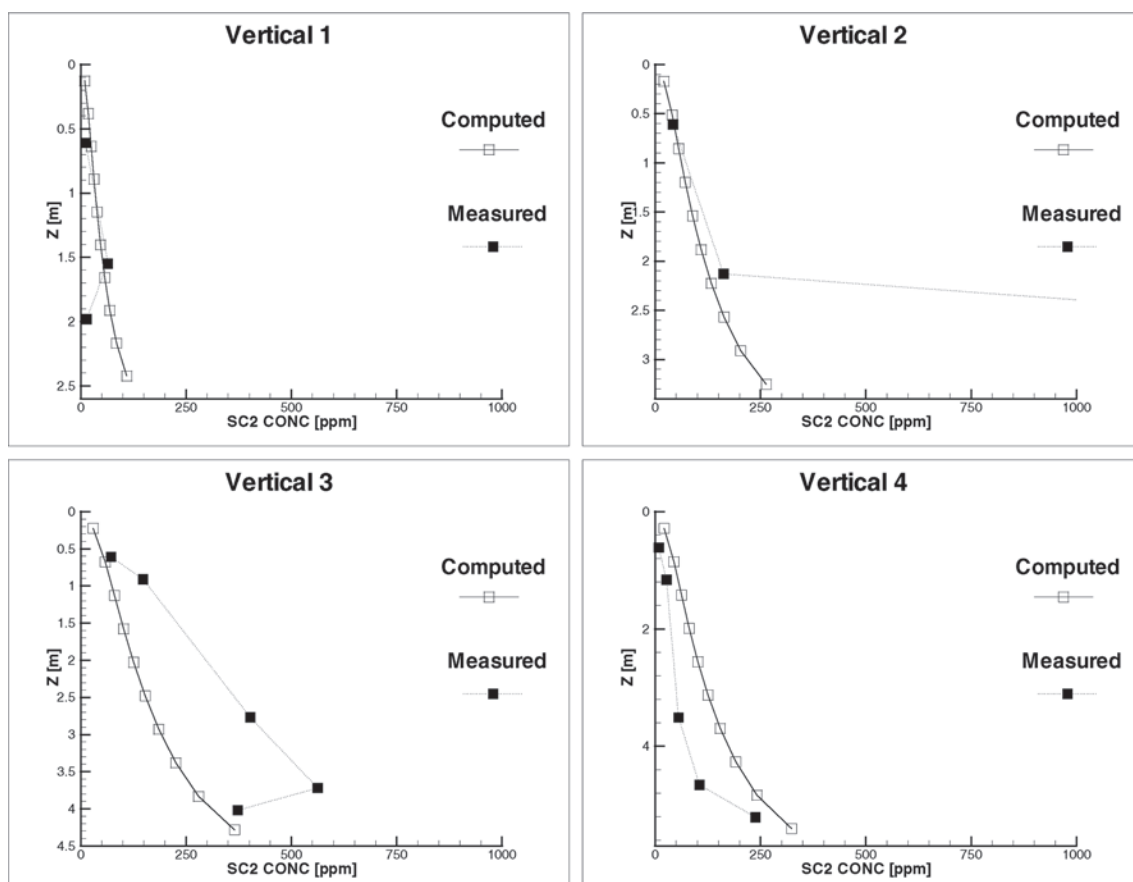


Fig. 15-13. Sample of computed and measured suspended-sediment concentrations for June 2000 event.

measured concentrations were simply ignored. The model also successfully reproduced the observed small size class 3 concentrations, although missing the few excessive measured values.

At the end of the one-day combined flow and sediment simulation period, preceded by the 12-h flow-stabilization period, the flow and the sediment reached a quasi-equilibrium state. Except for some local spots, the total (cumulative) deposition and erosion at the end of the simulation period varied between +10 and -10 cm throughout the model domain. This moderate bed-elevation change validates the reasonable choice of initial sediment conditions. As before, the spots with larger cumulative erosion and deposition found around dikes or close to banks are attributed to errors in the initial bathymetry.

The computed fine sediment (size class 1) fraction was practically zero throughout the domain. A small amount of the fine sediment, up to 2%, was computed at near-bank areas. The initially assigned size class 2 fraction was 0.53 (53%) throughout the domain. The computed size class 2 fraction at the end of the one-day simulation period, as shown in Fig. 15-14, showed a range of variation quite similar to the observed one. The depletion of size class 2 in the upstream portion of the model domain indicates insufficient supply of this size class through the inflow boundary, probably due to the approximate boundary conditions. The June

2000 data set did not contain enough information in that area. The most upstream data line with bed-sediment data is line 108, which had only two bed-sediment samples. The computed distribution of the size class 3 fraction throughout the domain was practically a mirror image of the size class 2 fraction distribution. Size class 3 also showed a variation range similar to the observed one.

15.11.3.7 Use of Model to Study Proposed Habitat Restoration Measures

The complete model, as described in the previous sections, required quite extensive CPU time (2 to 2.5 times longer than real time on a state-of-the-art 2002 personal computer) for simulation runs. Due to the prohibitive CPU time, it was decided to extract a small portion of the complete model and apply the proposed habitat restoration modifications to this submodel. The submodel included approximately the area between data lines 28 and 48 (Fig. 15-9). The submodel computational grid, the bathymetry, and the dikes representation were kept the same as for the corresponding portion of the complete model. The total number of computational-grid cells for the submodel was 121×27 . Figure 15-15 shows the submodel domain.

A proper transition from the complete model to the submodel could be achieved by using the entire set of the complete-model results as initial and boundary data for the submodel. However, this would require hot-start capability, unavailable in the CH3D-SED code as of this writing.

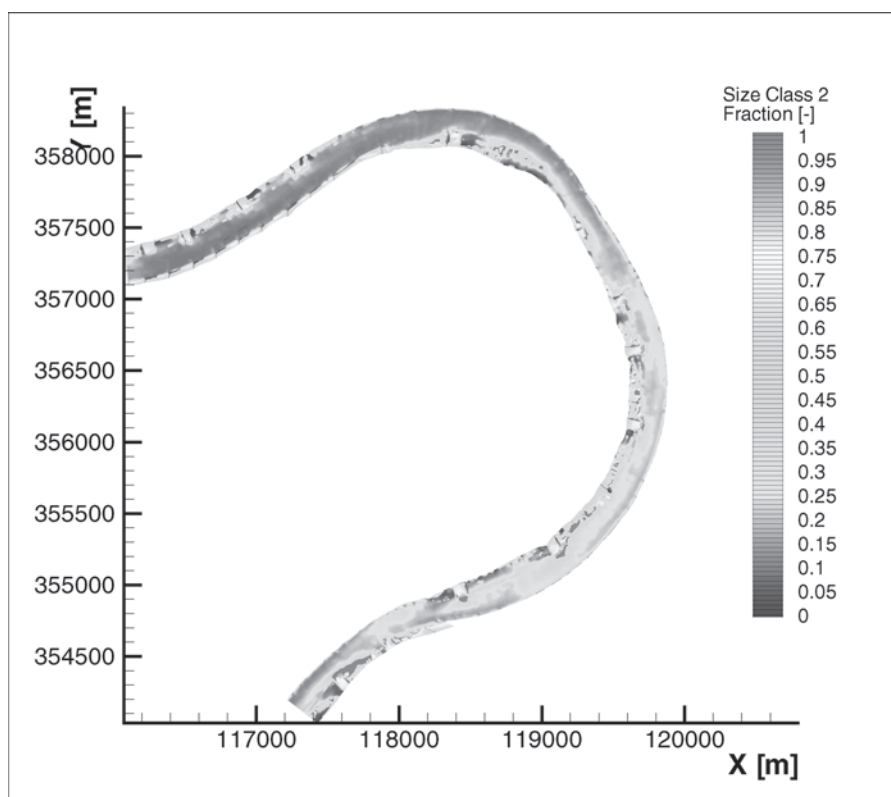


Fig. 15-14. Computed size class 2 fraction at the bed surface, June 2000 event.

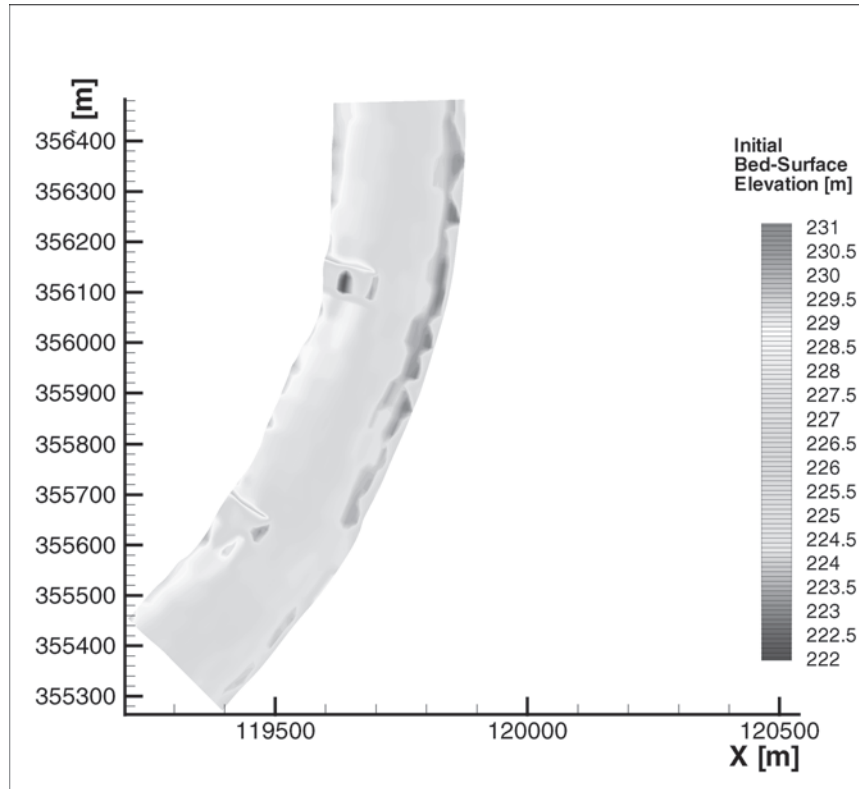


Fig. 15-15. The submodel domain.

Therefore, boundary and initial conditions for the submodel computations were constructed based partly on the complete model simulations of the June 2000 event, and partly on the available June 2000 data within the submodel domain.

Boundary conditions for the submodel flow computations were the approximated elemental-discharge distribution at the upstream inflow boundary (Line 48, Fig. 15-9) and the free-surface elevation, extracted from the complete model results, at the downstream outflow boundary (Line 28, Fig. 15-9). Zero-flow initial conditions were used for the flow computations. The friction coefficient was kept the same as the friction coefficient for the corresponding portion of the complete model, defined during the calibration of the complete model.

Boundary conditions for the submodel sediment computations were suspended-sediment concentration profiles and bed-sediment size-class fraction distributions extracted from the complete-model results. Initial conditions for sediment computations were constructed based on the June 2000 data, available within the submodel domain. The sediment characteristic size classes and physical calibration parameters (fine-sediment characteristic diameter and near-bed distances a and $a + \Delta a$) were kept the same as determined during the complete-model calibration.

The submodel produced discharges and free-surface elevations with the same accuracy as the complete model.

The computed submodel velocity and suspended-sediment concentration profiles showed the same agreement with the corresponding data as achieved with the complete model. However, the submodel cumulative erosion and deposition, as well as the size-class fractions at the bed surface, were not entirely the same as for the corresponding portion of the complete model. This suggests that the difference between the submodel and the corresponding portion of the complete model stems from the imbalance between initial and boundary conditions used for the small-model bed sediment computations. Thus, the submodel, and not the corresponding portion of the large model, was used as the reference for analyzing changes due to the proposed river-restoration modifications. The simulation period of five days was used for all submodel runs, both without and with modifications.

The first proposed modification included river widening and modifying the existing dikes into so-called rootless dikes. To widen the river, a channel, approximately 30 ft (9.14 m) wide and 10 ft (3.05 m) deep, was added along the concave bank. To modify the existing dikes into rootless ones, the near-bank portions of the existing dikes, approximately 30 ft (9.14 m) long, were removed. The cumulative bed-surface elevation changes after a 5-day simulation period for the submodel with the river widening and rootless dikes were compared with the same results for the submodel

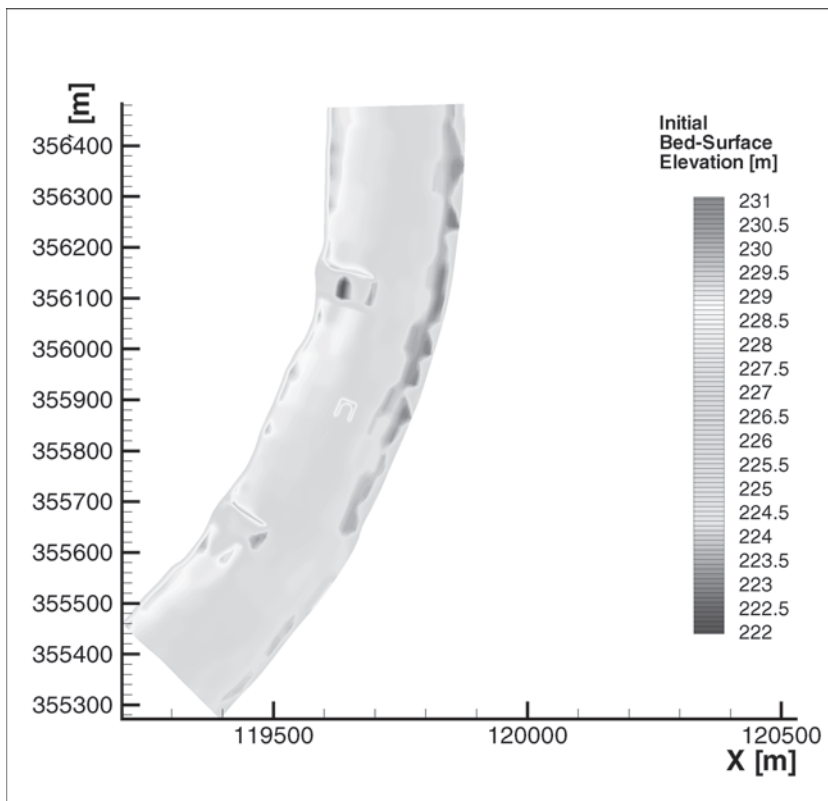


Fig. 15-16. River widening with rootless dikes and far chevron.

without any modifications. The comparison shows almost no difference between the two cases. Both computations show no significant change in the bed-surface elevation next to the concave bank. The intermittent erosion and deposition in the main channel and around dikes is quite similar in both cases, suggesting minimal influence of the proposed change.

A second proposed modification was a so-called far chevron dike added to the original modification (river widening with rootless existing dikes), as shown in Fig. 15-16. The schematic chevron dike was about 120 ft long (36.6 m) and 120 ft (36.6 m) wide. Its upstream end was about 720 ft (219.4 m) downstream from the upstream existing dike (Fig. 15-16), whereas its downstream end was about 750 ft (228.6 m) upstream from the downstream existing dike. An imaginary mid-chevron line, approximately parallel to the riverbanks, was located about 370 ft (112.8 m) away from the right descending bank, i.e., about 430 ft (131.1 m) away from the left bank. The dike was submerged with the crest elevation 3 ft (1 m) below the water surface; i.e., its height varied between about 8 (2.4 m) and 10 ft (3.05 m).

Figure 15-17 shows the cumulative bed-surface elevation changes, after a 5-day simulation period, for the model with river widening, rootless existing dikes, and the added far chevron dike. The cumulative bed-surface elevation changes away from the dike are quite similar to those for the original modifications. The area where the far chevron was intro-

duced did not suffer any large erosion or deposition due to the initial modifications. Therefore, the computed local bed-surface elevation changes around the dike can be attributed to the dike alone. The maximum erosion immediately downstream from the dike was about 2.5 m. The eroded material was deposited further downstream, over a larger area with maximum deposition of about 1.4 m.

As a third proposed modification, a so-called close chevron dike was added to the original modification (river widening with rootless existing dikes). The schematic close chevron dike had the same dimensions as the far chevron dike. The near chevron was located on the same perpendicular section as the far chevron; i.e., its upstream end was about 720 ft (219.4 m) downstream from the upstream existing dike (Fig. 15-16), whereas its downstream end was about 750 ft (228.6 m) upstream from the downstream existing dike. The imaginary mid-chevron line was located about 280 ft (85.3 m) away from the right descending bank; i.e., the dike was about 90 ft (27.9 m) closer to the right bank than the far chevron. The dike was submerged with the crest elevation 3 ft (1 m) below the water surface.

The cumulative bed-surface elevation changes after a 5-day simulation period, for the model with river widening, rootless existing dikes, and the added close chevron dike, in the area away from the chevron were again quite similar to those for the initial modifications. The close chevron

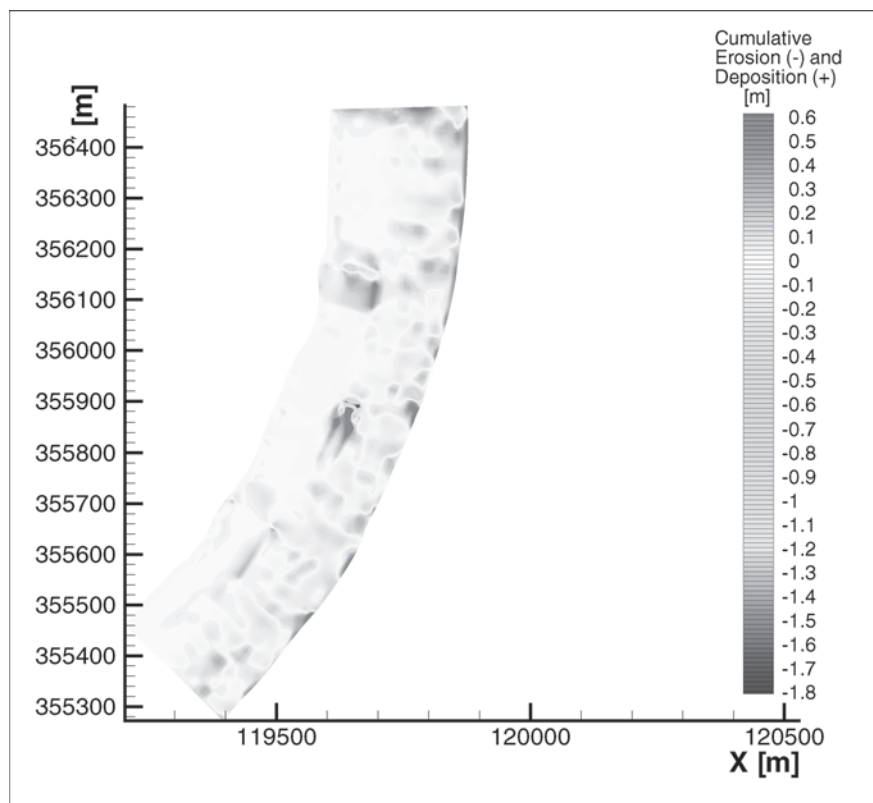


Fig. 15-17. Cumulative erosion and deposition after a five-day simulation period: submodel with river widening, rootless dikes, and far chevron.

affected a smaller local area than did the far chevron. The maximum erosion immediately downstream from the dike was about 1.4 m. The eroded material was deposited further downstream, over a larger area with maximum deposition of about 0.8 m.

This example effectively demonstrates the power of a three-dimensional mobile-bed model to provide indications of the response of a mobile-bed river to modifications imposed upon it, even if CPU time restrictions (as of this writing) make it impossible to perform truly long-term simulations (e.g., one or more complete hydrographs). There is nothing in CH3D-sed or the model data set that would preclude doing simulations for part or all of one or more hydrographs, if the supporting computer hardware were one or more orders of magnitude faster than what was available as of this writing.

15.11.4 Coralville, Saylorville, and Red Rock Reservoirs, Iowa

15.11.4.1 Introduction Two-dimensional mobile-bed models cannot capture the hydrodynamic and sediment processes associated with secondary flow, vertical acceleration around structures, etc. On the other hand, they offer the possibility of relatively long-term unsteady simulations when their

simplifying assumptions are appropriate for the problem under study. This can be illustrated through a summary description of the application of the MOBED2 two-dimensional mobile-bed program to the prediction of long-term sedimentation in the three major flood-control reservoirs of Iowa.

The mathematical and numerical basis for MOBED2 is described in Spasojevic (1988), and Spasojevic and Holly (1990a). This example is extracted from the report by Savic and Holly (1993).

The MOBED2 code comprises a numerical procedure for simulation of two-dimensional (plan view) unsteady interaction of sediment movement and hydrodynamics in natural watercourses. The basic governing equations for the flow are the momentum Eqs. (15-14) and (15-15) and the continuity Eq. (15-9). The basic sediment equations are the mass conservation equations for the channel bed (Eqs. 15-63) and (15-64) and the two-dimensional advection-diffusion equation for suspended-sediment transport (Eq. 15-71), both for any number of distinct sediment size classes. Auxiliary relations used for system closure are discussed in Sections 15.8.4 and 15.8.5 of this chapter. The tensor forms of the governing water and sediment equations in an orthogonal curvilinear system are used, permitting ready representation of the boundaries of natural watercourses. The entire code and associated numerical techniques are structured to avoid use of any

particular empirical relation until very late in the derivations. Therefore, the overall structure of the computation is independent of particular empirical expressions used to evaluate auxiliary relations, and thus they can be exchanged rather easily.

The hydrodynamic (depth-averaged Reynolds) equations are solved numerically using a split-operator procedure (momentum advection and diffusion steps had not yet been implemented in the code at the time of this project), and the resulting system of linear algebraic equations is solved by the alternative direction implicit method.

The sediment equations (including bed load for each size class and bed evolution) are solved simultaneously for each computational point using the Newton-Raphson method. Some of the important features of MOBED2 include the following:

The global set of sediment equations for all size classes, taken as a whole and solved simultaneously, describes the behavior of a mixture, including natural phenomena such as differential settling, armoring, and hydraulic sorting.

Sediment particles can move either in suspension or as bed load, depending on local flow conditions. Criteria for distinguishing between bed-load and suspended-sediment transport, as well as mechanisms defining exchange between the two, are incorporated into the code.

Sediment mixtures in natural watercourses are represented through a suitable number of discrete size classes.

Both the hydrodynamic and sediment equations are solved in a curvilinear coordinate system, which implies transformation of the governing equations in the real coordinates $X-Y$ of the so-called physical plane into the computational $\xi-\eta$ plane.

The goals of this study were to demonstrate the ability of MOBED2 to simulate unsteady water-sediment flow for the three Iowa reservoirs (Coralville, Saylorville, and Red Rock) and to provide a preliminary calibration of the data sets preliminary to transfer of the code and data sets to the sponsoring user, the Rock Island District of the U.S. Army Corps of Engineers.

15.11.4.2 Data Sources and Model Construction Topographical data came from two sources:

1. 1:24,000 U.S. Geological Survey topographic maps
2. U.S. Army Corps of Engineers Sedimentation Survey Reports

Because the computational-grid spacing was much denser than the spacing of the sedimentation survey sediment ranges (SR), an interpolation procedure, performed by University of Iowa GIS specialists, was used to obtain the computational-grid topology and topography. Numerous manual modifications of the data sets were performed in an iterative process, using the preliminary computation runs, to ensure correct numerical solution of the governing equations. This manual grid adjustment and refinement were a preliminary calibration of the model data sets.

The hydrologic data were provided by the Rock Island District of the U.S. Army Corps of Engineers. For the purpose of preliminary calibration the data were used to set inflow discharges and suspended sediment concentrations for the test runs. The most important data—regarding suspended-sediment size and bed-load size and distribution—were not available, and were thus assumed from Spasojevic (1988).

Specification of the two-dimensional plan-view grid is relatively simple for rectangular (or nearly rectangular) channels, and/or if the expected variations of free-surface elevations are small. However, in natural watercourses, any significant change of the free-surface level may notably change the plan-view contour of the flow domain. One approach to resolving this problem is to define the maximum model-domain contour based on the maximum expected free-surface level, and to treat the periodically dry areas of the model by a special procedure if the water level lowers significantly, so that the flow domain shrinks. However, at the time of this study, MOBED2 was not designed to cope easily with frequent and large changes in wetted and dry areas within the model domain. For this particular study, in which the Old River channels were permanently submerged below the dam-maintained reservoir elevation and the reservoir banks were relatively steep, it was possible to simulate extended periods of time with a single computational grid.

For the Iowa reservoir models, the downstream boundary was the dam itself, the impermeable side boundaries were determined by the maximum water levels, and the upstream boundaries were selected in consultation with Rock Island District engineers so that the major part of the sediment entrapped in the reservoir lay within the computational domain. The computational grid was specified to provide sufficiently detailed information on the studied reservoirs, yet not so detailed as to unnecessarily encumber the already time-consuming computations.

15.11.4.3 General Boundary and Initial Conditions

For initial conditions, MOBED2 requires known values or hydrodynamic and sediment quantities appropriate to the beginning of the simulation period: water-surface elevations and two-directional velocity fields for the hydrodynamic equations, and suspended-sediment concentration and distribution of the bed material for each size class and the initial bed elevation for the sediment equations.

Both inflow (upstream) and (outflow) downstream boundary conditions are required for the hydrodynamic computation. The outflow boundary condition can be a rating curve or a given discharge or free-surface elevation hydrograph, whereas the inflow boundary condition can be a discharge or free-surface elevation hydrograph only. For the sediment equations, boundary conditions are required only at inflow (hydrodynamic) boundaries, with prescribed evolution of suspended-sediment concentrations, bed-material distribution, and the bed elevation for each computational point across the inflow boundary.

The test cases for the preliminary calibration were selected to demonstrate the ability of the model to simulate two-dimensional unsteady water-sediment flow in the three Iowa reservoirs, that is, to show that the code can provide long-term simulations without numerical problems.

Accordingly, the test cases presented here were selected to treat a hypothetical hydrological situation, i.e., not to follow the strict details of a particular hydrological time-series. Moreover, even in a less hypothetical application of the models, it is suggested that only major flood events be simulated, i.e., those in which the majority of the sediment inflow occurs. (For example, one may simulate the important sedimentation features of a 50-year period by running only 100–200 months.) In addition to significant savings of CPU time, this helps to alleviate potential dry-bed problems (as explained earlier), because the large flood-flow discharges tend to correspond to the higher pool elevations for which the computational grids were laid out.

Initial data for the hydrodynamic computations required the initial distribution of both components of the depth-averaged velocity and the free-surface elevations. A zero-flow initial condition was assumed, implying a horizontal water level and a zero velocity field for the entire computational domain.

The hydrodynamic boundary condition along the upstream inflow boundaries was the distribution of unit discharge across the boundary. Because measured data for the flow distributions was not available, a reasonable estimate was obtained by distributing the total discharge across the upstream boundary in accordance with the cross-sectional area distribution. Imposition of the free-surface elevation along the dam cross section seemed to be an appropriate boundary condition at the downstream boundary, given the small velocities in the vicinity of the dam.

The sediment computations require representation of the natural sediment mixture in the reservoir by an appropriate number of size classes and their distribution. Measurements and analyses of size distributions for natural sediment mixtures in the Iowa reservoirs are extremely scarce, especially for the bed material. Therefore, the values from Spasojevic (1988) were used as a reasonable assumption for all three reservoirs. Only two size classes were chosen to simulate the natural sediment mixture. Size class 1 represents fine sediment capable of moving in suspension, whereas size class 2 represents coarser sediment mainly confined to the bed. A characteristic diameter of $D = 0.0025$ mm, taken from the size-distribution curve for suspended sediment at the Marengo gauging station (Spasojevic 1988), was used as an equivalent diameter for size class 1, whereas a diameter of $D = 0.6$ mm was used as the equivalent diameter for size class 2. It was assumed that, immediately after the dam was built, the bed consisted predominantly of coarser sediment (size class 2); thus, the initial active-layer size fractions were assigned to be zero for size class 1 and unity for size class 2. Initial bed elevations (as well as the entire geometry of the

model domain) were defined based on the original reservoir survey data.

The dam section was treated as an outflow boundary with zero bed-load flux during sediment computations. Imposed suspended-sediment concentrations (obtained from the data provided by the Rock Island District) defined the inflow boundary condition for the suspended sediment; a zero bed-load influx and constant bed elevations, were assumed to be appropriate upstream assumptions for the bed-load boundary conditions, given the lack of meaningful field data.

Ten-year periods were simulated for each of the reservoirs. The first year represented a schematic annual hydrological cycle to demonstrate that the code can perform under unsteady-flow conditions (see Fig. 15-18). The upstream hydrodynamic boundary condition was a schematic discharge hydrograph with a base of Q_{\min} and peak of Q_{\max} , whereas the similar schematic pool-elevation hydrograph determined the downstream boundary condition; the suspended-sediment concentration variations were assumed to correspond to the inflow hydrograph variations (Fig. 15-19). The remaining portion of the 10-year period was simulated with a constant discharge at the representative flood peak Q_{\max} , the maximum pool elevation Z_{\max} , and the maximum suspended sediment concentration C_{\max} , for each of the three reservoirs.

15.11.4.4 Coralville Reservoir The Coralville Reservoir is a flood-control impoundment located on the Iowa River near Iowa City, Iowa. The Coralville reservoir model represents the part of the reservoir from the Coralville Dam up to Sediment Range (SR) No. 21. To define the computational domain of the Coralville model, a flood situation with free-surface elevation around 217 m (roughly 712 ft) was adopted. For this condition the reservoir can be thought of as consisting of two parts with distinctly different hydraulic characteristics, as seen in Fig. 15-20. The part between Coralville Dam and the Curtis Bridge is relatively narrow, with the majority of the cross sections being either roughly trapezoidal or triangular in shape. The part between the Curtis Bridge and the upstream boundary is primarily a broad valley with dominant flood plains.

Fig. 15-20 shows the two-dimensional (plan-view) contour of the model domain, together with the orthogonal curvilinear computational ($\xi-\eta$) grid constructed to fit the model domain. The total number of computational points was 2,937, with $I = 267$ points in the ξ -direction (which is roughly the direction of the flow) and $J = 11$ points in the η -direction (which is roughly the direction perpendicular to the flow).

As described earlier, a zero flow state, with horizontal free-surface elevations and zero flow field, was used for the hydrodynamic initial condition. The initial suspended-sediment concentration for size class 1 (fine sediment) was set to 100 ppm over the entire domain; for size class 2 (coarse sediment), a global zero concentration was assigned as an initial condition.

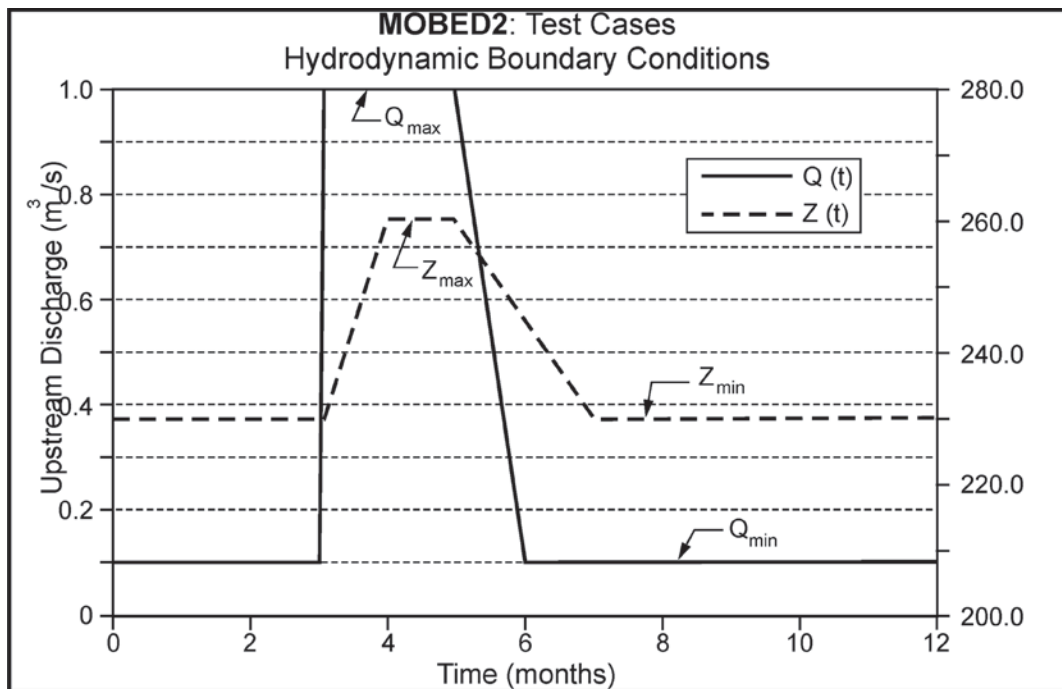


Fig. 15-18. Hydrodynamic boundary conditions for the test cases.

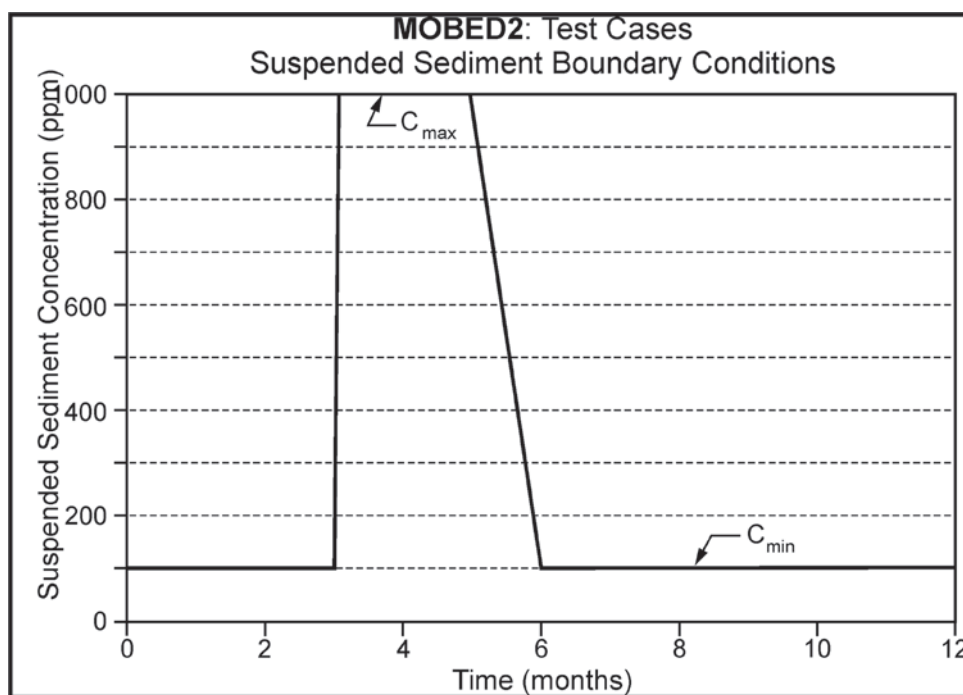


Fig. 15-19. Suspended-sediment boundary conditions for the test cases.

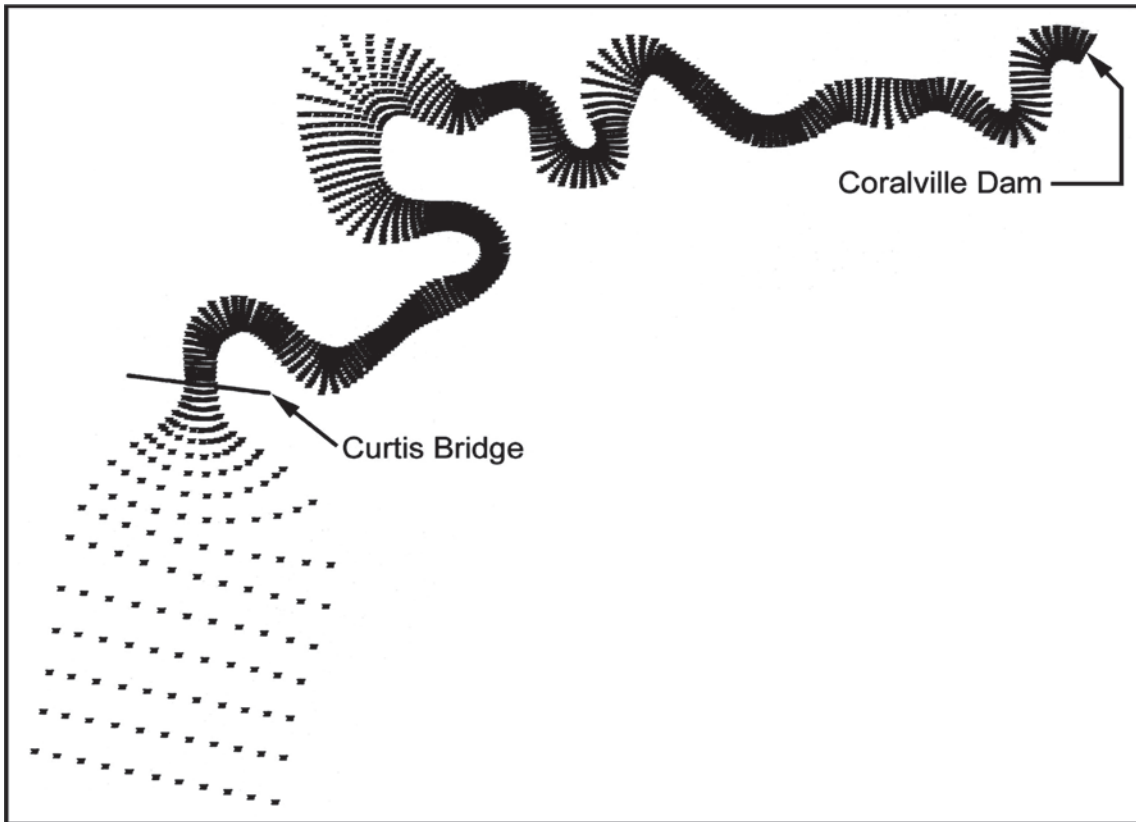


Fig. 15-20. Bed-elevation changes for Section $I = 228$ of Coralville Reservoir for simulation times of $t = 8.2$ and 11 years.

The maximum and minimum discharges of $Q_{\max} = 300 \text{ m}^3/\text{s}$ (10,600 cfs) and $Q_{\min} = 50 \text{ m}^3/\text{s}$ (1,765 cfs) for the upstream boundary condition (see Fig. 15-18) were selected in accordance with the historical hydrologic data. For the downstream boundary condition, free-surface elevations of $Z_{\max} = 217 \text{ m}$ (712 ft) and $Z_{\min} = 213 \text{ m}$ (698 ft) were selected, thus obviating possible dry-bed conditions, but still leaving the possibility to simulate pool-management operations during flood periods. The suspended sediment concentrations of $C_{\max} = 1,000 \text{ ppm}$ and $C_{\min} = 100 \text{ ppm}$ (Fig. 15-19) were considered to be a reasonable approximation for the purpose of preliminary calibration.

Two characteristic cross sections were chosen to present flow and sediment variables for this test simulation. Figures 15-21 to 15-24 show selected flow/sediment variables at cross section $I = 228$ (corresponding approximately to sediment range SR-5), whereas Figs. 15-25 to 15-28 show cross section $I = 7$ (close to sediment range SR-20). Cross section $I = 228$ (i.e., range SR-5) is located in the narrow part of the reservoir, whereas cross section $I = 7$ (SR-20) is in the wide inundation area upstream of Curtis Bridge.

The distribution of the unit discharge component in the flow direction (U_{st} discharge) across the section $I = 228$ is presented in Fig. 15-19. As expected, larger discharges occur in the zones of larger depth, and the suspended-sediment concentration distribution (for size class 1, i.e., fine sediment)

roughly follows the U_{st} discharge pattern (Fig. 15-20). The bed deposition (shown in Fig. 15-21) reflects closely the suspended-sediment concentration distribution, because the deposition component of the suspended-sediment source term (which is the dominant source of bed deposition) is mainly governed by the depth-averaged concentrations and the flow field.

The picture is somewhat different for the section $I = 7$, where the wide cross section produced the velocity field less dominated by ξ -direction velocities, and where the influence of the upstream boundary was felt more strongly. The result was a more evenly distributed bed-deposition (Fig. 15-28), which is in general agreement with the observed field data.

Due to an effective Courant-number limitation, the hydrodynamic computational time step had to be limited to 1 h. This relatively small time step is impractical for simulation of slowly varying sediment movement. Sediment variables changed very little during 1 h; moreover, the sediment computations are extremely time-consuming, and a sediment time step of 1 h would have enormously increased the CPU time. For a slowly varying flow field the problem is circumvented by choosing a “global” time step (for sediment computations) to be much longer than the hydrodynamic one. Hence, within a single global time step, water computations are performed for several short “water” time steps, only the first and latest computed flow fields being used in sediment

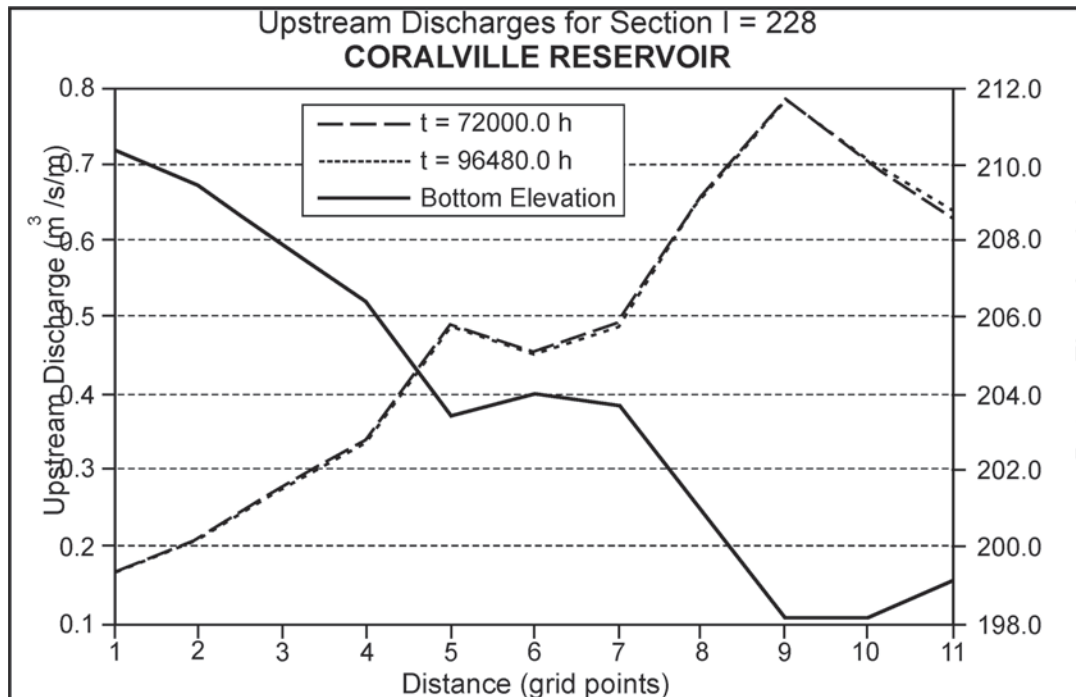


Fig. 15-21. Numerical grid for Coralville Reservoir.

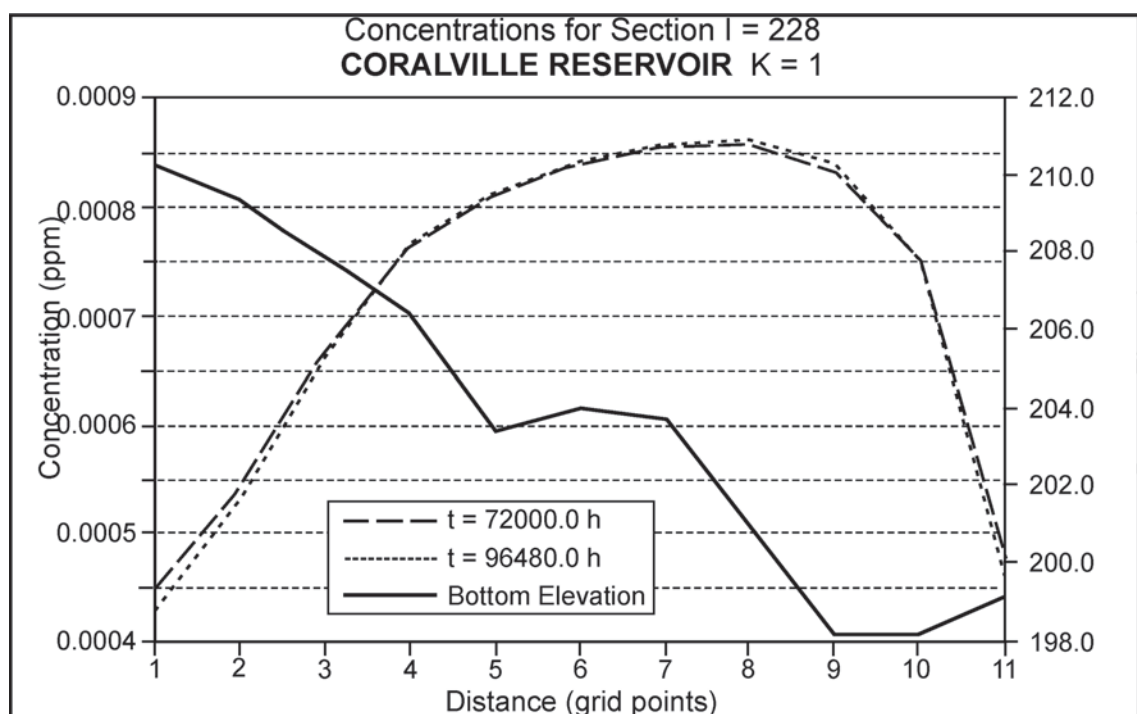


Fig. 15-22. Unit longitudinal staggered discharges for Section $I = 228$ of Coralville Reservoir for simulation times of $t = 8.2$ and 11 years.

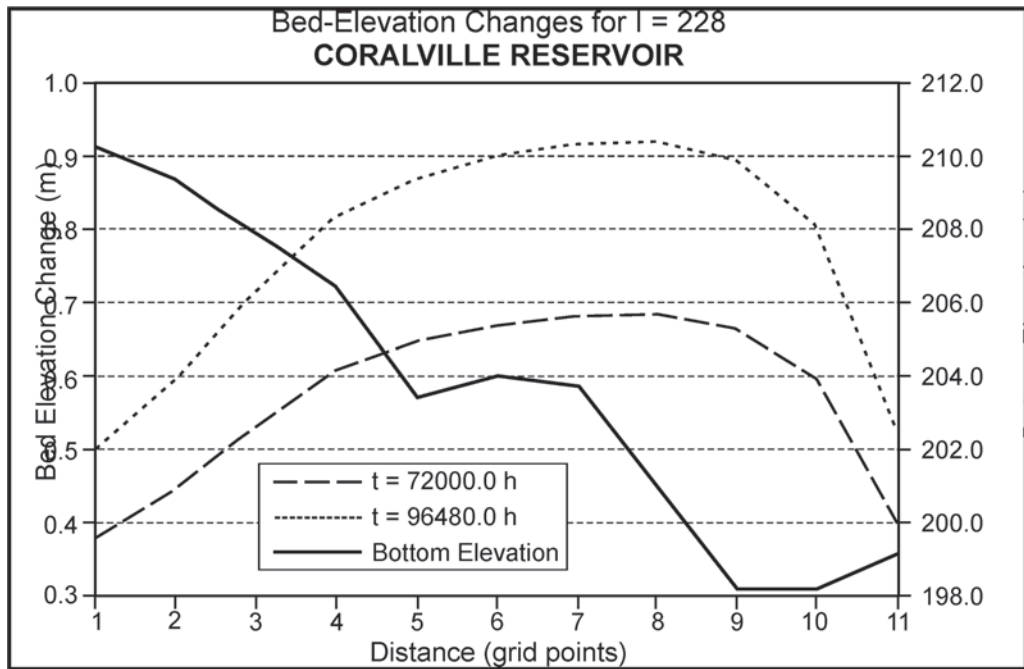


Fig. 15-23. Suspended-sediment concentrations for Section $I = 228$ of Coralville Reservoir for simulation times of $t = 8.2$ and 11 years.

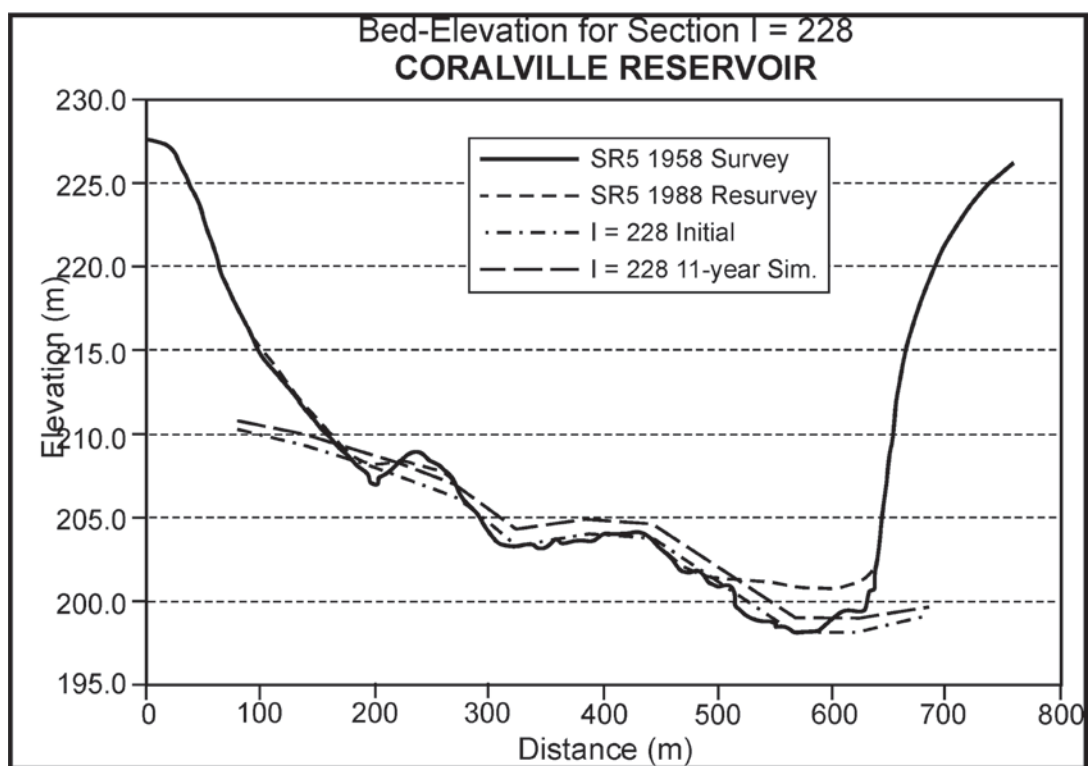


Fig. 15-24. Bed elevations for the Coralville-model Section $I = 228$ at the beginning and end of the 11-year simulation, compared to Sediment Range SR-5 (1958 and 1988) surveys.

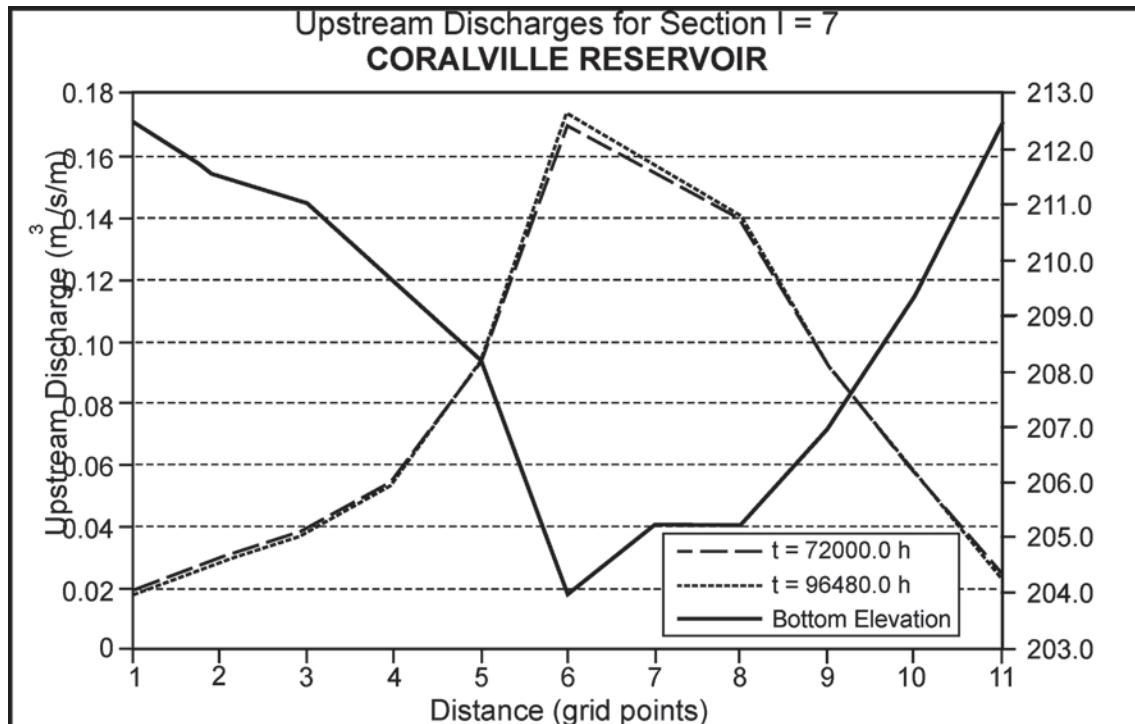


Fig. 15-25. Unit longitudinal staggered discharges for section $I = 7$ of Coralville Reservoir for simulation times of $t = 8.2$ and 11 years.

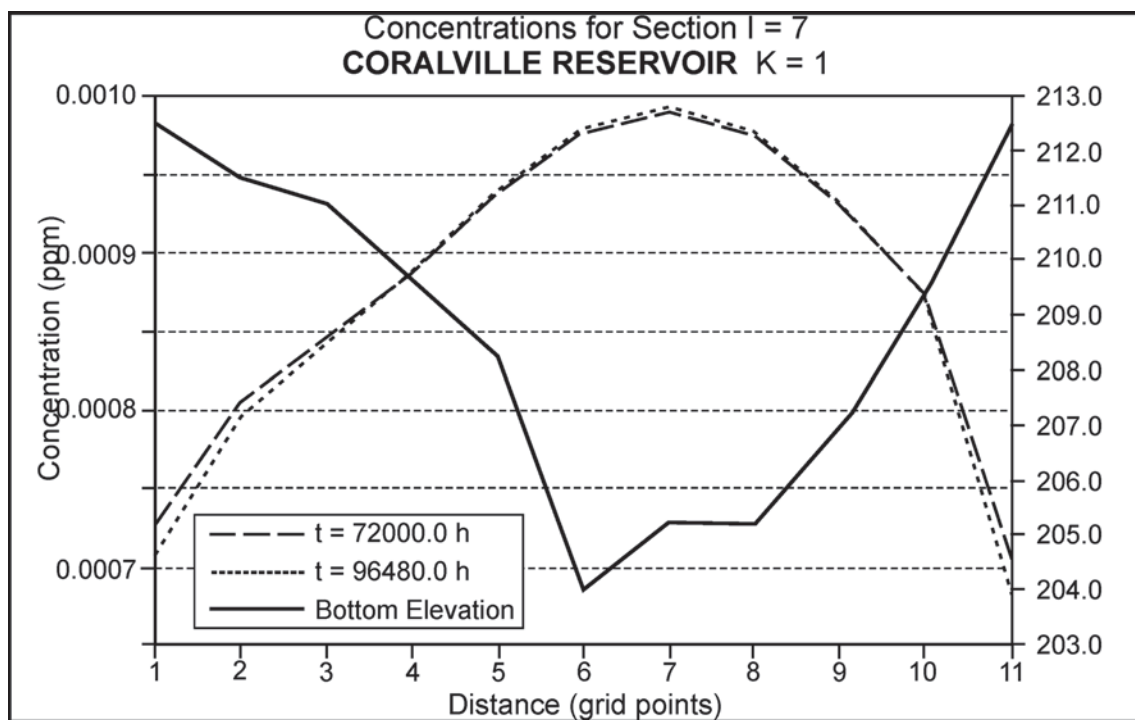


Fig. 15-26. Suspended-sediment concentrations for section $I = 7$ of Coralville Reservoir for simulation times of $t = 8.2$ and 11 years.

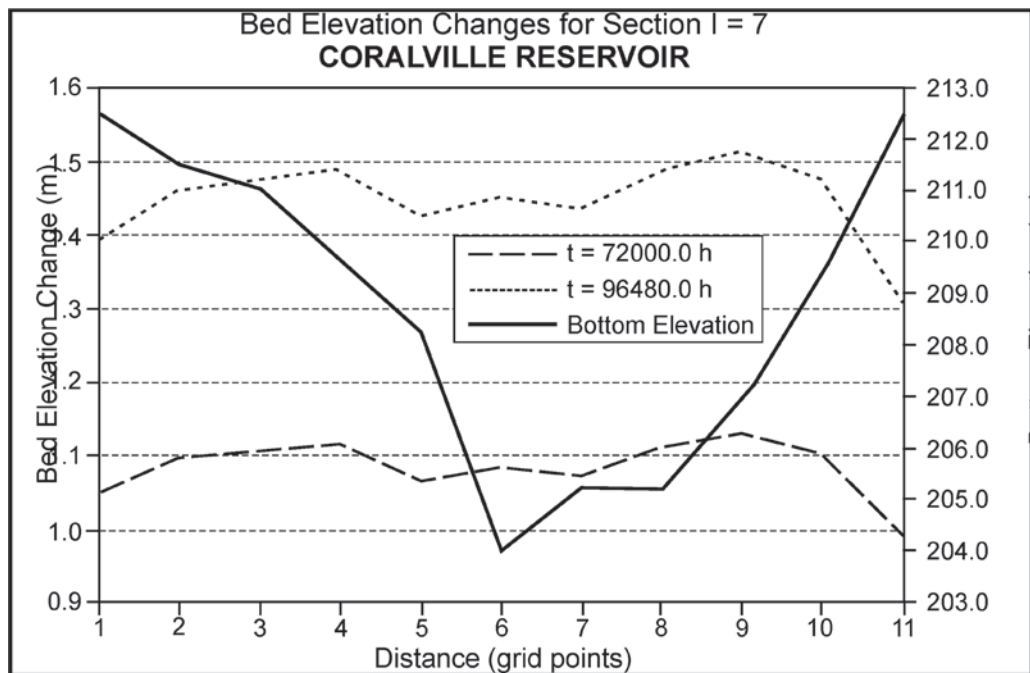


Fig. 15-27. Bed-elevation changes for Section $I = 7$ of Coralville Reservoir for simulation times of $t = 8.2$ and 11 years.

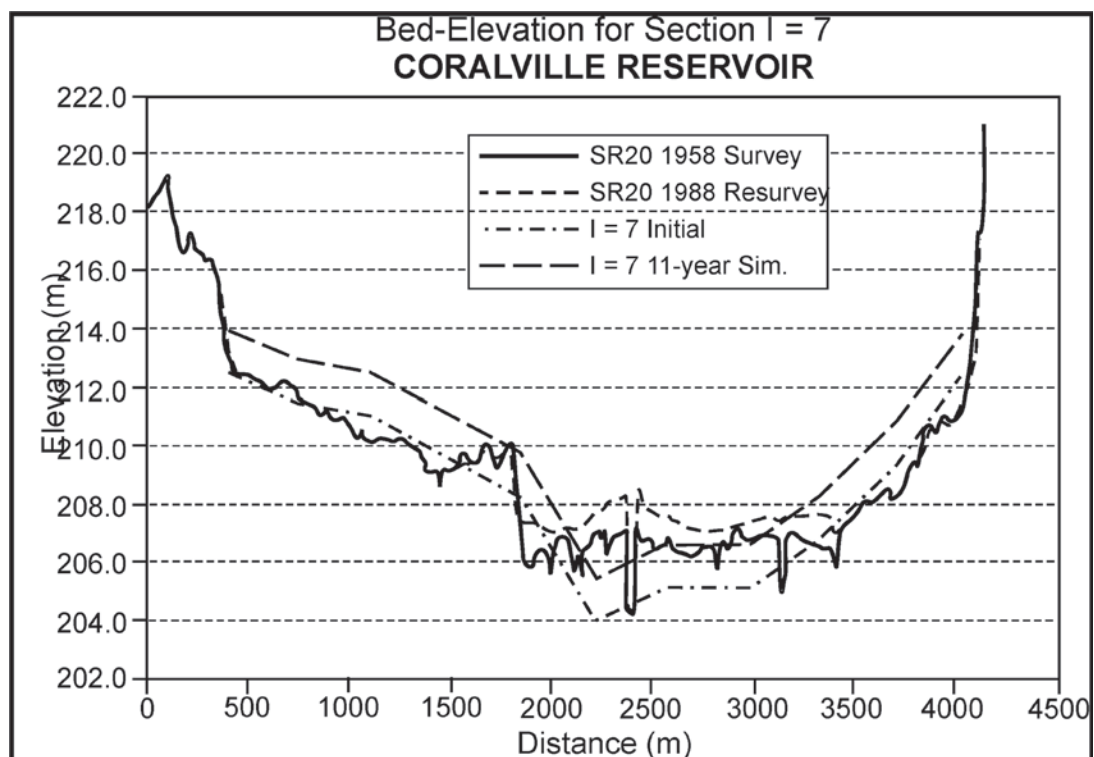


Fig. 15-28. Bed elevations for the Coralville-model Section $I = 7$ at the beginning and end of the 11-year simulation, compared to Sediment Range SR-20 (1958 and 1988) surveys.

computations. A global time step of 24 h was found to be an optimum value for the Coralville Reservoir model.

The CPU time required for the described 11-year simulation was around 200 h on a 486/33 MHz personal computer, using the Lahey 32-bit compiler; one would expect the same run to have taken only about 6 h on a state-of-the-art personal computer. (More iterations, and accordingly, more CPU time were needed for the unsteady part of the computations, i.e., for the first year of the simulation.) The storage memory requirements, beyond the 500K required for the program load module, were 1,650K for the Coralville model.

15.11.4.5 Saylorville and Red Rock Reservoirs The Saylorville and Red Rock reservoir model construction and operation followed the same general pattern as for the Coralville reservoir. Therefore in this section only brief descriptions of the physical situation and model grids are given.

The Saylorville Reservoir is located on the Des Moines River upstream of Des Moines, Iowa. The Saylorville Reservoir model represents the part of the reservoir from the Saylorville Dam up to Sediment Range (SR) No. 15. The computational domain of the model is defined for a flood situation, with pool elevation at 271.3 m (890 ft). Cross-section sediment range 1 is immediately upstream of the dam site, whereas Sediment Range SR-15 is close to the upstream boundary of the model domain. Fig. 15-29 shows the two-dimensional contour of the model domain and the computational grid. The total number of computational points was 1,144, with $I = 104$ points in the ξ -direction (the direction of the flow) and $J = 11$ points in the η -direction.

The Red Rock Reservoir is located on the Des Moines River, downstream of Des Moines, Iowa. The model represents the part of the reservoir from the dam up to Sediment Range (SR) No. 19. The computational domain of the model is defined for a flood situation, with the pool elevation at 237.75 m (780 ft). Cross-section Sediment Range 1 is upstream of the dam site, whereas Sediment Range SR-19 is close to the upstream boundary of the domain. Fig. 15-30 shows the contour of the model domain and the computational grid. The total number of computational points was 781, with $I = 71$ points in the ξ -direction (the direction of the flow) and $J = 11$ points in the η -direction.

15.11.4.6 Summary This two-dimensional example has been included primarily to point out the possibility—even in 1993, when this study was done—of making multi-year simulations to detect sedimentation trends subject to a succession of real or schematic hydrographs. As of this writing, it is not possible to envision such long-term simulations with three-dimensional models, even those based on the hydrostatic pressure assumption. As long as vertical accelerations and secondary flows are relatively unimportant to the problem under study, two-dimensional modeling offers a great deal of power at relatively low computational cost, and therefore is a viable tool within its known constraints.

15.12 CRITICAL ASSESSMENT OF STATE OF THE ART AND FUTURE PERSPECTIVES

As of this writing, two-dimensional (depth-averaged) fixed-bed modeling has reached a certain maturity and seen moderate use. But after a promising beginning, development of two-dimensional (depth-averaged) mobile-bed modeling has taken a back seat to three-dimensional. Meanwhile, three-dimensional fixed-bed modeling is rapidly becoming an effective engineering tool, and its mobile-bed counterpart is receiving considerable developmental attention and enjoying some success in practical engineering use.

It is unfortunate that development and application of two-dimensional (depth-averaged) mobile-bed modeling has become somewhat of an orphan in the rush to develop three-dimensional tools. Two-dimensional modeling, although unable to resolve mobile-bed responses closely related to secondary flow, detailed water and sediment dynamics around structures, and other three-dimensional effects, still offers the possibility of making truly long-term simulations in a way that is currently unthinkable with three-dimensional models. To exploit this potential fully, two-dimensional models need to be based on unstructured or nonorthogonal curvilinear structured grids, have robust wetting and drying capability for application to multiyear hydrologic series, and include both bed-load and suspended-load transport mechanisms in a nonuniform sediment environment.

In both two- and three-dimensional modeling, there is the issue of structured versus unstructured grids. Structured grids (usually nonorthogonal curvilinear and associated with finite-difference methods) are not well suited to grid refinement around local areas of interest or adjacent to hydraulic structures, but are generally attractive for their minimization of computational time (and thus their enabling of longer-term simulations and/or finer resolution of nonuniform sediment). Structured grids (e.g., finite-element or finite-volume, usually associated with flux-based methods) offer great flexibility in grid refinement around structures and local features of interest and lend themselves well to dynamic adaptive refinement, at the cost of relatively high demands on computer resources. Although it is tempting to believe that continuing rapid increases in computer processor speed and parallel systems will eventually make the speed advantages of structured grids irrelevant, experience has shown that this is unlikely to be the case. Indeed, it is always desirable to use a finer grid resolution, adopt more sediment size classes, run for longer periods, or test a greater number of cases, i.e., to push the limits of practical CPU time with whatever numerical tool is being used. It is likely that there will continue to be partisans of, and real needs for, both structured and unstructured modeling systems into the foreseeable future.

Another issue of importance as of this writing is that of fully three-dimensional versus quasi-three-dimensional

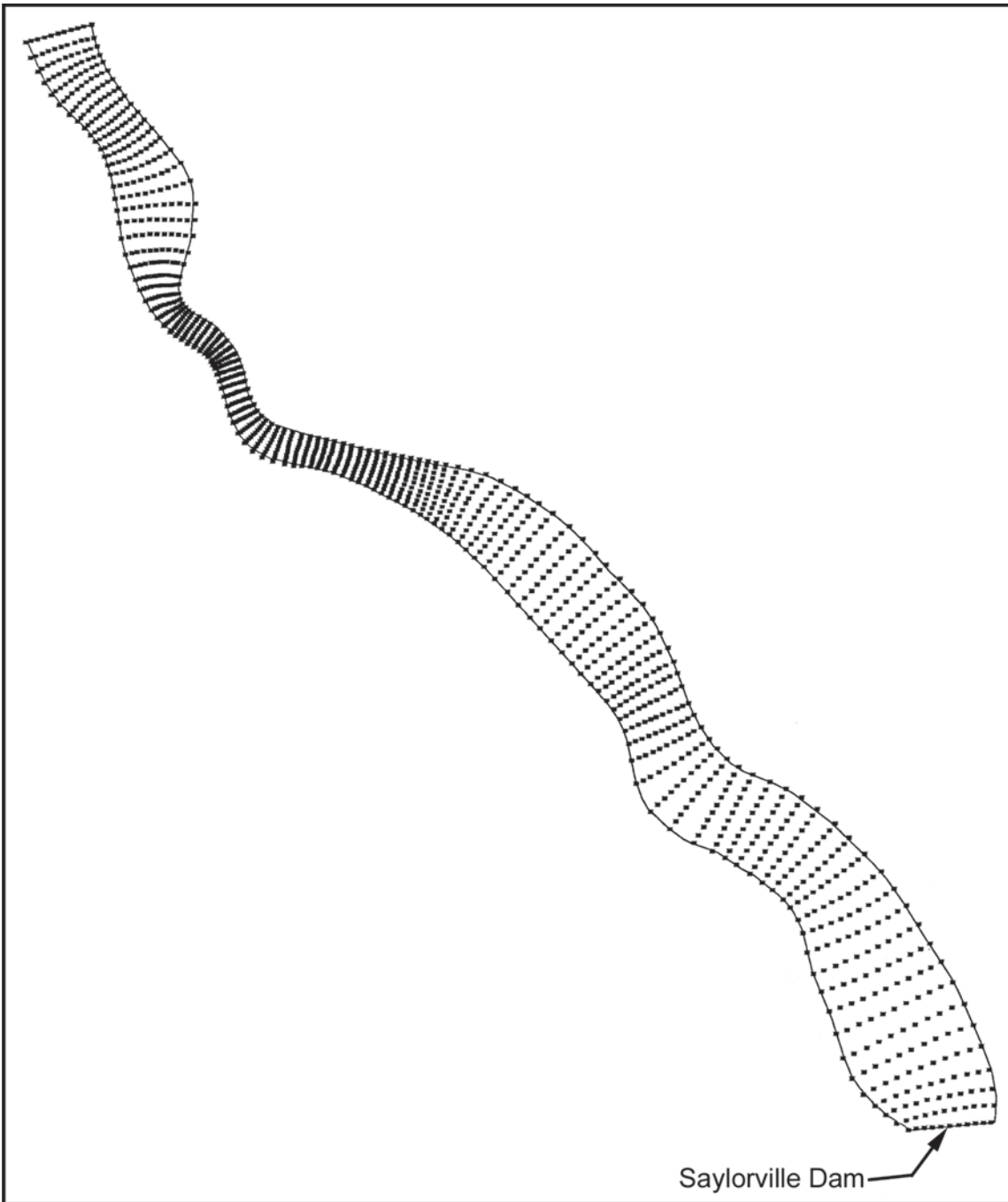


Fig. 15-29. Numerical grid for Saylorville Reservoir.

(i.e., hydrostatic) hydrodynamic modeling as a framework for mobile-bed models. Experience has shown that water and sediment movement in the immediate vicinity of structures (e.g. submerged dikes and bridge piers) can be correctly represented only if vertical acceleration components are explicitly taken into account, i.e., only if the model explicitly includes the vertical momentum equation. Quasi-three-dimensional models, in which the vertical momentum equation is replaced by the hydrostatic pressure assumption, offer the considerable

advantage of orders of magnitude decreases in computational time (the solution essentially comprises a two-dimensional one followed by application of the three-dimensional water continuity equation to recover vertical velocities). At the present time, truly unsteady simulations of any significant duration cannot be performed using full three-dimensional models, whereas they are becoming feasible with models based on the hydrostatic pressure assumption, as described in the examples of the previous section. In time, increases of computing speed

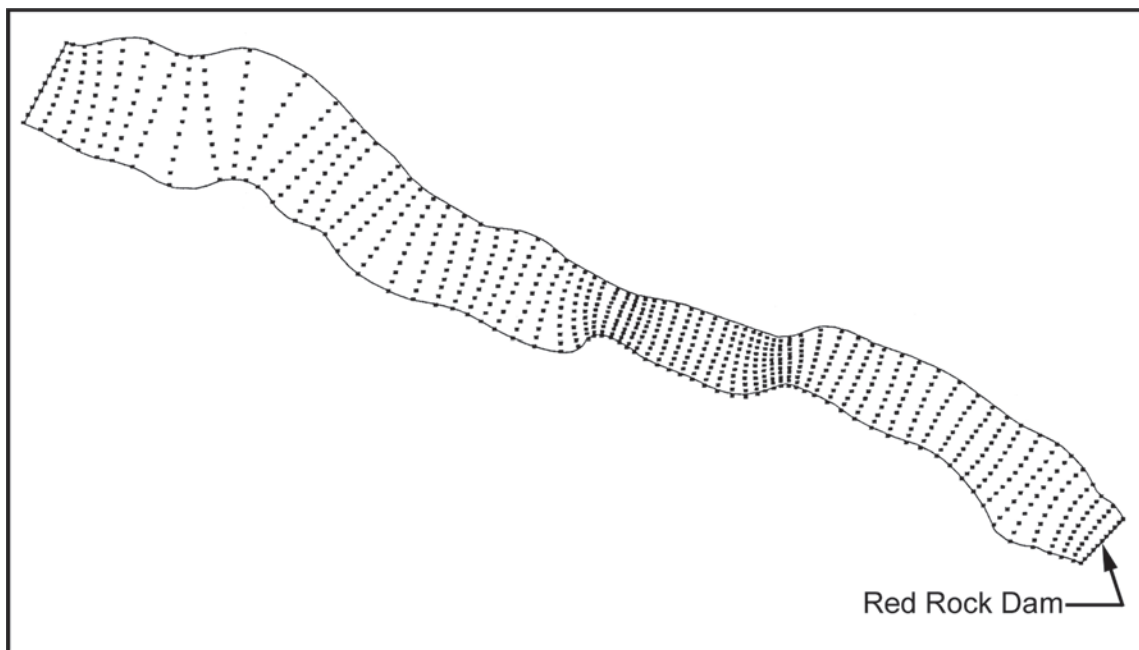


Fig. 15-30. Numerical grid for Red Rock Reservoir.

may obviate the need to use the hydrostatic pressure assumption. For the near- to mid-term, however, the best situation is to have the option of using fully three-dimensional modeling to obtain steady-state solutions including the best possible detail of flow around structures; or to use quasi-three-dimensional hydrostatic modeling to obtain unsteady simulations for prototype time periods of the order of days to weeks. Future three-dimensional developmental efforts should be based primarily on the full nonhydrostatic equations, even though at the present time this appears to exclude unsteady simulation for practical reasons.

The preceding paragraphs deal with dimensionality (two-dimensional, quasi three-dimensional, fully three-dimensional), and structured/unstructured grid issues. An equally important issue is related to the basic mathematical formulation of noncohesive sediment processes and their interaction with the flow. One can argue that this is not a subject for mathematical modelers because the basic understanding of physical processes, which is a basis for mathematical formulations, typically comes from experimental work. However, authors believe that there is a need for mathematical modelers to become more involved in guiding experimental programs that can be focused on the need to improve basic sediment formulations for computational models. Today's finest flow and sediment models, with features such as fully three-dimensional computation, unstructured and adaptive grids, and advanced turbulence models, may easily choke on imperfect, and often stale, formulations of sediment processes.

Even the advection-diffusion equation with the fall-velocity term, typically used as the governing equation for

suspended-sediment processes, brings up many questions. Is there a better formulation for the fall velocity of multiple particles in a moving fluid than typically used relations developed for a single particle in quiescent water? What are the real values of the turbulent Schmidt number σ_c , relating the sediment mass-diffusivity coefficient ε_s to the turbulent eddy viscosity v_t , which even some of the most sophisticated contemporary models assume to be equal to unity? What are the consequences of the assumption that the velocity of suspended-sediment particles is the same as that of the fluid for the accuracy of the suspended-sediment advection-diffusion equation? Or alternatively, what is the effect of an experimentally demonstrated lag between the fluid and suspended-sediment particle velocities on an overall sediment quantity such as the total suspended-sediment load?

Additional difficult questions arise concerning mathematical formulation of bed and near-bed processes. Even though one can talk about several prevailing alternative conceptual models of bed processes, as of this writing there is still no generally accepted unified theory for conceptual and mathematical formulation of these processes. In this area there is even more need for communication and coordination between researchers involved in sediment-related numerical and experimental work. One example concerns the issue of bed-form-related flow roughness. It is tempting to expect that computational grids will eventually become fine enough to resolve the details of bed forms, so that the flow and sediment equations themselves can capture their effects on flow and sediment processes. But this may never occur, and until it does, it may still be necessary to bring empirical representations of bed-form

effects on flow and sediment processes into two- and three-dimensional models. Another example concerns the fact that practically all bed-load formulas are developed from steady equilibrium conditions, whereas most models operate in an unsteady nonequilibrium environment. In general, unsteady-flow effects on sediment processes are seldom addressed in experimental work in a way that can be used to improve sediment modeling. This is all the more true when one considers the complicating factor of nonuniform sediment mixtures in the natural environment.

Especially important and difficult is the question of interaction between suspended-sediment and bed and near-bed processes. Prevailing modeling approaches, most of which rely on an empirical near-bed concentration in one way or another, simply bypass the role of near-wall turbulent events on sediment entrainment and deposition. Even though considerable experimental work on such events has been carried out, some of it including sediment, the results cannot be used in present mathematical models, partly because of CPU limitations and limits to model resolution in space and time, not to mention the stochastic nature of these processes. Therefore there is still a large gap between detailed experimental knowledge of turbulent events, including sweeps and streaks, and formulations that can be used effectively in the existing mathematical-modeling context of relatively coarse computational grids.

As challenging the disciplines of two- and three-dimensional noncohesive mobile-bed modeling are, there is a growing need for development of equivalent cohesive capability. Indeed, contaminants in waterways are most often associated with (sorbed to) fine silts and clays, whose cohesive properties are extremely difficult to capture in entrainment and deposition relations. Yet the need to study the transport and fate of contaminated sediment in waterways subject to exceptional hydrological events or disasters is likely to be a major driving force in the development and application of mobile-bed models in the coming decades. Cohesive sediment processes appear to be far less susceptible to rational analysis than their noncohesive counterparts, and numerical formulation of the mechanisms of exchange of sediment-borne contaminants among the multiple transport media (dissolved, suspended, bed, subsurface, etc.) is in its infancy and quite problematic. Contaminant-sediment capability should be a high developmental priority in current and future two- and three-dimensional modeling systems.

Can the model be separated from its developer? In the early days of one-dimensional unsteady-flow models, it was axiomatic that one would be naïve to consider making effective use of a code without having the telephone number of its developer close at hand. To some extent, that remains true today of one-dimensional mobile-bed models, though many organizations have achieved a certain autonomy in the use of HEC-6 (one-dimensional mobile-bed) without needing to consult with its developer on a

regular basis. Such autonomous use is not yet possible for some one-dimensional mobile-bed codes such as the authors' CHARIMA, which still require as much art as science for effective use.

Two- and three-dimensional mobile-bed modeling has not achieved, as of this writing, the maturity that would allow general use of most codes by engineers not in reasonably close contact with the code developer. However, the authors expect that such codes will fairly rapidly mature to enable generalized use by nonspecialists, or at least by specialists not in direct contact with the developers. An important reason for this anticipated acceleration to maturity has to do with the relative roles of science and art in one-, two-, and three-dimensional mobile-bed modeling.

In one-dimensional mobile-bed modeling, the highly heterogeneous processes of sediment entrainment, deposition, bed-load movement, etc. must be described for the cross section as a whole as functions of bulk channel properties such as average velocity, overall discharge, average depth, bulk shear stress, and average bed-material composition in the section. As much art as science is needed in selecting channel properties, and indeed in locating cross sections, in the effective use of one-dimensional models for engineering studies. The code developer is generally the one who is best positioned to combine science with art in extracting viable and useful results from a one-dimensional model.

In two- and three-dimensional mobile-bed models, the mathematical formulations of sediment processes are localized to a particular point on or above the bed, and thus need only be related to the hydrodynamic and bed-material conditions at that point. To be sure, there is still some art in knowing which relations are most appropriate for the area under study, and in relating local processes to depth-averaged hydrodynamic and sediment properties in the two-dimensional domain. But the higher the dimensionality of the model, the more local are the numerical formulations, and local formulations fall more into the realm of science than art. It may appear that multidimensional models are still heavily dependent on empirical auxiliary relations and calibration (as in the examples of Section 15.11). Yet these localized relations and calibrations have a much more physical/scientific basis than their counterparts in one-dimensional modeling, and thus are far more likely to support reliable model use in situations for which the model was not specifically calibrated. To the extent that this is true, the role of the model developer, and his or her skill in teasing the best information and behavior out of cross-sectional properties, becomes less important in enabling use of the model by engineers who are not closely associated with its development. Still, the most effective use of any mobile-bed model comprises close collaboration between model developer and user.

What should be the priorities for further two- and three-dimensional model development? In the authors' view, the

areas of greatest weakness at present are threefold: (1) inability to capture large temporal scales of change (e.g., seasons if not years) due to the sheer computational time burden of such complex computations; (2) inability to resolve subgrid scale processes, such as dune movement, due to computer speed and memory limitations; and (3) continuing inadequate descriptions of physical processes such as particle entrainment, deposition, and mixing. Weaknesses (1) and (2) will (presumably) progressively disappear as computational resources and speed continue their astounding rate of progress. Weakness (3) will not disappear simply because more powerful computers become available. There is a continuing need for research and development efforts focused on laboratory and field experiments specifically designed to improve the physical-process formulations adopted in numerical models. It is perhaps ironic that the rush to replace physical hydraulic investigations with numerical modeling, in both applications and research, has deprived numerical modelers of what they most need—improved understanding of some of the most complex physical processes on earth.

REFERENCES

- Ashida, K., and Okabe, T. (1982). "On the calculation method of the concentration of suspended sediment under non-equilibrium condition." *Proc. 26th Conference on Hydraulics*, Japan Society of Civil Engineers, Tokyo, 153–158 (in Japanese).
- Bennett, J. P., and Nordin, C. F. (1977). "Simulation of sediment transport and armoring." *Hydrological Sciences Bulletin*, XXII, 4(12), 555–569.
- Benqué, J. P., Cunge, J. A., Feuillet, A., Hagué, A., and Holly, F. M., Jr. (1982). "New method for computation of tidal currents." *Journal of the Waterways and Harbors Division, ASCE*, 108(WW3), 396–417.
- Borah, D. K., Alonso, C. V., and Prasad, S. H. (1982). "Routing graded sediments in streams: formulations." *Journal of the Hydraulics Division, ASCE*, 108(HY12), 1486–1505.
- Brors, B. (1999). "Numerical modeling of flow and scour at pipelines." *Journal of Hydraulic Engineering, ASCE*, 125(5), 511–523.
- Cao, Z. X., Wei, L. Y., and Xie, J. H. (1995). "Sediment-laden flow in open channels from two phase flow viewpoints." *Journal of Hydraulic Engineering, ASCE*, 121(10), 725–735.
- Catalyst-Old River Hydroelectric Limited Partnership d.b.a. Louisiana Hydroelectric Limited Partnership. (1999). *Lower Mississippi River Sediment Study*, Louisiana Hydroelectric Limited Partnership, Vidalia, La.
- Celik, I., and Rodi, W. (1984). "A deposition-entrainment model for suspended sediment transport." *Report. SFB 210/T/6*, University of Karlsruhe, Karlsruhe, Germany.
- Celik, I., and Rodi, W. (1988). "Modeling suspended sediment transport in nonequilibrium situations." *Journal of Hydraulic Engineering, ASCE*, 114(10), 1157–1191.
- Chapman, R. S., and Johnson, B. H. (1996). *User's guide for the sigma stretched version of CH3D-WES—A three-dimensional hydrodynamic, salinity, and temperature model*, Hydraulics Laboratory, U.S. Army Engineer Waterways Experiment Station, Vicksburg, Miss.
- Crowe, C. T., Troutt, T. R., and Chung, J. N. (1996). "Numerical models for two-phase turbulent flows." *Annual Review of Fluid Mechanics*, 28, 11–43.
- Damgaard, J. S., Whitehouse, R. J. S., and Soulsby, R. L. (1997). "Bed-load sediment transport on steep longitudinal slopes." *Journal of Hydraulic Engineering, ASCE*, 123(12), 1130–1138.
- Demuren, A. O. (1991). "Development of a mathematical model for sediment transport in meandering rivers." *Bericht No. 693*, Institut für Hydromechanik an der Universität Karlsruhe, Karlsruhe, Germany.
- Drew, D. A. (1983). "Mathematical modeling of two-phase flow." *Annual Review of Fluid Mechanics*, 15, 261–291.
- Duan, J. G., Wang, S. S. Y., and Jia, Y. (2001). "The applications of the enhanced CCHE2D model to study the alluvial channel migration process." *Journal of Hydraulic Research*, 39(5), 469–480.
- Elghobashi, S. E. (1994). "On predicting particle-laden turbulent flows." *Applied Science Research*, 52, 309–329.
- Fagerburg, T. L. (1998). "Discharge and velocity measurements on the Mississippi River at the Old River Control Structure Complex." *Progress Report, Lower Mississippi River Sediment Study*, U.S. Army Engineer Waterways Experiment Station, Vicksburg, Miss.
- Fang, H. W. (2000). "Three-dimensional calculations of flow and bed-load transport in the Elbe River." *Report No. 763*, Institut für Hydromechanik an der Universität Karlsruhe, Karlsruhe, Germany.
- Fang, H. W., and Rodi, W. (2000). "Three-dimensional calculations of flow and suspended sediment transport in the neighborhood of the dam for the Three Gorges Project (TGP) Reservoir in the Yangtze River." *Report No. 762*, Institut für Hydromechanik an der Universität Karlsruhe, Karlsruhe, Germany.
- Fennema, R. J., and Chaudhry, M. H. (1990). "Numerical solution of two-dimensional transient free-surface flows." *Journal of Hydraulic Engineering, ASCE*, 116(8), 1013–1034.
- Ferziger, J. H., and Peric, M. (2002). *Computational methods for fluid dynamics*, 3rd Ed., Springer, New York.
- Fletcher, C. A. J. (1991). *Computational techniques for fluid dynamics*, Vol. I, Springer, Berlin.
- Flokstra, C. (1977). "The closure problem for depth-averaged two-dimensional flow." *Publication No. 190*, Waterloopkundig Laboratorium, Delft Hydraulics Laboratory, Delft, The Netherlands.
- Gessler, D., Hall, B., Spasojevic, M., Holly, F. M., Pourtaheri, H., and Raphelt, N. K. (1999). "Application of 3-dimensional mobile bed, hydrodynamics model." *Journal of Hydraulic Engineering, ASCE*, 125(7), 737–749.
- Greimann, B. P., Muste, M., and Holly, F. M., Jr. (1999). "Two-phase formulation of suspended sediment transport." *Journal of Hydraulic Research*, 37(4), 479–500.
- Hervouet, J.-M., and Bates, P., eds. (2000). "The Telemac modeling system." Special Issue, *Hydrological Processes*, 14(13).
- Hirsch, C. (1991). *Numerical computation of internal and external flows*, Vols. I and II, Wiley, New York.
- Holly, F. M., Jr., and Rahuel, J. L. (1990). "New numerical/physical framework for mobile-bed modelling. I: Numerical and physical principles." *Journal of Hydraulic Research*, 27(4), 401–416.

- Holly, F. M., Jr., and Spasojevic, M. (1999). "Three-dimensional mobile-bed modeling of the Old River Complex, Mississippi River," *Proc. XXVIIIth IAHR Congress*, Graz, Austria.
- Holly, F. M., Jr., and Usseglio-Polatera, J. M. (1984). "Dispersion simulation in two-dimensional tidal flow." *Journal of Hydraulic Engineering, ASCE*, 110(7), 905–926.
- Ishii, M. (1975). *Thermo-fluid dynamic theory of two-phase flow*. Eyrolles, Paris.
- Jankowski, J. A., Malcherek, A., and Zielke, W. (1994) "Numerical modeling of sediment transport processes caused by deep sea mining discharges." *Proceedings of the OCEANS 94 Conference, Brest*, Vol. III, IEEE/SEE, Piscataway, N.J., 269–276.
- Jia, Y., Kitamura, T., and Wang, S. S. Y. (2001). "Simulation of scour process in plunging pool of loose bed-material." *Journal of Hydraulic Engineering, ASCE*, 127(3), 219–229.
- Jia, Y., and Wang, S. S. Y. (1999). "Numerical model for channel flow and morphological change studies." *Journal of Hydraulic Engineering, ASCE*, 125(9), 737–749.
- Jin, Y. C., and Steffler, P. M. (1993). "Predicting flow in curved channels by depth-averaged method." *Journal of Hydraulic Engineering, ASCE*, 119(1), 109–124.
- Jobson, H. E., and Sayre, W. W. (1970). "Vertical transfer in open channel flow." *Journal of Hydraulic Engineering, ASCE*, 96(HY3), 703–724.
- Karim, F., and Kennedy, J. F. (1982). "IALLUVIAL: A computer-based flow and sediment-routing model for alluvial streams and its application to the Missouri River." *Technical Report No. 250*, Iowa Institute of Hydraulic Research, University of Iowa, Iowa City, Iowa.
- Kitamura, T., Jia, Y., Tsujimoto, T., and Wang, S. S. Y. (1998). "Sediment transport capability in channels with vegetation zone." *Advances in Hydro-Science and Engineering (CR-ROM)*, Vol. III, K. P. Holz, W. Bechteler, S. S. Y. Wang, and M. Kawahara, eds., Center for Computational Hydroscience and Engineering, University of Mississippi, University, Miss.
- Kovacs, A., and Parker, G. (1994). "A new vectorial bedload formulation and its application to the time evolution of straight river channels." *Journal of Fluid Mechanics*, 267, 153–183.
- Lau, Y. L., and Engel, P. (1999). "Inception of sediment transport on steep slopes." *Journal of Hydraulic Engineering, ASCE*, 125(5), 544–547.
- Leonard, B. P. (1979). "A stable and accurate convective modelling procedure based on quadratic upstream interpolation." *Computer Methods in Applied Mechanics and Engineering*, 19, 59–98.
- Lin, B., and Falconer R. A. (1996). "Numerical modeling of three-dimensional suspended sediment for estuarine and coastal waters." *Journal of Hydraulic Research*, 34(4), 435–456.
- Liu, Q., Chen, L., and Liu, D. (1997). "Effects of existence of sediment particles on the energy loss of flow." *International Journal of Sediment Research*, 11(3), 18–24.
- Minh Duc, B., Wenka, Th., and Rodi, W. (1998). "Depth-average numerical modeling of flow and sediment transport in the Elbe River." *Proc. 3rd Int. Conf. on Hydroscience and Engineering*, Brandenburg University of Technology, Cottbus, Germany.
- Morlock, S. E., Nguyen, H. T., and Ross, J. H. (2002). "Feasibility of acoustic Doppler Velocity meters for the production of discharge records from U.S. Geological Survey streamflow-gaging stations." *Water-Resources Investigations Report 01-4157*, U.S. Geological Survey, Indianapolis, Ind.
- Muste, M., Yu, K., and Spasojevic, M. (2004a). "Practical aspects of ADCP data use for quantification of mean river flow characteristics. Part I: Moving-vessel measurements." *Flow Measurements and Instrumentation*, 15(1), 1–16.
- Muste, M., Yu, K., Pratt, T., and Abraham, D. (2004b). "Practical aspects of ADCP data use for quantification of mean river flow characteristics. Part II: Fixed-vessel measurements." *Flow Measurements and Instrumentation*, 15(1), 17–28.
- Nagata, N., Hosoda, T., and Muramoto, Y. (2000). "Numerical analysis of river channel processes with bank erosion." *Journal of Hydraulic Engineering, ASCE*, 126(4), 243–252.
- Nakagawa, H., and Tsujimoto, T. (1980). "Sand bed instability due to bed load motion." *Journal of the Hydraulics Division, ASCE*, 106(HY12), 2029–2951.
- Ni, H. Q., Huang, Z. C., Zhou, L. X., and Zhou, J. Y. (1996). "Numerical simulation of sedimentation using a two-fluid model of turbulent liquid solid flows." *Flow Modeling and Turbulence Measurements VI*, Balkema, Rotterdam, The Netherlands, 781–788.
- Nordin, C. F., and Queen, B. S. (1989). "Particle size distributions of bed sediment along the thalweg of the Mississippi River, Cairo, Illinois to Head of Passes, September 1989." *Report 7*, Potamology Program (P-1), submitted to U.S. Army Corps of Engineers, Lower Mississippi Valley Division, Vicksburg, Miss.
- Olsen, N. R. B. (1999). "Two-dimensional numerical modeling of flushing processes in water reservoirs." *Journal of Hydraulic Research*, 37(1), 3–16.
- Olsen, N. R. B., Jimenez, O., Lovoll, A., and Abrahamsen, L. (1999). "3D CFD modeling of water and sediment flow in hydropower reservoir." *International Journal of Sediment Research*, 14(1), 16–24.
- Olsen, N. R. B., and Kjellesvig, H. M. (1998). "Three-dimensional numerical flow modeling for maximum local scour depth." *Journal of Hydraulic Research*, 36(4), 579–597.
- Olsen, N. R. B., and Melaaen, M. C. (1993). "Three-dimensional calculation of scour around cylinders." *Journal of Hydraulic Engineering, ASCE*, 119(9), 1048–1054.
- Olsen, N. R. B., and Skoglund, M. (1994). "Three-dimensional numerical modeling of water and sediment flow in a sand trap," *Journal of Hydraulic Research, IAHR*, 32(6), 833–844.
- Onishi, Y., and Thompson, F. L. (1984). "Mathematical simulation of sediment and radionuclide transport in coastal waters." *Report No. 5088-1*, Vol. 1, Pacific Northwest Laboratory (PNL), Richland, Wash.
- Onishi, Y., and Trent, D. S. (1982). "Mathematical simulation of sediment and radionuclide transport in estuaries." *Report No. 4109*, Pacific Northwest Laboratory (PNL), Richland, Wash.
- Onishi, Y., and Trent, D. S. (1985). "Three-dimensional simulation of flow, salinity, sediment, and radionuclide movement in the Hudson River estuary." *Proceedings, Specialty Conference: Hydraulics and Hydrology in Small Computer Age, ASCE*, New York, 1095–1100.
- Phillips, B. C., and Sutherland, A. J. (1989). "Spatial lag effects in bed load sediment transport." *Journal of Hydraulic Research, IAHR*, 27(1), 115–133.
- Rodi, W. (1993). *Turbulence models and their application in hydraulics*, 3rd Ed., Balkema, Rotterdam, The Netherlands.

- Rodi, W. (2000). "Numerical calculation of flow and sediment transport in rivers." *Proc. Eighth Int. Symp. on Stochastic Hydraulics*, Z.-Y. Wang and S.-X. Hu, eds., A. A. Balkema, Rotterdam, The Netherlands, 15–30.
- Savic, Lj., and Holly, F. M., Jr. (1993). "Numerical modeling of reservoir sedimentation. MOBED2 program. Programmer's and user's manual." *Limited Distribution Report No. 204*, Iowa Institute of Hydraulic Research, Univ. of Iowa, Iowa City, Iowa.
- Shen, H. W., and Lu, J. Y. (1983). "Development and prediction of bed armoring." *Journal of Hydraulic Engineering, ASCE*, 109(4), 611–629.
- Sheng, Y. P. (1983). "Mathematical modeling of three-dimensional coastal currents and sediment dispersion: Model development and application." *A.R.A.P. Report No. 485*; also as *Technical Report CERC-83-2*, Waterways Experimental Station, Vicksburg, Miss.
- Shimizu, Y., Yamaguchi, H., and Itakura, T. (1990). "Three-dimensional computation of flow and bed deformation." *Journal of Hydraulic Engineering, ASCE*, 116(9), 1090–1108.
- Simmonds, J. G. (1994). *A brief on tensor analysis*. Springer, New York.
- Spasojevic, M. (1988). "Numerical simulation of two-dimensional (plan-view) unsteady water and sediment movement in natural watercourses." Ph.D. thesis, University of Iowa, Iowa City, Iowa.
- Spasojevic, M., and Holly, F. M., Jr. (1990a). "MOBED2—Numerical simulation of two-dimensional mobile-bed processes." *Technical Report No. 344*, Iowa Institute of Hydraulic Research, The University of Iowa, Iowa City, Iowa.
- Spasojevic, M., and Holly, F. M., Jr. (1990b). "2-D bed evolution in natural watercourses—New simulation approach." *Journal of Waterway, Port, Coastal, and Ocean Engineering, ASCE*, 116(4), 425–443.
- Spasojevic, M., and Holly, F. M., Jr. (1993). "Three-dimensional numerical simulation of mobile-bed hydrodynamics." *Technical Report No. 367*, Iowa Institute of Hydraulic Research, The University of Iowa, Iowa City, Iowa; also as *Contract Report HL-94-2*, Waterways Experimental Station, Vicksburg, Miss., 1994.
- Spasojevic, M., and Muste, M. (2002). "Numerical model study of Berwick Harbor, Morgan City, Louisiana." *Technical Report No. 422*, Iowa Institute of Hydraulic Research, The University of Iowa, Iowa City, Iowa.
- Spasojevic, M., Muste, M., and Holly, F. M., Jr. (2001). "3-D modeling of the Missouri River at Leavenworth Bend." *Limited Distribution Report No. 298*, Iowa Institute of Hydraulic Research, The University of Iowa, Iowa City, Iowa.
- Thomas, W. A., and McAnally, W. H., Jr. (1985). "User's manual for the generalized computer program system open-channel flow and sedimentation—TABS-2, main text." *Instruction Report HL-85-1*, Waterways Experiment Station, U.S. Army Corps of Engineers, Vicksburg, Miss.
- Thuc, T. (1991). "Two-dimensional morphological computations near hydraulic structures." Ph.D. dissertation, Asian Institute of Technology, Bangkok, Thailand.
- Usseglio-Polatera, J. M., and Cunge, J. A. (1985). "Modelling of pollutant and suspended-sediment transport with Argos Modelling System." *Proc. International Conference on Numerical and Hydraulic Modelling of Ports and Harbors*, BHRA, Fluid Engineering Centre, Cranfield, U.K., 83–92.
- van Rijn, L. C. (1984a). "Sediment transport. I: Bed load transport." *Journal of Hydraulic Engineering, ASCE*, 110(10), 1431–1456.
- van Rijn, L. C. (1984b). "Sediment transport. II: Suspended load transport." *Journal of Hydraulic Engineering, ASCE*, 110(11), 1613–1641.
- van Rijn, L. C. (1986). "Mathematical modeling of suspended sediment in nonuniform flow." *Journal of Hydraulic Engineering, ASCE*, 112(6), 433–455.
- van Rijn, L. C. (1987). "Mathematical modeling of morphological processes in the case of suspended sediment transport." *Delft Hydraulics Communication No. 382*, Delft Hydraulics, Delft, The Netherlands.
- Villaret, C., and Davies, A. C. (1995). "Modeling sediment-turbulent flow interactions." *Applied Mechanics Research*, 48(9), 601–609.
- Wang, S. S. Y., and Adeff, S. E. (1986). "Three-dimensional modeling of river sedimentation processes." *Proc., Third International Symposium on River Sedimentation*, IRTCES, IWHR, Beijing, China.
- Wellington, N. W. (1978). "A sediment-routing model for alluvial streams." MEngSc dissertation, University of Melbourne, Australia.
- Wu, W., Rodi, W., and Wenka, T. (2000). "3D numerical modeling of flow and sediment transport in open channels." *Journal of Hydraulic Engineering, ASCE*, 126(1), 4–15.
- Zaghoul, N. A., and McCorquodale, J. A. (1975). "A stable numerical model for local scour." *Journal of Hydraulic Engineering, ASCE*, 13(4), 425–444.

This page intentionally left blank